ERDC/CHL TR-13-3

Coastal and Hydraulics Laboratory

US Army Corps
of Engineers®
Engineer Research and
Development Center

ERDC
INNOVATIVE SOLUTIONS
for a safer, better world

Physical Model Study of Flowerpot Discharge Outlet, West Closure Complex, New Orleans, Louisiana

Stephen T. Maynord

May 2013

The US Army Engineer Research and Development Center (ERDC) solves the nation's toughest engineering and environmental challenges. ERDC develops innovative solutions in civil and military engineering, geospatial sciences, water resources, and environmental sciences for the Army, the Department of Defense, civilian agencies, and our nation's public good. Find out more at www.erdc.usace.army.mil.

To search for other technical reports published by ERDC, visit the ERDC online library at http://acwc.sdp.sirsi.net/client/default.

ERDC/CHL TR-13-3
May 2013

Physical Model Study of Flowerpot Discharge Outlet, West Closure Complex, New Orleans, Louisiana

Stephen T. Maynord

Coastal and Hydraulics Laboratory
US Army Engineer Research and Development Center
3909 Halls Ferry Road
Vicksburg, MS 39180

Final report

Prepared for US Army Corps of Engineers
441 G Street NW
Washington, DC 20314-1000

Abstract

The physical model investigation of the West Closure Complex (WCC) Pump Station evaluated flow leaving the 1740 cfs pumps through the flowerpot discharge outlet (FPDO). The model study evaluated stability of flow in the FPDO, head loss through the FPDO to use in pump head estimation, downstream riprap stability, and performance of keel coolers both inside the FPDO and downstream of the FPDO in the tailwater. The recommended Type 8 Design FPDO has a 14-in.-wide rounded lip with its top located at elevation (el) 14, the chamber floor at el 11, and the roof at el 23. The diameter of the outlet at the top of the semicircular lip at el 14 was 169.5 in. Two 3-ft-wide piers at the downstream end of the chamber were found to not have adverse effects on pump head or flow exiting the chamber. Pressures measured in the pump column and dye injections in the flowerpot section showed stable flow conditions in the vertical column above the pump. Water levels in the chamber were well below the roof and should allow air bulking of the flow without filling of the chamber.

Contents

Figures and Tables

Figures

Tables

Preface

This study was conducted for the US Army Engineer Districts, Rock Island and New Orleans.

The work was performed by the Navigation Branch (CN-N) of the Navigation Division (CN), US Army Engineer Research and Development Center – Coastal and Hydraulics Laboratory (ERDC-CHL). At the time of publication, Dr. Richard Styles was Chief, CEERD-CN-N and Dr. Rose Kress was Chief, CEERD-CN. The Deputy Director of ERDC-CHL was Jose Sanchez and the Director was Dr. William Martin.

COL Kevin J. Wilson was the Commander of ERDC, and Dr. Jeffery P. Holland was the Director.

Unit Conversion Factors

Multiply	By	To Obtain
cubic feet	0.02831685	cubic meters
feet	0.3048	meters
inches	0.0254	meters
pounds (mass)	0.45359237	kilograms

1 Introduction

1.1 Background

At the request of the US Army Engineer Districts, Rock Island and New Orleans (RINO), the US Army Engineer Research and Development Center (ERDC) conducted physical model studies of the proposed Flowerpot Discharge Outlets (FPDO) used on the discharge side of each pump in the West Closure Complex (WCC) pumping station. The WCC is located just downstream of the confluence of the Harvey and Algiers Canals as shown in Figure 1. The WCC consists of levees, navigation channels, storm surge gates, and a pumping station initially having 13 pumps at 1,540 cfs per pump for a total station capacity of 20,000 cfs. The station was modified to have 11 pumps at 1,740 cfs per pump for a total station capacity of 19,140 cfs. These discharges are based on the design intake elevation of 2.0 ft (el 2). All elevations are in feet relative to the vertical datum of NAVD88 (2004.65). At the minimum intake el 0, discharge per pump was 1,710 cfs for a total capacity of 18,810 cfs. At the maximum intake el 7, discharge per pump was 1,815 cfs for a total station capacity of 19,965 cfs.[1]

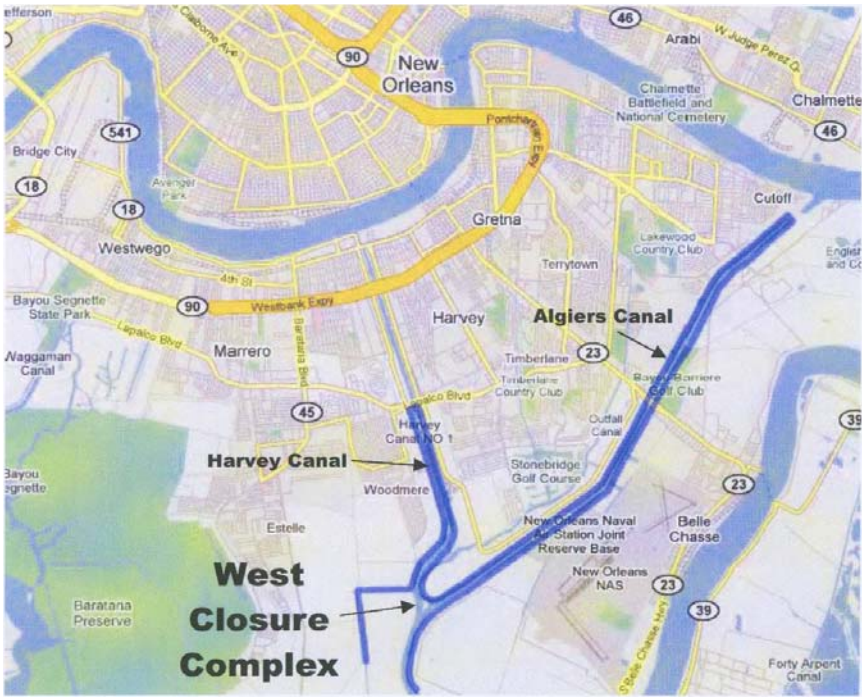

Figure 1. Location of WCC.

[1] All elevations (el) cited herein are in feet referenced to the National Geodetic Vertical Datum.

The discharge side of a pump can be configured to either discharge above or below the downstream water level. Discharge below the downstream water level is used to achieve siphonic recovery and thus reduce pump head. The reduced pump head is important in reducing operating costs for stations that operate a large amount of the time. One drawback of discharging below the downstream water level is that valves or other devices must be used to prevent backflow through the pump when stages on the discharge side exceed stages on the intake side of the pump and the pump is not operating. The alternative to discharging below the downstream water level and including backflow prevention devices is to discharge above the highest downstream water level to insure that backflow cannot occur. The FPDO studied herein, discharges above the highest downstream water level. The drawback of discharging above the downstream water level is that the pump head is larger than in a station having siphonic recovery. For stations that only operate a small portion of the time such as at the WCC, the increase in operating costs due to the higher head can be acceptable because of the elimination and possible failure of devices that prevent backflow through the pumps.

1.2 The flowerpot concept and need for modeling

An early design of the FPDO is shown in Figure 2. Horizontal flow enters the formed suction intake (FSI) at the bottom left, exits the pump vertically, and enters the rectangular discharge chamber. Flow turns from vertical to horizontal and exits out the right side of the box and drops into the downstream tailwater. The flowerpot name comes from the flare of the pump column above the pump. This flare increases the pipe diameter and reduces the velocity entering the chamber above the vertical pipe. Lower velocity entering the chamber should reduce losses through the chamber and thus head on the pump. This study found that flare that is too great results in flow separation in the vertical column above the pump and instability of flow in the column and chamber.

The ERDC recommended that a model study be conducted because few FPDO have been built and ERDC could not find any physical model investigations of the FPDO concept. Appendix E in EM 1110-2-3105, “Mechanical and Electrical Design of Pump Stations,” shows discharge into a chamber from a vertical non-flared pipe but the chamber dimensions do not match the WCC configuration. The manual does not provide a reference for this plot, but it was traced back to information from Flygt Pump Company. Additional information was obtained from Flygt, but this also did not match the configuration of the WCC.

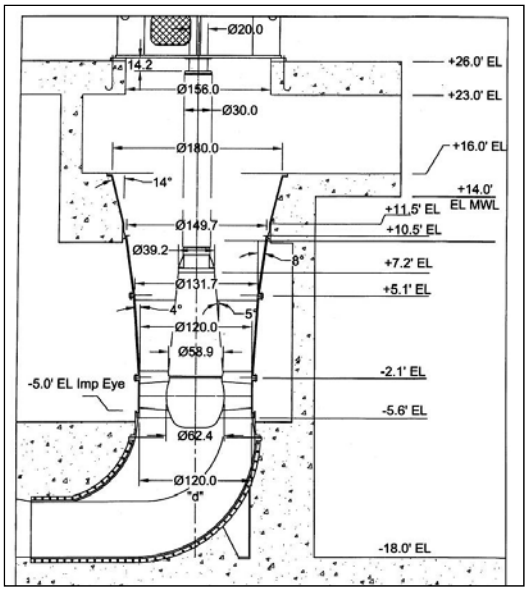

Figure 2. Side view of Type 3 design flowerpot discharge outlet. This was an early design of the flowerpot that will be discussed subsequently and was later modified. Flow enters the pump at the bottom left and exits at the top right.

There were two primary goals for this study. The first was the stability of flow in the discharge outlet chamber. The ERDC was concerned that the outlet chamber above the vertical flared pipe could alternate between flowing full and not flowing full in an unstable manner, which could induce head fluctuations on the pump. During the first phase of this study, it became apparent that a second and equally important goal had to be accomplished. The second goal of this modeling effort was to determine the head loss through the flared pipe and outlet chamber to develop an accurate system curve to use in pump sizing requirements. These two goals lead to construction and testing of two types of physical models that will be discussed subsequently. Near the end of the study, downstream riprap stability and performance of radiators (called keel coolers) used to cool pump station engines and other mechanical equipment became items that needed to be addressed in the models.

1.3 Models used in this study

Two model designs were used in this study. The first model built was with an impeller pump installed just below the chamber to generate the model flow similar to the proposed FPDO. The objective of this model was to simulate the swirl and turbulence from the pump and its influence on the performance of the box. The focus of this model was the hydraulic

performance of the box insuring that the flow conditions in the box were stable. The primary drawback of this model design was that there was no way to measure the head on the pump in the model reliably because of the complex flow conditions in the column above the pump, in the chamber, and chamber exit. Figure 3 shows the model test setups for the two models used in this study. Figure 3a shows the setup with the pump immediately below the discharge outlet chamber. The full scale FPDO uses a formed suction intake (FSI) on the intake side of the pump. The Figure 3a model used a suction bell instead of an FSI but this difference was not important to the study of performance of the FPDO.

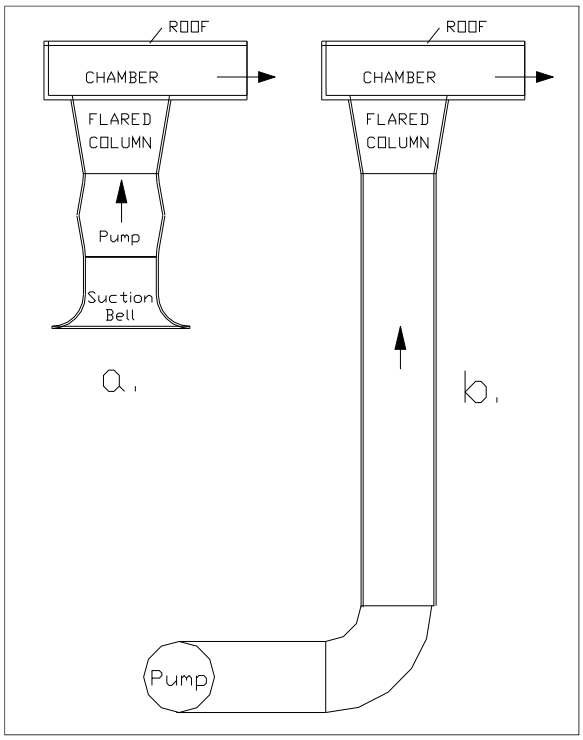

Figure 3. Concept drawings of two types of flowerpot models used in this study. Not to scale.

During the course of this study, the sponsor looked at the possibility of reducing the original number of pumps from 13 to either 12 or 11 pumps to reduce cost. The final plan was to use 11 pumps. The sponsor needed accurate estimates of the head losses to generate an accurate system curve to evaluate pump size requirements. Other losses used in developing a system curve, such as through the trash rack and FSI, are well known and commonly accepted. Losses through the pump including losses as a result of the center shaft enclosure were reflected in the pump curve. Only the FPDO losses were unknown and had to be determined in the model. From

observing flow conditions in the Figure 3a physical model, it was apparent that the head could not be measured accurately in the FPDO model with the pump immediately below the chamber because of the large turbulence and complex flow patterns just above the pump impeller. For these reasons a second model design was used to determine the head loss through the FPDO. The model pump was located away from the FPDO and a 10-diameter length of straight pipe was placed upstream of the FPDO. Piezometer taps were installed at four locations at 90 deg around the perimeter of the straight pipe to measure the static head, and discharge was measured with a Venturi meter to determine the velocity head at the location of static head measurement. This approach isolated the head loss through the FPDO. Figure 3b shows the setup with the straight pipe immediately below the discharge outlet chamber.

1.4 Riprap stability and alternate locations of keel coolers

In addition to the performance of the flowerpot, the Figure 3a FPDO model was used to evaluate riprap requirements and velocities near keel coolers in the tailwater downstream of the pump station. The Figure 3b FPDO model with straight pipe below the outlet chamber was also used to evaluate keel cooler effects on pump head, loadings on keel coolers, and velocities near keel coolers.

2 Flowerpot Model with an Impeller Pump Immediately Beneath the FPDO

2.1 Model description

The test facility (Figure 4) reproduced the FPDO for one pump at a model to prototype scale ratio of 1:15. The flume consisted of an outer flume that was the sump for the pump and an inner flume that had a sharp-crested weir at the downstream end that was used for flow measurements. Note that the inner flume was 41.5-ft wide, which was the width of the FPDO plus 1/2 of a divider wall width on each side. This resulted in the inner flume representing the correct width of the discharge channel for one pump. A framework held the 15-hp motor, pump with a suction bell, the pump column, and the FPDO. The FPDO emptied into the inner flume. The 15-hp motor was controlled by a variable frequency drive unit. A tachometer was used to measure the shaft speed and once set, the motor speed was constant. Figure 5 shows the model impeller that was not a scaled impeller from the WCC pump. The model impeller had three blades with a vane angle at the tip of 19 deg. The model used a bell mouth intake having a diameter of 15 in. on the 8-in.-diameter pump.

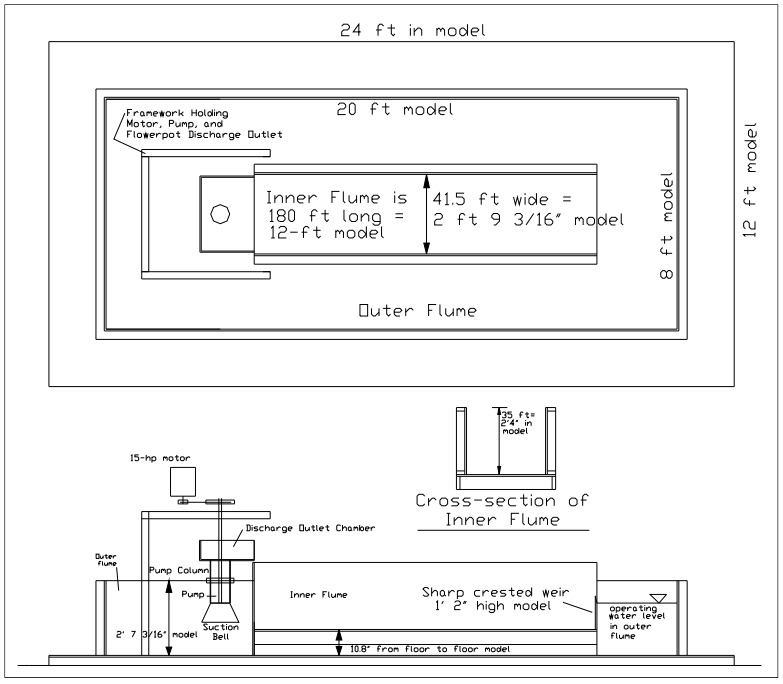

Figure 4. Schematic of 1:15-scale model facility used to test FPDO with an impeller pump immediately below FPDO.

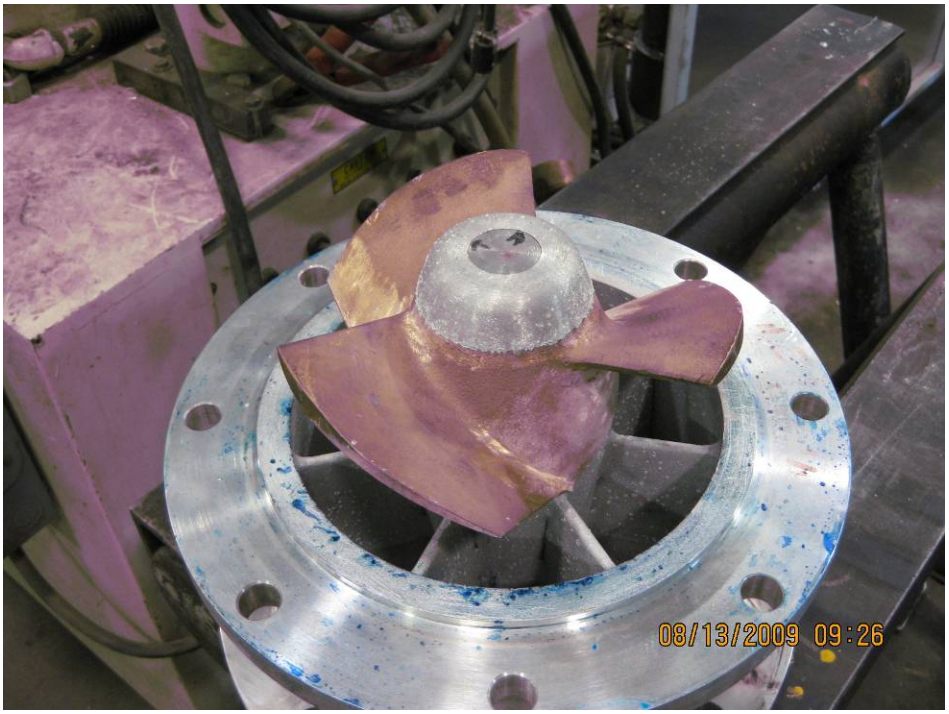

Figure 5. Impeller used in 1:15-scale FPDO. Picture shows model pump turned upside down.

2.2 Scale selection and scale relationships

The FPDO chamber has a free surface, which requires that the Froude number be the same in the model and prototype to result in similar flow patterns. Equality of Froude number means that the ratio of inertial forces to gravitational forces is the same in the model and prototype.

Equality of Froude number results in the following relations to transfer quantities from model to prototype:

Length ratio:	$L_r = L_p/L_m$
Discharge ratio:	$Q_r = Q_p/Q_m = L_r^{2.5}$
Velocity ratio:	$V_r = V_p/V_m = L_r^{0.5}$
Time ratio:	$T_r = T_p/T_m = L_r^{0.5}$
Frequency ratio (such as rotational speed):	$f_r = f_p/f_m = 1/\ L_r^{0.5}$

where subscript, r, denotes ratio; p prototype; and m model.

The scale was selected based on a minimum Reynolds number and an available existing pump. The flowerpot outlet was composed of the vertical

flared pump column section, an abrupt expansion into the chamber, vertical flow transitioning to horizontal flow, and flow out/over the exit end of the chamber. Scale effects are minimized by keeping the model Reynolds number sufficiently large. Of the various components of the FPDO, the diffuser was the component that has the most information available about the effects of Reynolds number. The diffuser at the WCC has a center shaft enclosure that was not present in diffusers that have been tested for Reynolds number effects. Based on Miller (1978), the loss coefficient in a 6- and 8-deg diffuser with a thin inlet boundary layer was almost constant above a Reynolds number (R) of 2×10^5. At $R = 2 \times 10^5$, the loss coefficient was only two percent greater than at $R = 10^6$, the highest R presented in the plot.

An existing impeller pump had a diameter of 8-in. For the 120-in. prototype pump diameter, this existing pump resulted in a length ratio $L_r = 15$. At a full scale discharge of 1,540 cfs per pump, the 1:15-scale model had a discharge of 1.77 cfs. The resulting model R at 70 ^{O}F was 3×10^5, which was greater than the minimum R from Miller (1978). The subsequent change to 11 pumps resulted in discharge of about 1,740 cfs per pump and the model Reynolds number was further increased. The 1:15-scale was adopted for the FPDO model having the pump immediately beneath the FPDO.

2.3 Results with an existing impeller pump immediately beneath FPDO

Initial tests were conducted with an existing pump that did not reproduce details of the FPDO pump to try to gain insight into the issues important to the proper operation of the FPDO. Figure 6 shows a side view of the Type 1 Design having the existing pump and a straight pump column rather than a flared section. The Type 1 Design had the floor of the chamber at el 16 and the column diameter entering the chamber was 10-ft. A pressure transducer (Omega PX 309-002G5V, 0-2 psi) was installed in the pump column to measure static pressure and pressure variations. The pressure transducer measurements in the pipe below the FPDO were used as a qualitative indicator of the stability of the flow entering the FPDO. The discharge chamber in the Type 1 Design does not have the roof in the model that was added in subsequent tests. The top of the back and side walls in the Type 1 Design was at el 26. Table 1 summarizes the details of the Type 1 Design and all subsequent design types.

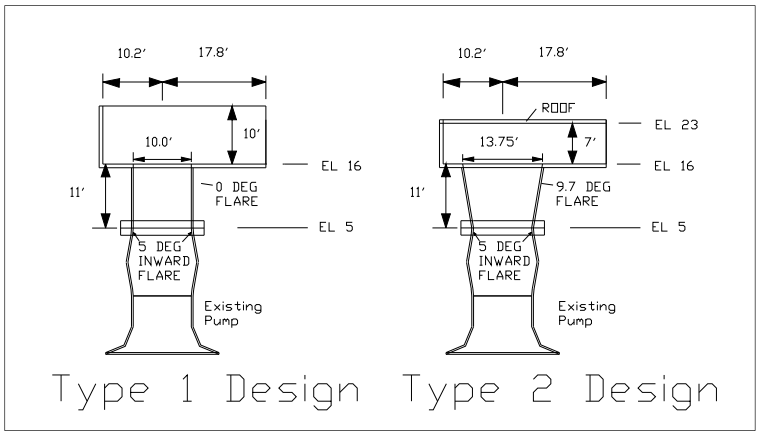

Figure 6. Side view of model with existing pump. Type 1 Design with uniform diameter pump column and Type 2 Design with 9.7-deg flared pump column.

Table 1. Summary of design types of FPDO.

Type (FPDO model)	Chamber el	Model Pump	Pump Column and flowerpot flare	Flowerpot Inside Diameter at top, ft (lip shape)	Top of Flowerpot el	Piers	Backwall Distance from center of pump, ft
1 (1)	16.0	Existing	No flare	10.0 (no lip)	16.0	None	10.25
2 (1)	16.0	Existing	Both 9.7-deg flare	13.75 (no lip)	16.0	None	10.25
3 (1)	16.0	Fairbanks	8- and 14-deg flare	15.0 (no lip)	16.0	None	10.25
4 (1)	11.5	Fairbanks	8- and 3.2-deg flare	13.5 (1-in.-thick)	16.0	None	15.25
5 (1)	11.5	Fairbanks	8- and 3.2-deg flare	13.5 (1-in.-thick)	16.0	None	10.25
6 (1)	11.5	Fairbanks	8- and 3.2-deg flare	13.5 (1-in.-thick)	16.0	Two	10.25
7 (1)	11.5	Fairbanks	8- and 3.2-deg flare	13.27 (2.3 in. thick)	14.0	Two	10.25
8 (2)	11.0	No Pump	6.1-deg flare, 2.2 in. offset, and 6.1- deg flare	14.125 (rounded plate with 7- in. radius)	14.0	Two	10.25
9 (2)	11.0	No Pump	6.1- and 6.1- deg flare	14.125 (rounded plate with 7- in. radius)	14.0	Two	10.25
10 (2)	11.0	No Pump	6.1-deg flare, 2.2 in. offset, and 6.1-deg flare	14.125 (rounded solid with 7- in. radius)	14.0	Two	10.25
11 (2)	11.0	No Pump	6.1-deg flare, 2.2 in. offset, and 6.1-deg flare	14.125 (rounded plate with 7- in. radius)	14.0	None	10.25

Figure 7 shows a side view of the Type 1 Design with 1,540 cfs. Note that the shaft was not enclosed as was done in the actual Fairbanks Morse design used in later tests. The black line on the side of the chamber was at el 23 and represented the position of the roof. Note that the water level

was well above the black line, which means the discharge chamber will likely flow full to some extent. A pressure transducer was installed in the Type 1 Design at el 7.7 in the pump column. The pressure transducer was located at 2:30 with 12:00 pointing downstream. The pressure transducer in the Type 1 Design measured a static head of el 20.5, as shown in Figure 8. The total energy elevation based on the sum of the static head and the velocity head in the 10-ft diameter pipe was el 26.5. The total energy elevation value should be viewed with caution because of the close proximity of the pressure measurement location and swirl, turbulence, and distorted velocity profile from the pump. In addition, the Type 1 Design did not have a roof that would have affected the measured pressure. The distorted flow could prevent the single static pressure measurement from being representative of the entire flow. The distorted flow could also result in a kinetic energy correction factor α greater than one but unknown.

These initial tests showed that the uniform pipe resulted in excessive velocity entering the discharge chamber. Flaring of the vertical pipe between the pump and the discharge chamber was needed to reduce the velocity entering the discharge chamber. These initial tests suggested that the 7.0 ft of clearance from the floor (el 16) and the roof of the discharge chamber (el 23) might not be enough. The pressure fluctuations had a standard deviation of 0.43 ft in full scale with the straight pump column. This value served as a baseline for pressure fluctuations from an impeller pump with no influence of pump column flaring.

The Type 2 Design had a 9.7-deg flare above the existing pump, as shown in Figure 6. Note that the Type 2 Design had a 13.75-ft column diameter at the entrance to the FPDO. The Type 2 Design was tested with the roof installed at el 23 and the outlet chamber flowed full over the upstream two-thirds of the chamber. Figure 9 shows the measured static head elevation for the Type 2 Design. The pressure transducer was located at 2:30 in clock frame with 12:00 pointing downstream. Note that the average static head elevation dropped about 2.2 ft, but the fluctuations increased based on the standard deviation. The influence of the 9.7-deg flare was shown by the increase in standard deviation of the pressure fluctuations. The Type 2 Design had a standard deviation of 0.4 ft greater than that with the Type 1 Design.

Figure 7. Side view of model with existing pump and uniform diameter pump column with 1,540 cfs. The black line is the location of the roof at el 23.

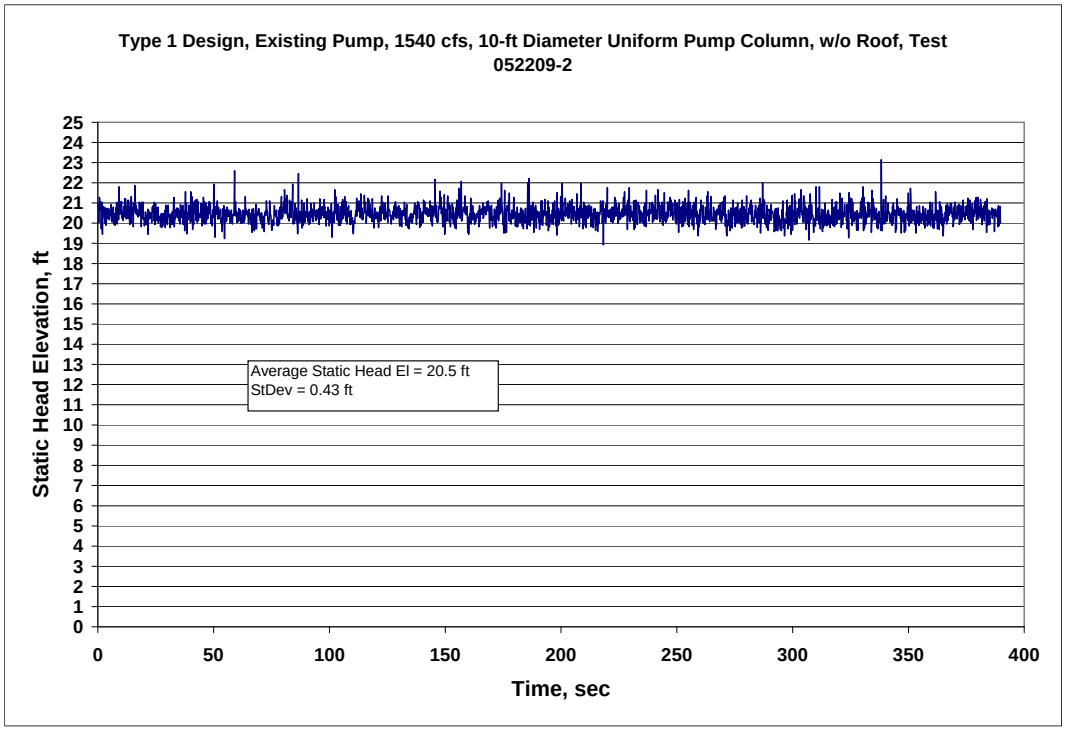

Figure 8. Static head elevation in Type 1 Design with existing pump immediately below FPDO, uniform 10-ft-diameter pump column.

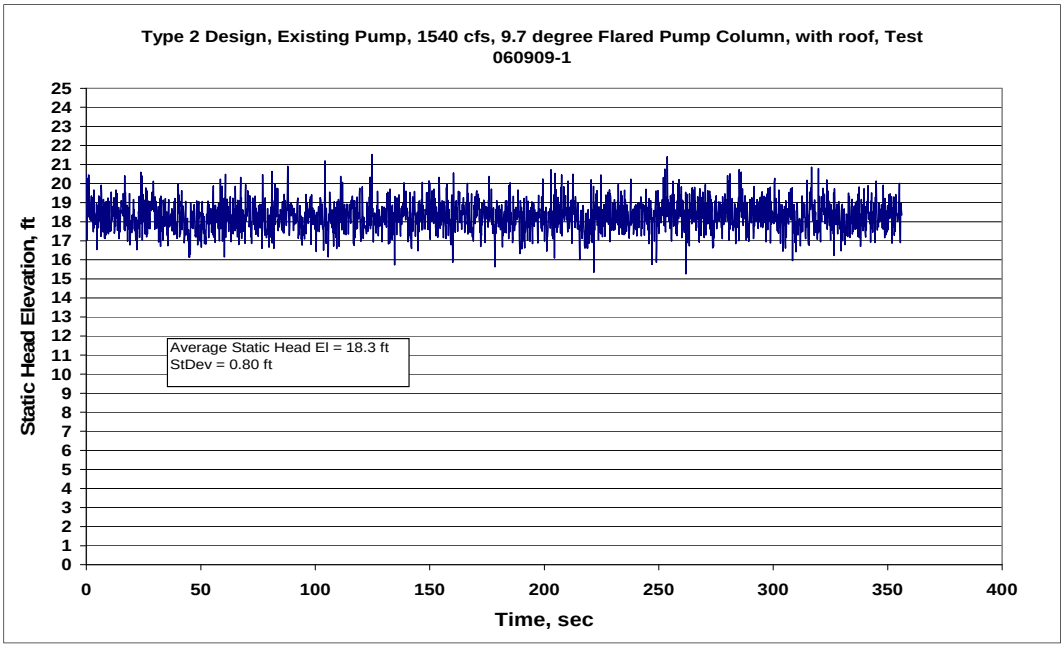

Figure 9. Static head elevation in Type 2 Design with existing pump immediately below FPDO, with 9.7-deg flared pump column.

2.4 Results with Fairbanks Morse column, vanes, shaft enclosure, and ERDC impeller immediately below FPDO

The pump model used in these tests was built at the ERDC and had the Fairbanks Morse diameters and flares in the model, as well as details of the center shaft enclosure. The pump impeller was similar to the full scale impeller but was not an exact scaled version. This model included one important error that resulted from a miscommunication between the ERDC and Fairbanks Morse. The vanes in the pump were built straight rather than curved. This error almost certainly resulted in turbulence exiting the pump and entering the FPDO at a greater rate than would occur in the real system.

The Type 3 Design is shown in Figure 2. Type 3A had the opening in the roof for pump removal whereas Type 3B had no opening in the roof other than for the 30-in.-diameter shaft enclosure. Tests with the two designs showed no difference so the Type 3A Design with the opening was preferred and was used in subsequent tests. The model reproduced all details except for the incorrect vane configuration discussed previously. The pump had the following parts:

- FSI up to el -5.6;
- 10-ft-diameter impeller section between el -5.6 and -2.1;

- The seven-vane section between el -2.1 and +5.1, which had wall divergence of 4-deg and shaft enclosure convergence of 5-deg;
- Pump column section between el 5.1 and 10.5, which had a wall divergence of 8-deg and a shaft enclosure that initially had the 5-deg convergence and then a change in diameter at el 7.2,;
- The flowerpot section between el 10.5 and 16.0, which had a wall divergence of 14-deg and a shaft enclosure of uniform diameter;
- Diameter of flowerpot section at entrance to discharge chamber of 15.0 ft; and
- Discharge chamber, which was 7-ft high and 38.5 ft wide being basically a rectangular box with an outlet on one end.

The discharge chamber had an opening at the top through which the pump can be removed for repair and maintenance.

The Type 3 Design described above had a significant amount of separation of flow due to the diverging pipe walls and the converging center shaft enclosure. The abrupt expansion between the vertical pipe and the discharge chamber was also a potential source of instability, particularly in combination with the 8-deg and 14-deg diverging pipe sections. Miller (1978) examined conical diffusers for flow stability. The conical diffusers of Miller were free outlets without a center shaft enclosure and straight uniform approach flow without turbulence from an impeller, but represent the best available information. The first (8-deg pump column) and second (14-deg flowerpot) sections were evaluated using the Miller (1978) guidance, which was based on the area ratio between the ends of the diffuser and the length of the diffuser relative to the radius of the inlet. The effects of the center shaft enclosure were ignored. The first diffuser section having the 8-deg wall flare fell between Miller's line for steady flow and the line for onset of small areas of flow separation with small amplitude fluctuations. The second diffuser section having the 14-deg wall flare fell well above the line for onset of small areas of flow separation with small amplitude fluctuations and close to the line for very unsteady flow with areas of stall moving around the diffuser and penetrating far into the flow. Miller (1978) stated that the severest pressure fluctuations occurred when a diffuser followed a component with which it interacts unfavorably. The second 14-deg diffuser, which fell close to Miller's "very unsteady" range, followed the first 8-deg diffuser and could result in an unfavorable interaction.

Modeling flow separation was extremely difficult because a variety of factors that affect the onset of separation were difficult to replicate in the model. In some cases these differences could be dealt with by running the model at increased velocity up to equal Reynolds number. This was not possible in the WCC flowerpot model because the model contained the discharge outlet having a free surface, which must be modeled by replicating the Froude number.

Results with the Type 3 Design showed unstable flow in the chamber with slugs of air rapidly moving from downstream to upstream as well as from back corners of the chamber toward the center of the box. In addition, dye injected inside the 14-deg flowerpot moved upstream indicating areas of significant flow separation. Figure 10 shows the measured static head elevation from two transducers positioned at 2:30 and 8:30 at el 7.7. Note that while the static pressure dropped about 1.0 ft from the Type 2 Design, the standard deviation increased significantly. The cells were swapped and each location showed the same standard deviation with both cells.

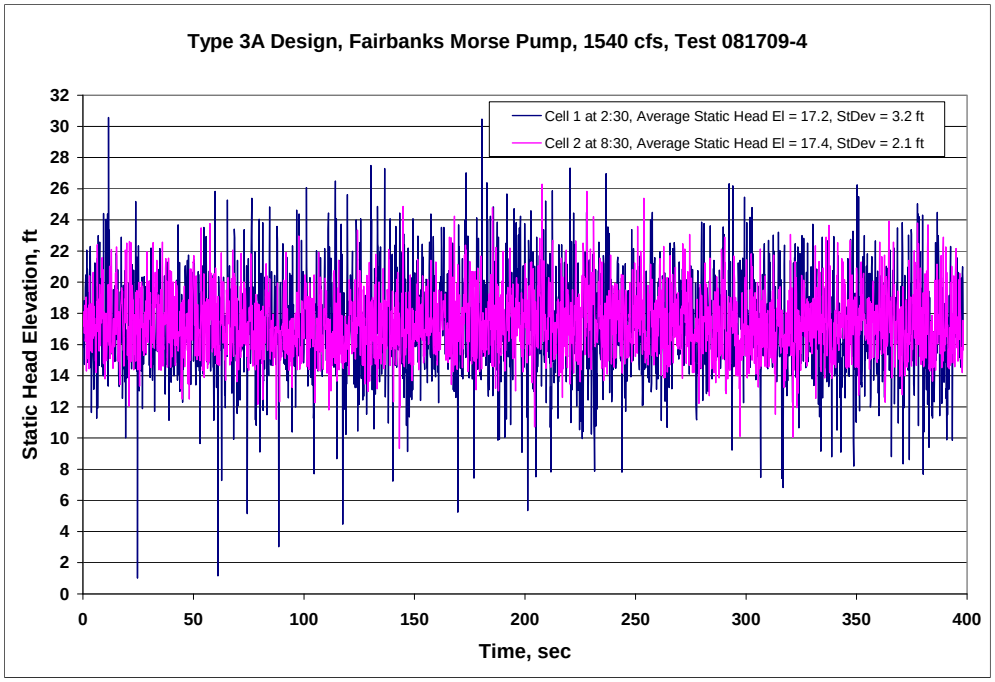

Figure 10. Static head elevation in Type 3A Design with Fairbanks Morse design except for incorrect vanes.

At this point in the testing, there was concern that the chamber was adversely affecting the flow exiting the flowerpot section. In addition, there was concern over the 14-deg flare that was believed to be the source of much of the flow separation indicated by the upstream movement of dye.

Reducing the 14-deg flare, increasing the backwall clearance, and reducing the floor elevation were tested to determine their impacts. In the Type 4 Design, all three were changed and in the Type 5 Design only the floor elevation and the flare angle were reduced. Figure 11 shows the Type 4 and Type 5 Designs. Consideration was given to the question: "What was the optimum diameter of the top of the pipe?" Note that the outlet diameter at the top of the flowerpot section with the reduced flare changed from 15 ft in the Type 3A Design to 13.5 ft in the Type 4 and 5 Designs. There were competing factors present in determining the best outlet diameter. Reducing the pipe outlet velocity favored as large an opening as possible. Preventing large scale separation and maintaining flow stability in the flared section favored a smaller diameter. The need to keep as large a space between the pipe and the backwall favored a smaller diameter. The flower-pot diameter was not optimized but 13.5 ft was considered a good compromise between these competing factors.

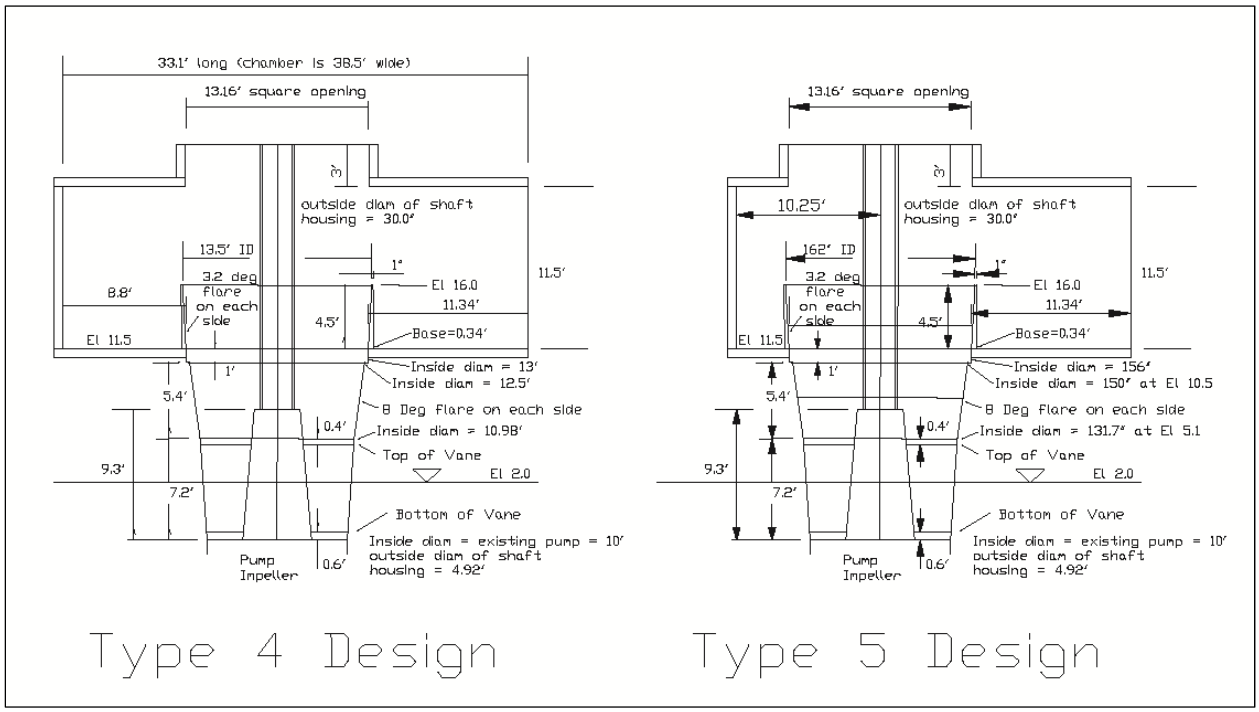

Figure 11. Type 4 and Type 5 Designs with lowered floor, reduced flare, and backwall distance increased by 5.0 ft (Type 4) and original backwall distance (Type 5).

Figures 12 and 13 show the measured static head elevation for the Type 4 and Type 5 Designs, respectively. Both show similar average static head elevations and standard deviations. Note that the standard deviation was significantly reduced from the Type 3A Design but still well above the Type 2 flared pump column design. This increased standard deviation showed the

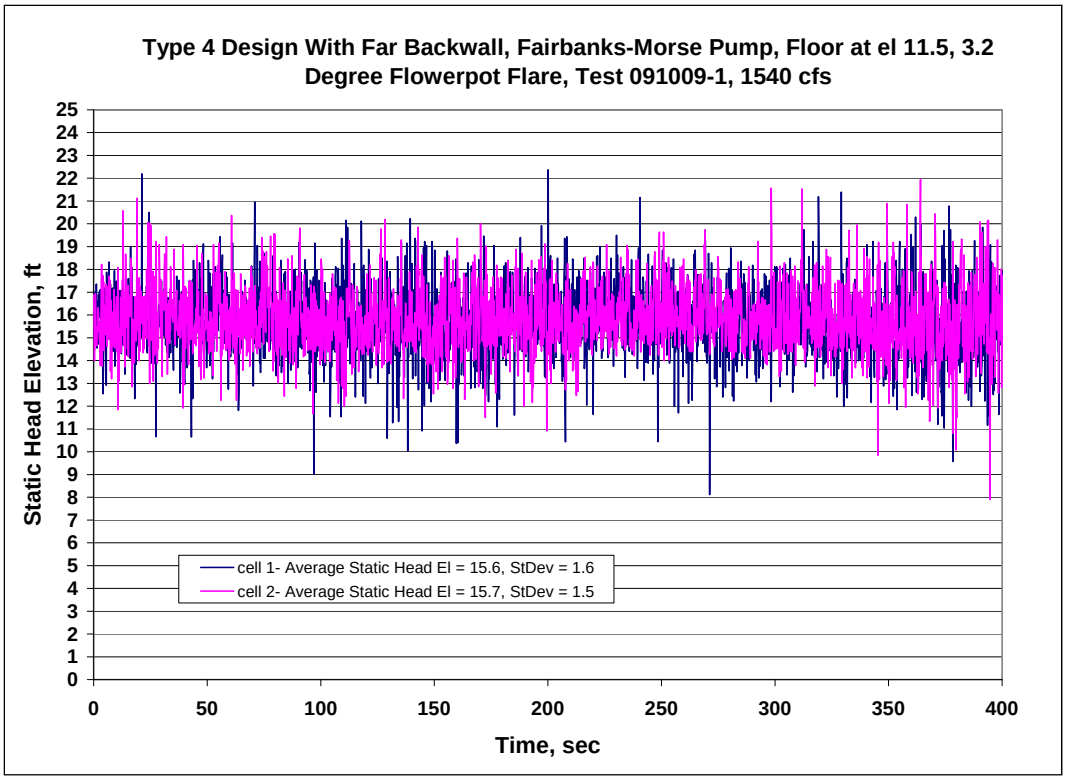

Figure 12. Static head elevation in Type 4 Design with Fairbanks Morse design except for incorrect vanes. Far backwall location, floor at el 11.5, and reduced flare angle in flowerpot section.

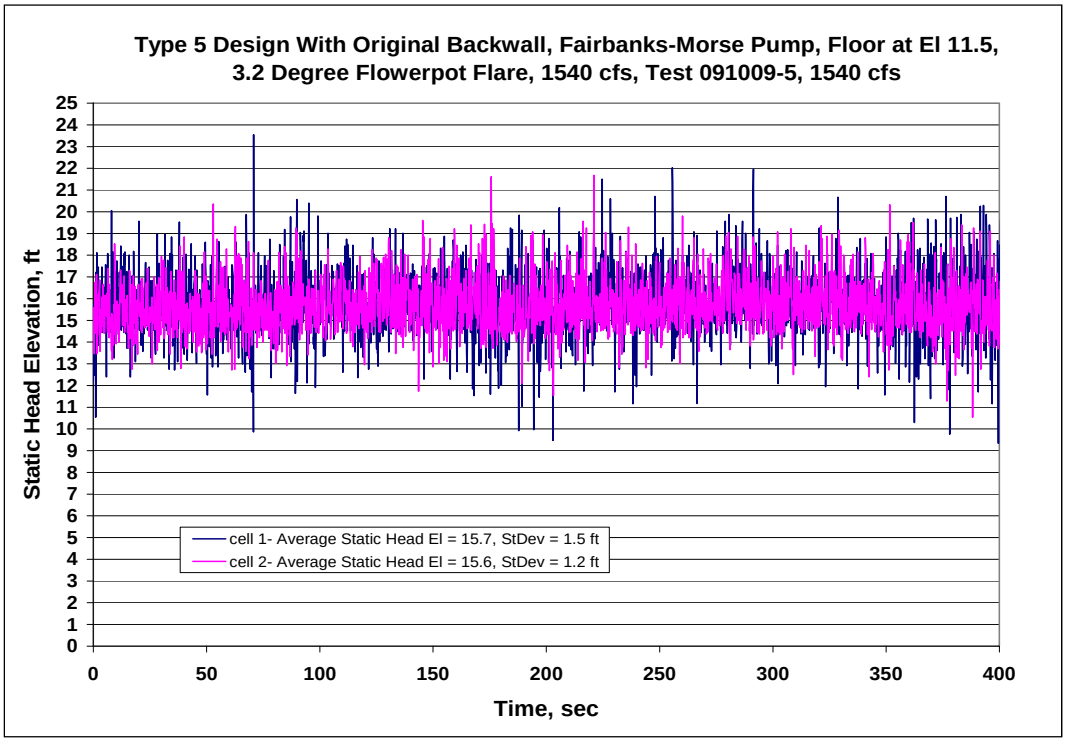

Figure 13. Static head elevation in Type 5 Design with Fairbanks Morse design except for incorrect vanes. Original backwall location, floor at el 11.5, and reduced flare angle in flowerpot section.

influence of the incorrect vanes in the model. Since the two backwall distances gave similar results, backwall distance did not explain the reduced standard deviation. While this could have been the result of the lowered floor, it was believed that the reduced standard deviation was primarily due to the elimination of the 14-deg flare angle. Although the standard deviation was reduced, dye injections in the 3.2-deg flared section periodically moved upstream still showing the presence of flow separation. The lowering of the floor to el 11.5 in the Type 4 and 5 Designs resulted in the discharge box not flowing full. Flow in the box was turbulent, particularly at the top of the flow above the vertical pipe. The ERDC believes that some of the roughness/ turbulence above the pipe was due to the vane error described previously. No large scale instability was seen in the box flow as opposed to the previous design where significant instability was seen in the box. Some flow rose above the roof elevation at el 23.0 into the square opening. The top of this opening at el 26.0 was left open in the model for viewing purposes. Some of the flow splashed above and out of the top of the square opening. The amount splashing up, above, and out of the opening tended to increase with increasing discharge.

Project designers asked whether support piers could be installed at the downstream opening of the FPDO. The piers were needed to reduce the cost of a beam that would have to span the entire width at the discharge exit end of the 38.5-ft-wide chamber. The designers provided the pier size and locations shown in Figure 14. The Type 6 Design adds the piers to the Type 5 Design, which consisted of the original backwall location, the floor at el 11.5, the el 16 sharp crested lip, and the reduced flare angle of the flowerpot section. The piers were added to the model and no difference in performance of the FPDO was observed. Later tests in the second FPDO model were discussed and subsequently confirmed this finding.

At this point in the model study, the sponsors were considering using fewer pumps with larger capacity per pump as a cost saving measure. Since the same pumps were going to be used, reducing the head on the pump was one way to increase the discharge per pump. One way to reduce pump head was to lower the lip of the discharge outlet, which was at el 16 in the Type 6 Design. The Rock Island/New Orleans Districts stated that the lip could not be lowered any more than 2.0 ft (down to el 14) and still maintain the required level of storm surge protection. The Type 7 Design, shown in Figure 15, had the lip lowered to el 14. Table 2 shows data collected on the Type 6 and Type 7 Designs. These tests in the 1:15-scale model showed that

lowering the lip from el 16 to el 14 only reduced pump head by about 0.6 ft. This limited reduction in head was the result of the lowered lip being affected to a greater extent by submergence of the flow from the pipe in the outlet chamber. This 0.6 ft lowering of head should be viewed with some caution because the FPDO model with the pump immediately below the outlet did not have a good location to measure the pump head caused by the FPDO. Note that the total head determined from the two different piezometer locations and based on the measured top of jet did not give consistent values. This highlights the difficulty of using the FPDO model with the pump immediately below the FPDO to determine total head on the pump.

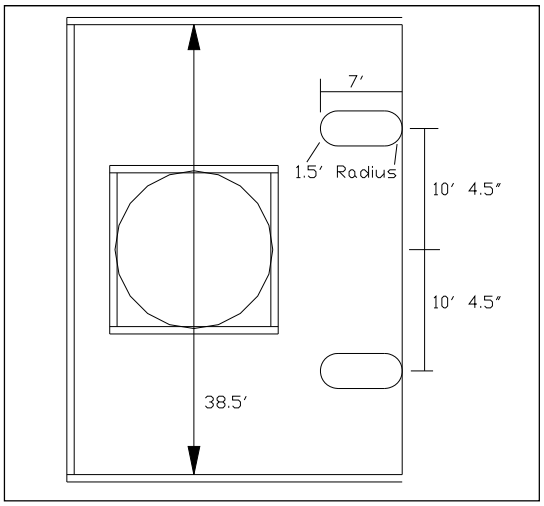

Figure 14. Pier size and location in Type 6 Design.

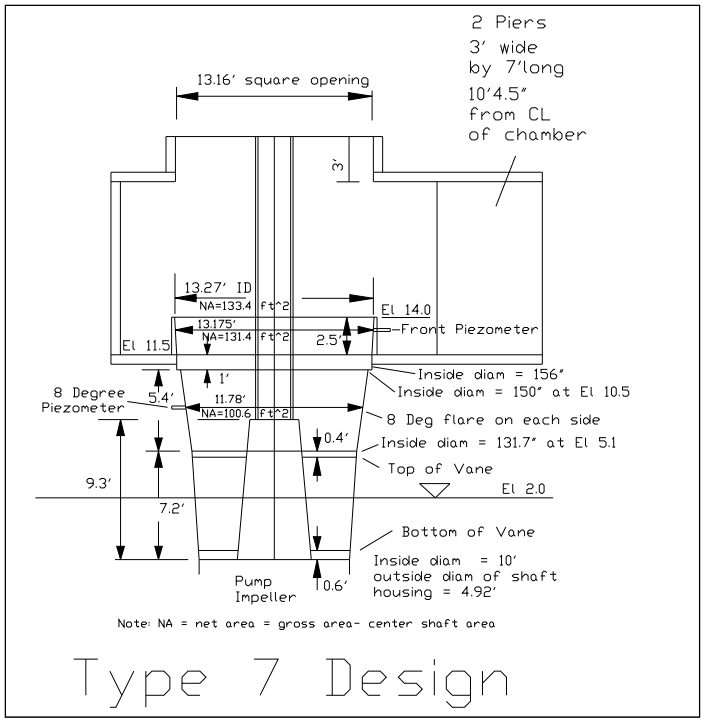

Figure 15. Type 7 Design with lip at el 14. NA = net area = total area - shaft area.

Table 2. Data from el 16 lip (Type 6) and el 14 lip (Type 7) in the 1:15 original FPDO model. Floor at el 11.5.

Design	Q, cfs (model rpm)	8-deg piezometer elevation, (Total Head)*	Front piezometer elevation, (Total Head)*	Top of jet, avg elevation	Water surface elevation at back corner, (depth, ft)
Type 6	1,680 (747)	14.50 (18.84)	17.88 (20.42)	22.44	19.4 (7.9)
Type 7	1,700 (747)	13.75 (18.19)	17.35 (19.95)	21.69	19.4 (7.9)
Decrease	NA	0.65	0.47	0.75	0.0
Type 6	1,825 (776)	13.94 (19.06)	17.65 (20.65)	23	19.75 (8.25)
Type 7	1,800 (776)	13.75 (18.81)	17.5 (20.47)	22.4	19.9 (8.4)
Decrease	NA	0.25	0.18	0.60	-0.15

*Piezometer locations shown in Figure 15.

3 Flowerpot Model with Straight Pipe Immediately Beneath the FPDO

3.1 General

Determination of the head in the FPDO model became a critical element because of the efforts to reduce the number of pumps from 13 to 11. Up until this point in the study, hydraulic equations based on horizontal pipe flow were used to determine the head on the pump from the various components of the FPDO. The velocity head was used to define the exit loss from the vertical pipe above the pump. The depth upstream from the free overfall was used to define the water level at the vertical pipe outlet. The application of these equations was made more difficult based on insight gained from a paper by Lawrence and Braunworth (1906, ASCE transactions) on flow issuing from a vertical pipe. Unlike the FPDO, their tests did not have a floor positioned at or below the pipe lip, which can lead to submergence effects on the flow exiting the pipe. Lawrence and Braunworth separate flow exiting a vertical pipe into three regimes. For a rise of the water level above the top of the pipe of up to 0.37 times the diameter of the pipe, the flow was weir flow. For weir flow conditions, the rise of the water level above the top of the pipe was greater than the velocity head in the pipe. For a rise of the water level above the top of the pipe of 1.4 times the pipe diameter, the jet flow regime begins. For jet flow, the rise of water level above the top of the pipe was about equal to the velocity head. Between these two regimes was the third or transitional regime. For the FPDO having a diameter of about 13.5 ft, the weir regime was up to 0.37 × 13.5 ft or 5.0 ft and the jet regime starts at 1.4 × 13.5 ft or 18.9 ft. Based on observations of depth above the outlet in the model, the WCC FPDO was in the Lawrence and Braunworth transitional regime for discharge of about 1,740 cfs. The WCC was far from the jet flow condition where the flow exiting the pipe will rise to a height equal to the velocity head. To complicate pump head determination using hydraulic equations even further, the depth in the chamber was sufficient to cause submergence effects on flow exiting the pipe. Submergence effects are affected strongly by the shape of the lip. For horizontal flow, a sharp crested lip is generally most affected by submergence, whereas a broad crested weir is least affected by submergence. The effect of submergence on flow from a vertical pipe was unknown. Accurate determination of pump head requires

proper integration of all of these factors and must be done in a physical model.

3.2 Preliminary FPDO model

3.2.1 Preliminary model description

Because of the importance of an accurate determination of pump head, a second FPDO model was constructed to study the head loss in the FPDO without the effects of the excessive swirl and turbulence present in the initial model. Design details were not available for the revised outlet to replace the Type 7 Design, which still had some performance concerns such as flow separation in the pump column. ERDC constructed a preliminary FPDO model to look at issues such as floor elevation effects and lip thickness and shape effects. These preliminary tests were conducted with a FPDO outlet having no flare of the column below the FPDO and a 13.5 ft inside diameter at the top of the outlet. Because these tests did not include the details of the actual design and only looked at effects of specific variables, they were not assigned design type numbers. The preliminary model was constructed from readily available pipe, which resulted in a scale ratio of 1:20.38. The model had a length of pipe equivalent to ten pipe diameters below the FPDO so that the flow entering the FPDO was relatively free of swirl and excessive fluctuations in velocity direction and magnitude. This straight length of pipe allowed for the determination of the total head in the FPDO using piezometers installed just upstream of the FPDO.

The model schematic is shown in Figure 16. The straight length of pipe was a 7.0-ft (model) length of 8.0 in. PVC pipe. The upstream end of the pipe had a 90-deg elbow. At the downstream end of the elbow, a honeycomb was installed using the material shown in Figure 17. This material had 1/4 in. diameter openings and was 2-in. thick to reduce the effects of the 90-deg bend. The initial tests had neither the center shaft enclosure nor the two structural piers and the lip was only tested at el 14. The floor of the FPDO was at el 11.75. The four piezometers at 90 deg around the pipe were located at el 0.9. Flow rate was measured with a venturi meter. The model is shown in Figures 18-20. The water surface at the top of the jet without the center shaft enclosure was smoother than subsequent tests with the center shaft enclosure.

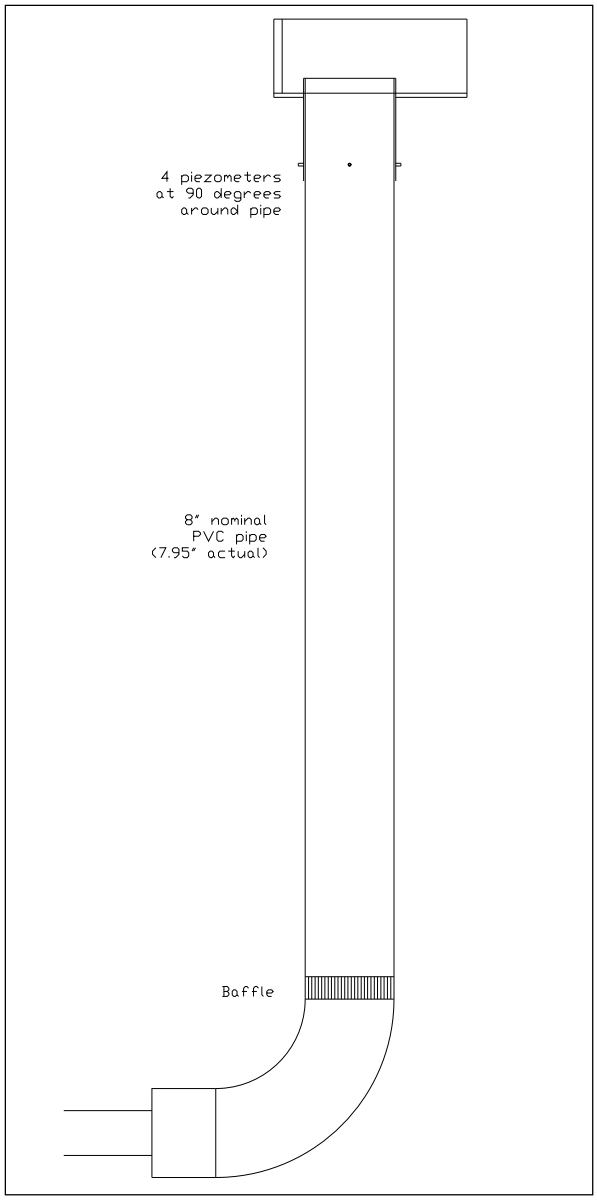

Figure 16. Schematic of FPDO without excessive swirl and turbulence.

This issue became important because the ERDC evaluated whether the total head on the pump should be determined using the measured top of the jet or the measured piezometer reading plus the velocity head. The ERDC believed that the most accurate determination of total energy to use in the pump head calculations was from the sum of the piezometer elevation and the velocity head at the piezometer location, as opposed to the top-of-jet measurements. Consideration should be given to increasing this value to account for some swirl, separation, and turbulence from the pump in the real system and will be discussed subsequently.

Figure 17. Honeycomb baffle material used at downstream end of 90-deg elbow.

Figure 18. 1:20.377-scale preliminary FPDO model showing 7-ft-long PVC pipe.

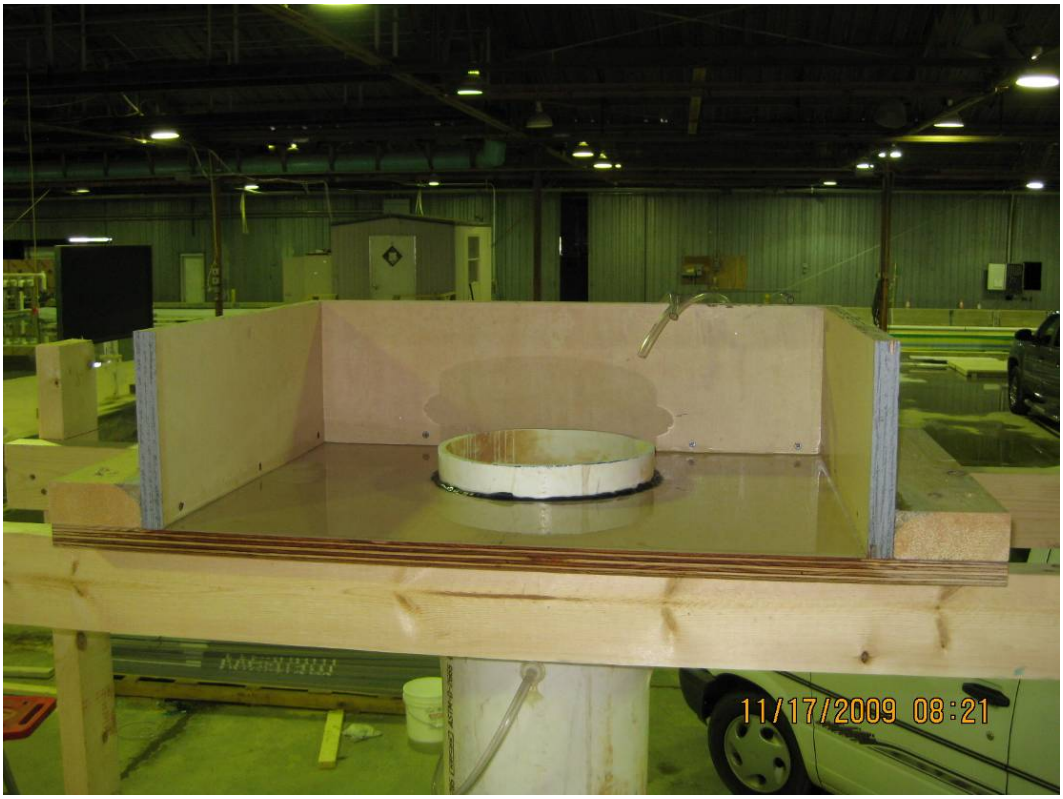

Figure 19. 1:20.377-scale preliminary FPDO model showing outlet chamber.

Figure 20. 1:20.377-scale preliminary FPDO model showing flow of 1,667 cfs in outlet chamber.

3.2.2 Evaluation of total energy for a range of floor elevations

Tests were conducted on the effects of floor elevation with the 30-in. diameter center shaft enclosure and with the two 3-ft-wide by 7-ft-long structural piers placed in the 1:20.377-scale model. The shaft enclosure extended about 5.5 ft (model) down into the 8.0 in. (model) PVC pipe. Another honeycomb baffle was installed at the upstream end of the center shaft enclosure. The lip of the discharge outlet was at el 14 for all tests and data are shown in Tables 3-6. The top of the lip had square corners and was 6.7-in. wide. Data are also provided for the depths in the chamber along the side walls to assess submergence effects. The inside diameter of the outlet simulated in the model was 13.5 ft.

Table 3. Effect of FPDO floor elevation on total energy and discharge profile with a floor located at el 10.

Q, cfs	Piezometer el	$V^2/2g$, ft	Total energy el	Top of jet el	Depth at back corner, ft	Depth at wall even with pump CL, ft
710	16.33	0.41	16.74	16.51	4.9	4.3
950	16.79	0.74	17.53	NM	5.8	4.9
1,200	17.25	1.17	18.42	17.99	6.5	5.9
1,490	17.79	1.81	19.60	NM	7.1	6.7
1,667	17.94	2.27	20.21	Not measured	Not Measured but other tests show depth = 7.5 ft	Not Measured but other tests show depth = 6.9 ft
1,834	18.17	2.74	20.91	19.77	Not Measured but other tests show depth = 7.9 ft	Not Measured but other tests show depth = 7.3 ft

Table 4. Effect of FPDO floor elevation on total energy and discharge profile with a floor located at el 11.

Q, cfs	Piezometer el	$V^2/2g$, ft	Total energy el	Top of jet el	Depth at back corner, ft	Depth at wall even with pump CL, ft
1,667	18.28	2.27	20.55	Not measured	Not Measured but other tests show depth = 7.5 ft	Not Measured but other tests show depth = 6.9 ft
1,834	18.48	2.74	21.22	20.26	Not Measured but other tests show depth = 7.9 ft	Not Measured but other tests show depth = 7.3 ft

Table 5. Effect of FPDO floor elevation on total energy and discharge profile with a floor located at el 11.75.

Q, cfs	Piezometer el	$V^2/2g$, ft	Total energy el	Top of jet el	Depth at back corner, ft	Depth at wall even with pump CL, ft
710	16.68	0.41	17.09	Not measured	4.5	4.1
950	17.1	0.74	17.85	17.7	5.3	4.7
1,200	17.7	1.17	18.87	18.4	6.3	5.5
1,490	18.31	1.81	20.12	19.4	7.1	6.5
1,667	18.57	2.27	20.84	20.1	7.5 ft	6.9 ft
1,834	18.82	2.74	21.56	20.75	7.9 ft	7.3 ft
1,834 repeat	18.72	2.74	21.46	Not measured	7.9	7.3

Table 6. Effect of FPDO floor elevation on total energy and discharge profile with a floor located at el even with lip.

Q, cfs	Piezometer el	$V^2/2g$, ft	Total energy el	Top of jet el	Depth at back corner, ft	Depth at wall even with pump CL, ft
1,667	20.46	2.27	22.73	22.1	6.9	6.8
1,834	20.69	2.74	23.43	22.55	7.3	7.1

Figure 21 shows the data from Tables 3-6 and a curve labeled “Lowest.” The Lowest curve was based on Lawrence and Braunworth (1906) assuming a fully aerated nappe of water out of a sharp crested vertical pipe that does not have an outlet chamber, shaft enclosure, or piers. The lowest curve represents the minimum total energy that can be expected with the pipe lip at el 14 with the following exception. Note that on the left side of the plot the data for the el 10 floor go below the Lowest curve. This could be the result of the flow in the outlet not having an aerated nappe that results in lower heads than a fully aerated nappe.

3.2.3 Effects of lip thickness

The initial test series in the preliminary 1:20.377-scale FPDO model not having the pump directly below the outlet chamber was conducted with a vertical pipe with no flare and a square lip having a scaled wall thickness of 6.7 in. The Type 7 Design in the Fairbanks Morse configuration had steel plate at the lip having a 1.0 in. thickness. The 1:20.377-scale model was tested with a lip having a scaled thickness of 1.3 in., which was about as close as could be obtained to the 1.0 in. actual thickness. The 1.3 in. thickness was achieved by grinding down the 6.7-in. thick lip. A schematic of these two lip configurations is shown in Figure 22. The 1.3 in. lip is also shown in the 1:20.377-scale model in Figure 23.

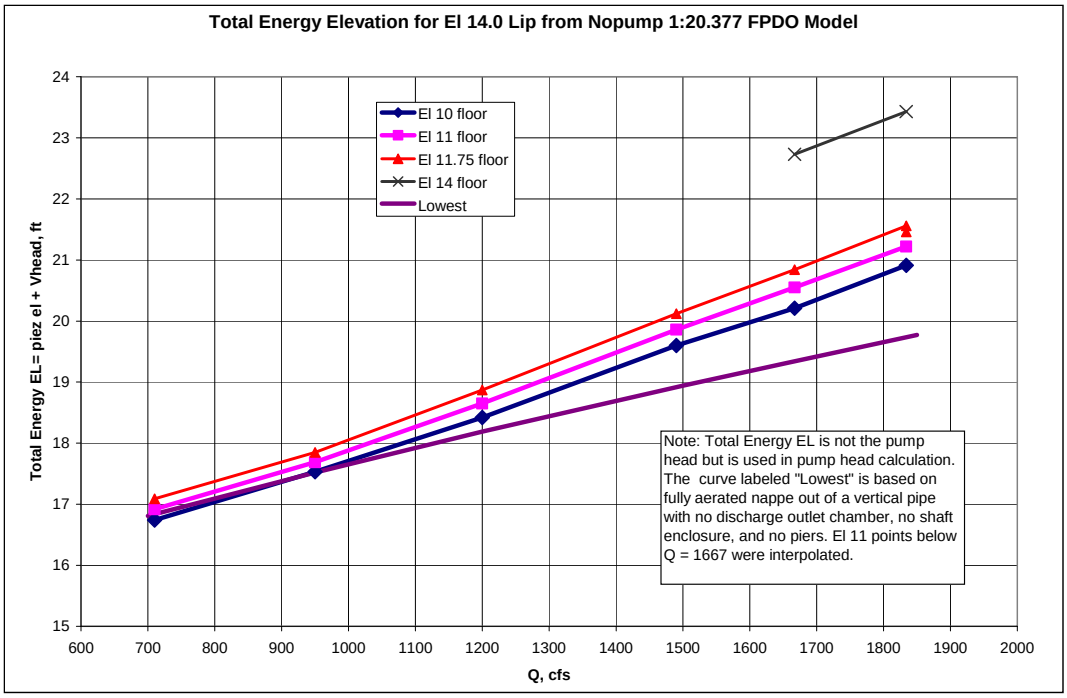

Figure 21. Effect of floor elevation on total energy elevation versus Q for FPDO. Based on the 1:20.377 preliminary model not having a pump immediately below the FPDO. Lip was square and 6.7-in.-wide for all floor elevations. No flare of the pump column.

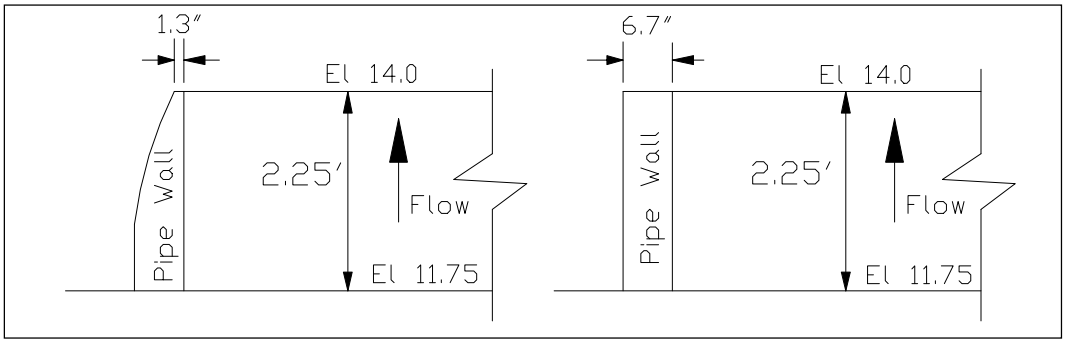

Figure 22. Schematic of two lip configurations tested in model.

Tests were also conducted with a 13.9-in.-wide-square-lip as shown in Figures 24 and 25 and a 13.9-in.-wide-rounded-lip shown in Figures 24 and 26. All lip tests were conducted with the floor at el 11.75. Results from the four lip designs are plotted in Figure 27. These results show that lip width and shape are important factors in the head on the pump. The thin lip having width of 1.3 in. resulted in the highest total energy. The 1.3-in. wide lip was the design closest to the 1.0-in.-wide-lip in the Type 7 Design. The 6.7-in. and 13.9-in.-wide-square-lip designs gave similar total energy. The 13.9-in. wide rounded lip resulted in the lowest total energy. At 1,834 cfs, the total energy for the 13.9-in.-wide-rounded-lip was about 0.6 ft below the curve for the 6.7-in. and 13.9-in.-wide-square-lip.

Figure 23. 1:20.377-scale preliminary model with 1.3 in. lip. The black material at base of pipe was a sealant used to close the gap between the chamber floor and pipe.

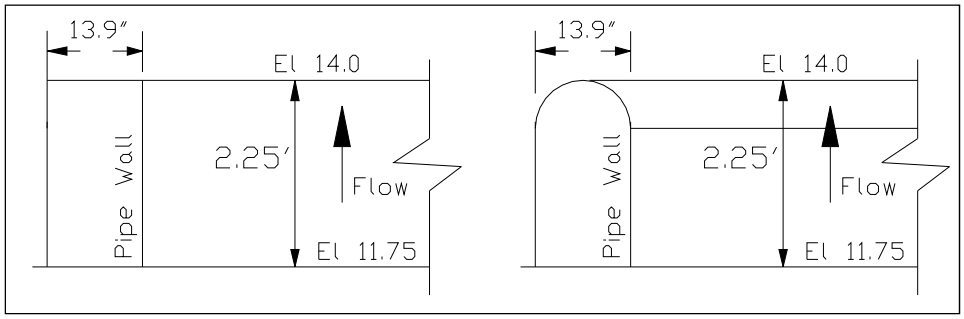

Figure 24. Square and rounded lip designs having width of 13.9 in.

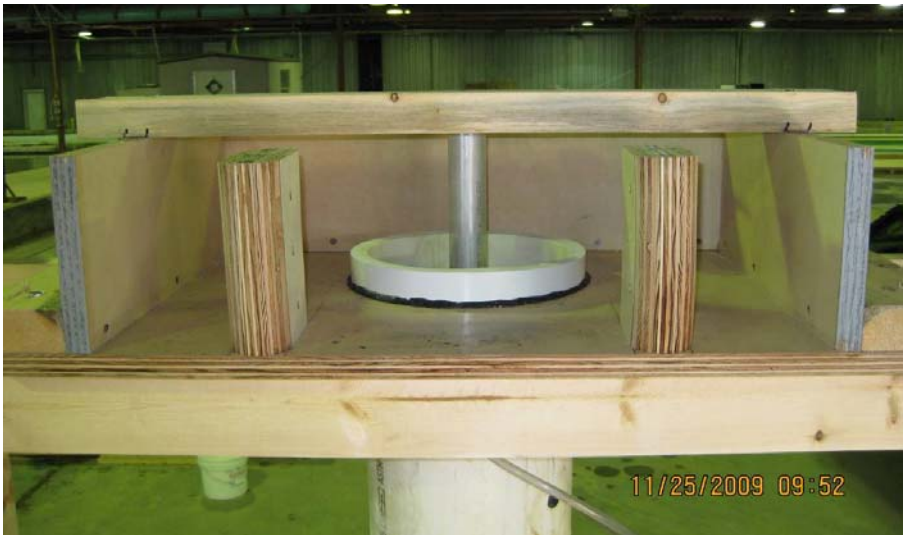

Figure 25. 13.9-in.-wide-square-lip with floor at el 11.75 in 1:20.377 preliminary model.

Figure 26. 13.9-in.-wide-rounded-lip with floor at el 11.75 in preliminary 1:20.377-scale model.

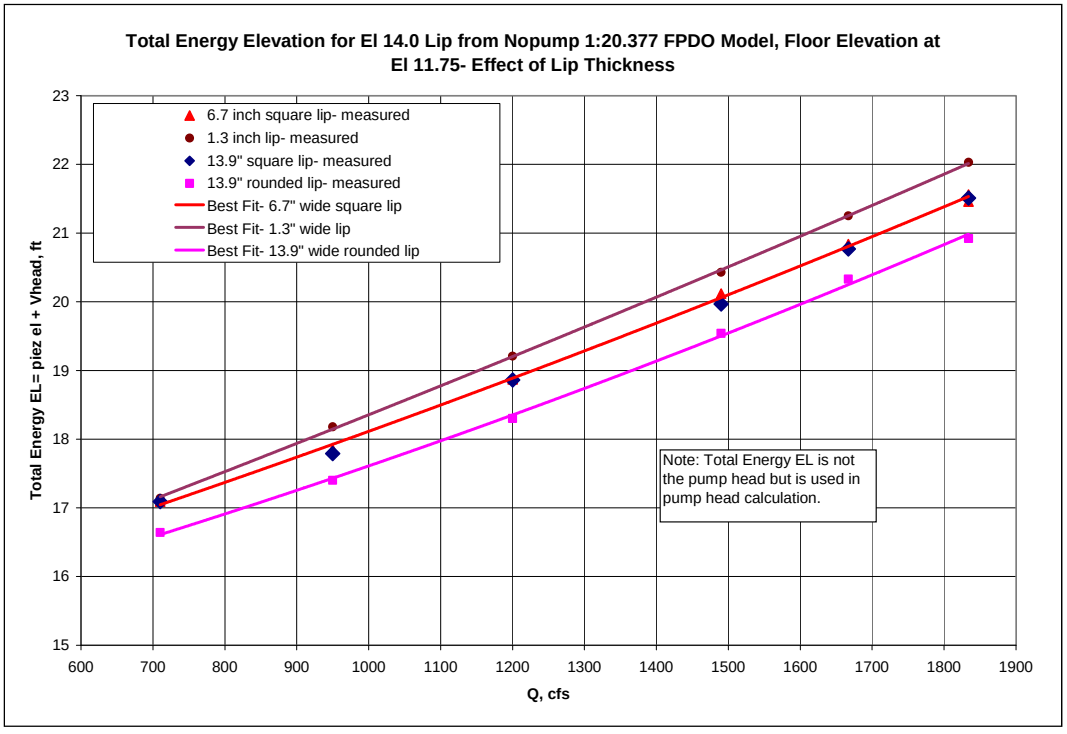

Figure 27. Effect of lip shape and thickness. All tests conducted with floor el 11.75. Tests in 1:20.377-scale preliminary model. No flare of the pump column.

The final tests in the preliminary model were conducted with a scale ratio of 1:19.25, semi-circular rounded lip at el 14, and floor elevation at el 11. The model scale was changed because it was the easiest way to construct the model of the additional lip designs that needed to be tested. These

tests were conducted in anticipation of the detailed Fairbanks Morse design that would have a flared pipe and outlet diameter of about 155.5 in. This preliminary model was built with straight pipe and an inside diameter of 154 in. The straight pipe with 154-in.-diameter was the ERDC's best estimate of how to model the flared pipe of 155.5-in. diameter so that the design team could develop a needed system curve to use in decision making. The detailed model containing flared pipe and all details was under construction during these final tests in the preliminary model. The resulting curves are shown in Figure 28 for the 13.1-in. and 19.3-in.-wide-rounded-lips from the 1:19.25-scale model and the 13.9-in.-wide-rounded-lip from the 1:20.377-scale model. Results comparing the 13.1-in.-wide and 13.9-in.-wide-lips (whose widths were essentially the same) showed that the change in opening diameter made a significant difference. The 13.1-in.-wide and 19.3-in.-wide-rounded-lips showed a small amount of improvement at low to intermediate flows of the wider lip. However, the wider lip resulted in water frequently splashing over the backwall, which was not seen with the narrower lip. This may be the result of the wider lip being too close to the backwall. An additional test was run to determine if the total energy head could be reduced by increasing the backwall distance by 4.0 ft. The test was run in the 1:19.25 model with the 19.3-in. wide lip. Although flow in the FPDO looked better because the flow depth was not as high on the backwall, no reduction in the total energy elevation was found with the increased backwall clearance.

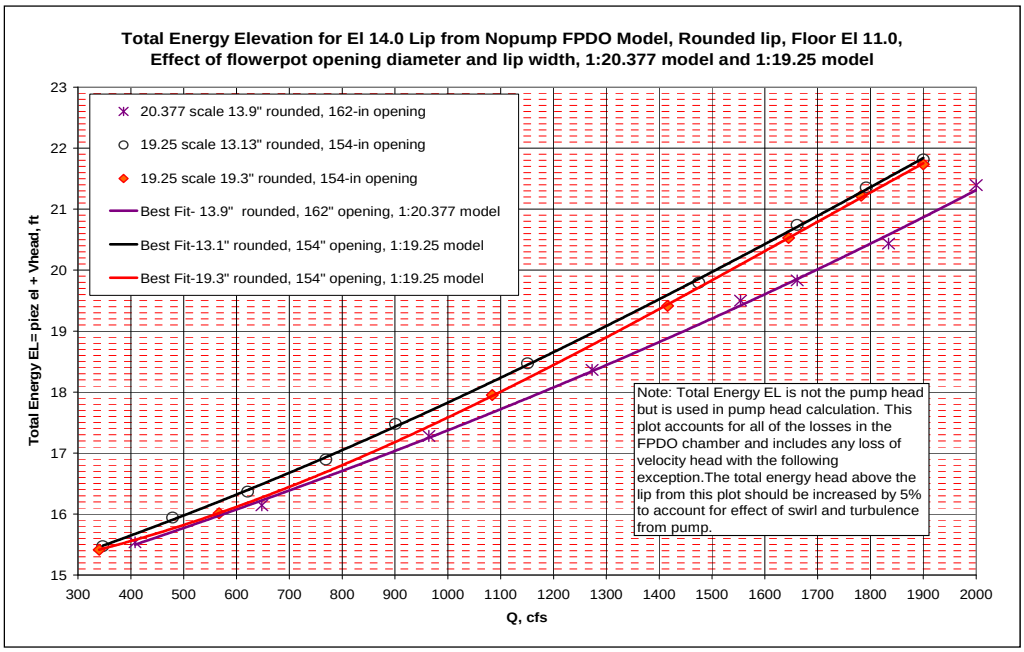

Figure 28. Total energy elevation for el 14 rounded lip, floor at el 11, effects of lip width and flowerpot opening diameter. Tests in 1:20.377-scale preliminary model. No flare of the pump column.

This concluded the tests in the preliminary FPDO model not having the pump immediately below the outlet chamber. At this point, the 13.1-in.-wide-rounded-lip curve with 154-in.-diameter opening represents the best estimate of the total energy in the actual FPDO for use in developing the system head curve.

3.3 Tests with detailed design of FPDO

In the Type 8 Design, shown in Figures 29 and 30, all details of the Fairbanks design above el 4.5 are incorporated into the model except for the enlargement of the shaft enclosure between el 4.5 and el 7, shown in Figure 2. The losses from this change in diameter in the shaft enclosure are already incorporated into the pump curve and were not included in the FPDO model. The 30 in. shaft was incorporated into the FPDO model because this shaft makes a difference in the nature of flow entering the FPDO. The floor was at el 11, the lip was at el 14, and the rounded lip had a 7-in. radius making it 14-in. wide. The pump column section and the upper part of the flowerpot section both had a 6.1-deg flare. Note that the junction between the flowerpot section and the pump column section had an offset of about 2.2 in. This offset was for placement and removal of the pump and pump column section while the flowerpot section remains in-place. The Type 8 Design was modeled at a scale ratio of 1:21.932. This allowed the use of a standard 6-in.-diameter PVC pipe for the straight pipe preceding the flared pump column. The Type 8 Design model is shown in Figures 31 and 32.

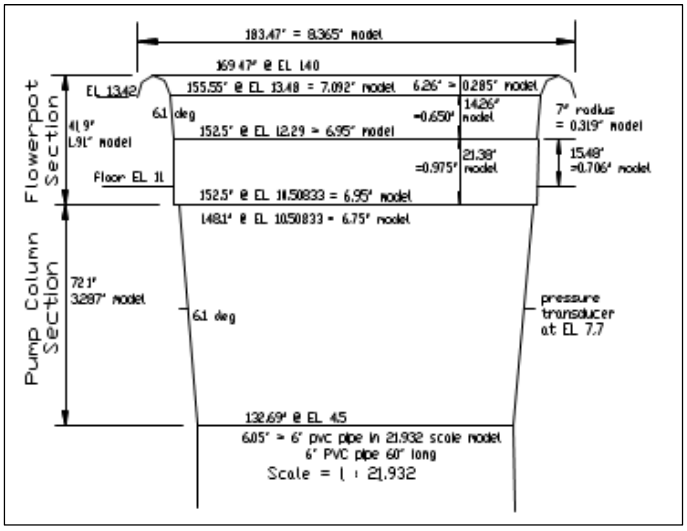

Figure 29. Type 8 Design FPDO.

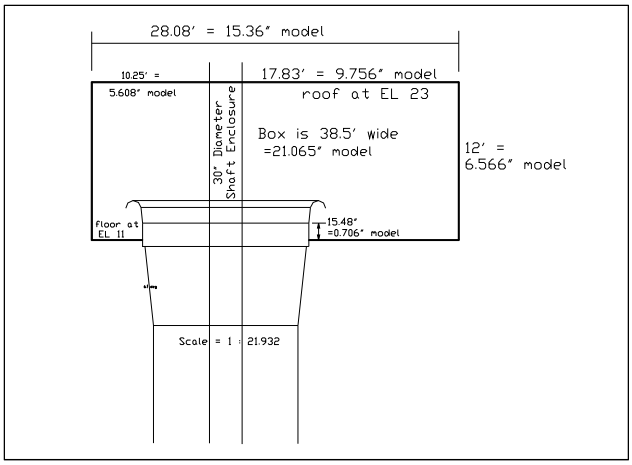

Figure 30. Type 8 Design with chamber dimensions.

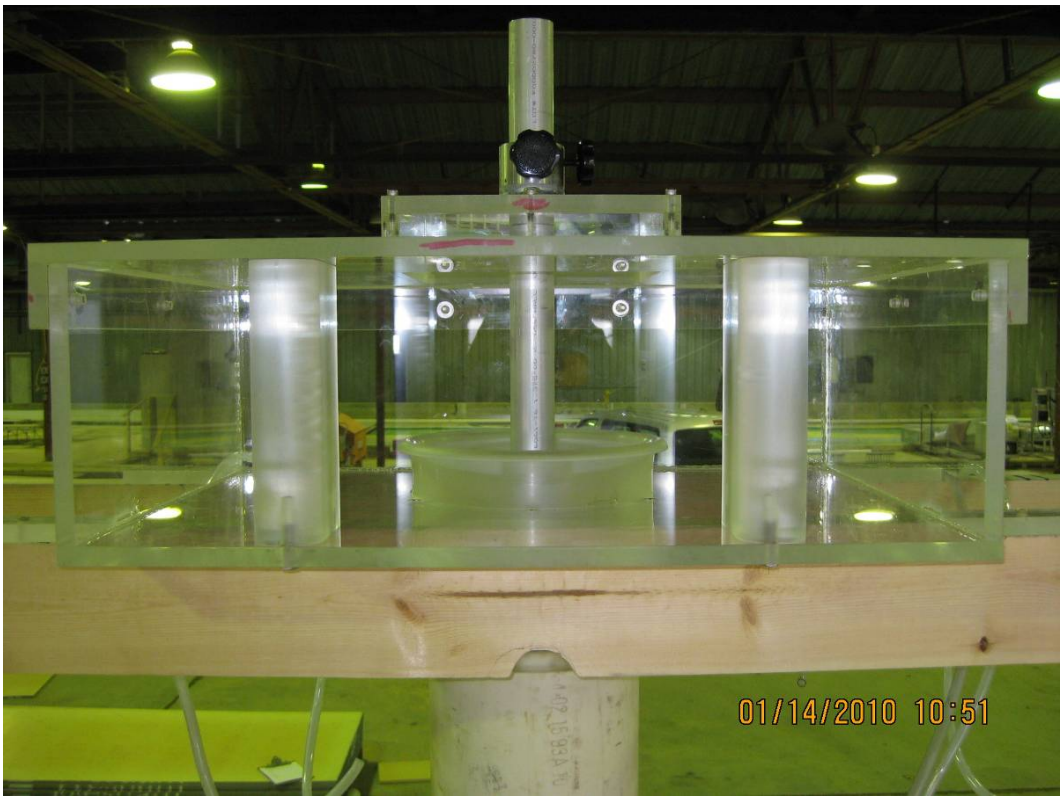

Figure 31. Front view of Type 8 Design 1:21.932-scale model.

In the 1:21.932-scale model, the Reynolds number in the pipe upstream of the flared pump column section of the FPDO at the design discharge of 1,740 cfs and 70 ^{0}F was 1.9 × 10^{5}, which was close to the desired R of 2 × 10^{5}. Based on Miller (1978), the loss coefficient in the flared pump column section will be about two percent greater than the highest Reynolds number tested.

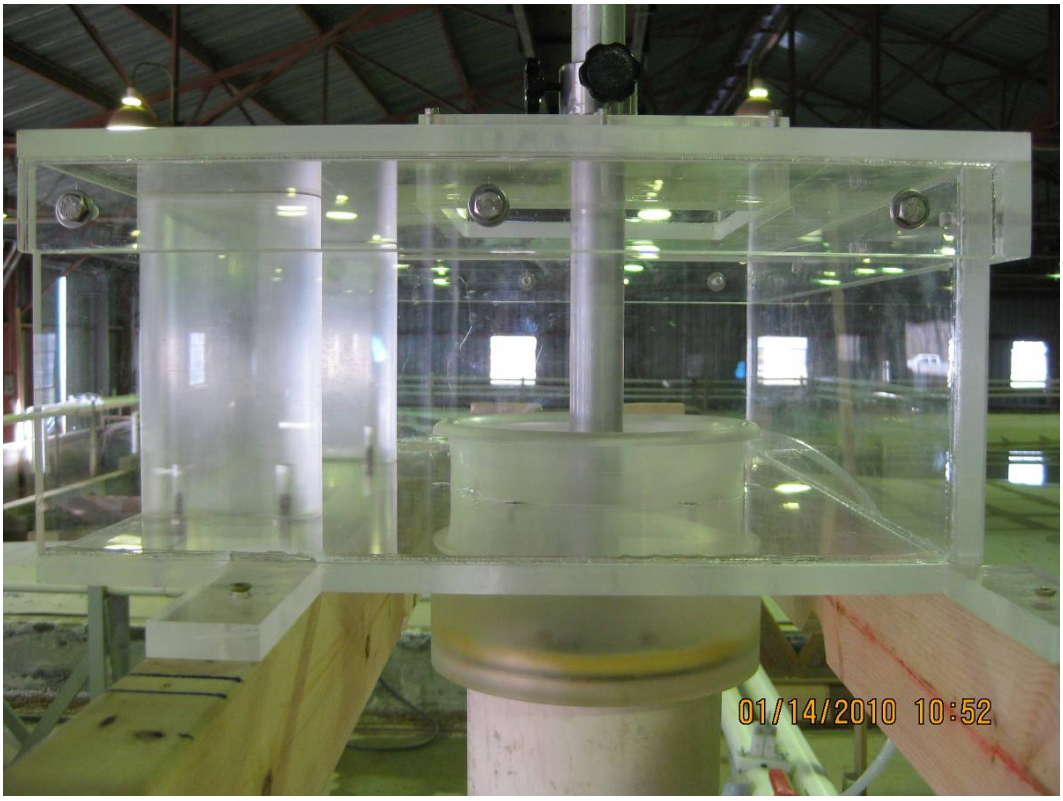

Figure 32. Side view of Type 8 Design 1:21.932-scale model.

Miller (1978) was discussed previously in this report regarding flow stability. The 6.1-deg flare of the pump column and flowerpot sections in the Type 8 Design fell into Miller's region of steady flow. This finding was important because the model was not trying to simulate flow conditions where unsteady separated flow could be expected.

Results from the Type 8 Design are shown in Figure 33 and Table 7. The curve from the preliminary model having the 13.1-in.-wide-rounded-lip and 154-in.-diameter opening is also shown. The best fit curve for the detailed Type 8 Design was based on all four replicates. The best fit curve from the Type 8 Design was up to 0.4 ft higher than the preliminary model. The data for the Type 8 Design were corrected for model scale effects that cause the friction losses to be greater in the model than in the prototype. The correction was not large and amounted to only 0.15 ft at a discharge of 1,740 cfs. Flow in the Type 8 Design is shown in Figures 34-37.

Dye was injected at various locations inside the flowerpot section to see if there was any indication of flow separation. None of the dye injection locations showed any indication of unstable flow in the pump column or flowerpot sections of the Type 8 Design.

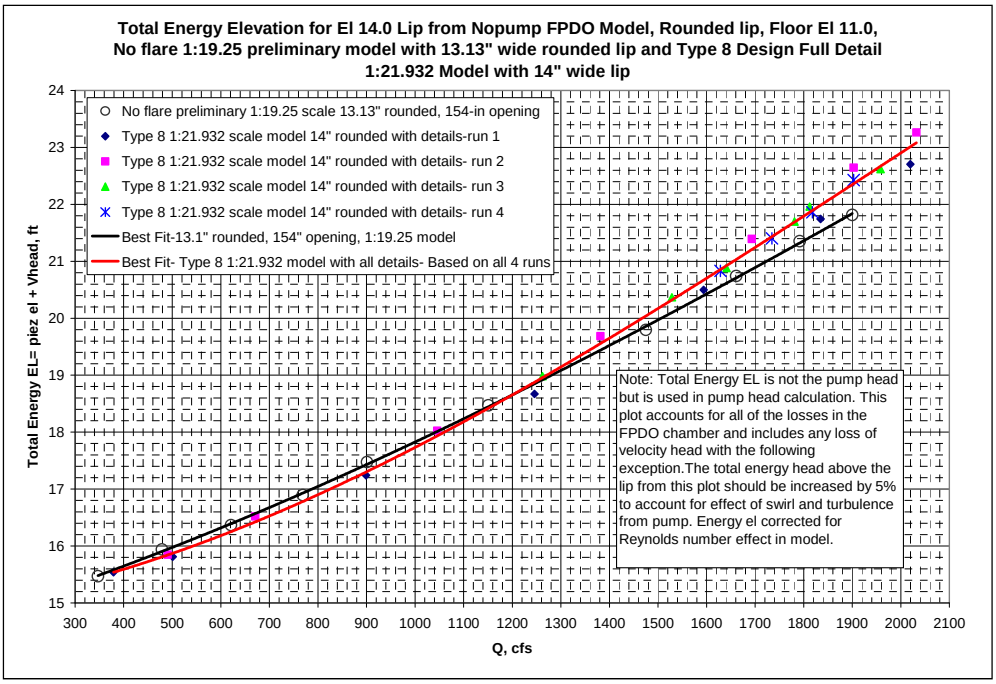

Figure 33. Results from Type 8 Design. Flared pump column in Type 8 Design.

Table 7. Test data from Type 8 Design.

Run	Q, cfs	Average Piezometer Head, el	V²/2g ft	Total Energy, el	Reynolds Number Correction, ft	Corrected Total Energy, el	Depth at Back Corner, ft	Depth at side wall at pump CL, ft
1	379	15.28	0.27	15.55	0.01	15.54	3.1	2.7
	501	15.36	0.47	15.83	0.02	15.81	3.5	3.2
	899	15.78	1.51	17.29	0.05	17.24	4.9	4.5
	1,246	15.85	2.91	18.75	0.08	18.67	6.0	5.5
	1,594	15.87	4.76	20.63	0.13	20.50	NM	NM
	1,835	15.61	6.30	21.91	0.16	21.75	7.9	7.1
	2,020	15.26	7.64	22.90	0.19	22.71	8.3	7.3
2	2,032	15.73	7.73	23.46	0.19	23.26	8.2	7.5
	1,903	16.04	6.78	22.82	0.17	22.64	8.0	7.0
	1,693	16.16	5.37	21.53	0.14	21.39	7.7	6.8
	1,382	16.21	3.57	19.78	0.10	19.69	6.9	6.0
	1,046	16.04	2.05	18.09	0.06	18.03	5.8	4.9
	671	15.70	0.84	16.55	0.03	16.52	4.3	3.8
	491	15.41	0.45	15.86	0.02	15.85	3.7	3.1
3	1,812	15.97	6.15	22.12	0.16	21.96	NM	NM
	1,641	15.97	5.04	21.02	0.13	20.88	NM	NM

Run	Q, cfs	Average Piezometer Head, el	$V^2/2g$ ft	Total Energy, el	Reynolds Number Correction, ft	Corrected Total Energy, el	Depth at Back Corner, ft	Depth at side wall at pump CL, ft
	1,958	15.62	7.18	22.80	0.18	22.62	NM	NM
	1,529	16.11	4.38	20.49	0.12	20.37	NM	NM
	1,262	16.08	2.98	19.07	0.08	18.98	NM	NM
	1,781	15.91	5.94	21.85	0.15	21.70	NM	NM
4	1,817	15.83	6.19	22.02	0.16	21.86	NM	NM
	1,903	15.82	6.78	22.60	0.17	22.43	NM	NM
	1,735	15.91	5.64	21.55	0.15	21.40	NM	NM
	1,629	16.00	4.97	20.96	0.13	20.83	NM	NM

NM = not measured

Figure 34. Rear view of Type 8 Design with 1,594 cfs.

Figure 35. Rear view of Type 8 Design with 1,834 cfs.

Figure 36. Side view of Type 8 Design with 1,693 cfs.

Figure 37. Side view of Type 8 Design with 1,902 cfs.

A pressure cell was installed at el 7.7 in the pump column section. The model was run at 1,740 cfs, which was the discharge for the design intake of el 2.0. The measured static head elevation is shown in Figure 38. The standard deviation was 0.27 ft and 0.28 ft for the two different locations of the pressure cell. This can be compared to Figures 8 and 9 where the standard deviation with an impeller pump having correct vanes was measured in the 1:15-scale model. Without any flare of the pump column, the standard deviation in Figure 8 was 0.43 ft. With a 9.7-deg flare, the standard deviation in Figure 9 was 0.8 ft.

Several tests were run to see if the total energy elevation could be reduced by changes to the Type 8 Design. In the Type 9 Design, an insert was made that eliminated the 2.2 in. offset between the flowerpot section and the pump column section, shown in Figure 29.

There was no significant difference between the total energy elevations in the Type 8 and Type 9 Designs. In the Type 10 Design, a skirt was added below the 7-in. radius to eliminate the cavity beneath the rounded lip and make the lip look more like the rounded lip tested in the preliminary model. There was no significant difference between the total energy elevations in

the Type 8 and Type 10 Designs. In the Type 11 Design, the piers were removed from the outlet chamber. There was no significant difference between the total energy elevations in the Type 8 and Type 11 Designs.

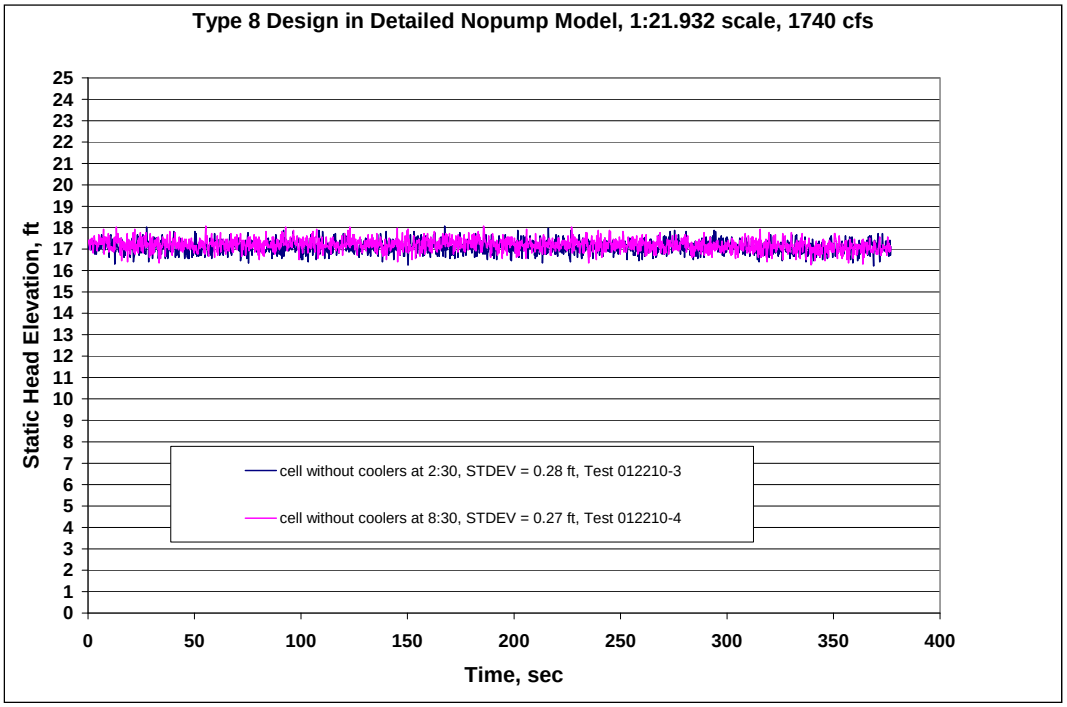

Figure 38. Type 8 Design, static head elevation in 6.1-deg flared section, pressure cell at el 7.7.

3.4 Adjustment in total energy to account for pump swirl and turbulence

Based on the magnitude of pressure fluctuations from the 1:15-scale model, having an impeller pump beneath the FPDO, in Figures 8 and 9, and the measurements in the detailed FPDO 1:21.932-scale model, in Figure 38, more turbulence and swirl would be present in the system with the pump immediately beneath the FPDO. This added swirl and turbulence could increase the head resulting from flow through the FPDO. There was not a rigorous basis for selecting the head increase but the diffuser was closest to the pump and likely to be most affected by the pump turbulence. Miller (1978) provides loss coefficient for diffusers downstream of pipe bends but not downstream of pumps. The most analogous situation found was in Miller (1978) for a diffuser having a thin boundary layer versus a thick boundary layer. Considering the pump column and flowerpot sections as being one diffuser, the area ratio was 1.37 and the length/inlet radius was 1.72. Based on these parameters, the loss coefficient for the thick boundary layer was about five percent greater than the loss coefficient for the thin

boundary layer. To account for the potential increase in loss through the FPDO, a five percent increase in the total energy above the el 14 outlet lip was recommended. For example, in the Type 8 Design, a discharge of 1,740 cfs had a total energy elevation of about 21.45. The total energy elevation of 21.45 results in 7.45 ft of total energy above the el 14 lip. A five percent increase results in 1.05 x 7.45 = 7.82 ft. The corresponding total energy elevation was 14 + 7.82 = 21.82 ft. This increase has not been added to any of the plots presented herein and was recommended for the design builder to make this increase in developing the system curve.

3.5 Calculation of pump head using total energy from model

As stated previously, the total energy elevation (TEE) plots presented herein were used in determining the system head loss curve to use in pump selection. The total pump head to develop the system curve was determined from:

$$\text{Total Head} = \text{TEE} + 0.05 \times (\text{TEE} - 14.0) + \text{other losses} - \text{intake el}$$

The other losses were defined by the design builder and result from the trash rack, FSI, contractions, and friction as follows:

- Approach channel to pump bay contraction loss = $0.6 \times (V_{bay}^2/2g - V_{approach}^2/2g)$;
- Trash Rack Loss = 0.21 ft;
- Friction loss in pump bay = $0.018 \times$ (length/hydraulic radius) $V_{bay}^2/2g$;
- Entrance loss at contracted section = $0.5 \times (V_{entrancetocontracted\ section}^2/2g)$;
- Gate slot loss = $0.2\ (V_{entrancetocontractedsection}^2/2g)$;
- Friction loss in contracted section = $0.0185 \times$ (length/hydraulic radius) $\times\ (V_{exitofcontractedsection}^2/2g)$;
- Contraction loss at end of contracted section = $0.3 \times (V_{beforeradius\ contraction}^2/2g - V_{exitofcontractedsection}^2/2g)$;
- Loss through FSI = $0.15 \times V_{FSIthroat}^2/2g$.

3.6 Bulking of flow due to air entrainment

Flow in the discharge outlet chamber was highly turbulent and entrained large quantities of air. Although the initial 1:15-scale model with the pump below the FPDO and the second 1:21.932-scale model were large models, both models entrained less air than would the full scale system. Flow in the full scale system would have more bulking of the flow due to greater air

entrainment. Flow in both models was examined to make certain that the water level in the outlet chamber was below the roof to insure the chamber does not confine the flow exiting the vertical pipe. These tests were conducted to insure that the chamber box was not close to flowing full to insure stable flow conditions in the outlet. Instability could occur if the box were to switch from flowing full to not flowing full. At the 1,800-1,825 cfs flows in the Type 6 and 7 Designs in the 1:15-scale model, the depth at the back corners was 8.25- to 8.4-ft. Depths were used rather than elevations because the Type 6 and 7 Designs had a floor at el 11.5. Note that the 1:15-scale model had excessive swirl and turbulence in the flow from the pump due to the vane issue. In the Type 8 Design in the 1:21.932-scale model at a similar discharge of 1,834 cfs, the depth in the back corners was 7.9 ft. At the side wall even with the centerline of the pump, the Type 8 Design in the 1:21.932-scale model at a discharge of 1,834 cfs had a depth of 7.1 ft. Considering that the box was 12-ft tall from roof to floor, depths from both models indicate a large margin of allowable bulking before the box will flow full.

4 Riprap Design for Downstream of the FPDO

4.1 General

Riprap stability tests were conducted on the downstream side of the pump station where the flowerpot discharge outlet (FPDO) discharges into the downstream tailwater (Figure 39). The floor of the FPDO was at el 11 and the exiting jet falls into tailwater, which can be as low as el -1.5 and as high as el 11. All riprap stability tests were conducted with the maximum discharge per pump of 1,815 cfs that occurs when the intake was at el 7. The jet falls through the tailwater onto a 40-ft-long concrete slab at el -18. The top of riprap was also at el -18. The unit discharge for the downstream channel was 1815/41.5 = 43.7 cfs/ft. The unit discharge leaving the FPDO was 1815/(38.5-6) = 55.8 cfs/ft. (The subtraction of 6.0 ft was because of the width of the two piers in the FPDO.) This was not a large unit discharge but the plunging nature of the jet and the lack of baffle blocks and/or an end sill may result in significant potential for excessive scour downstream of the structure. The objective of this portion of the study was to find the stable riprap size and required downstream length.

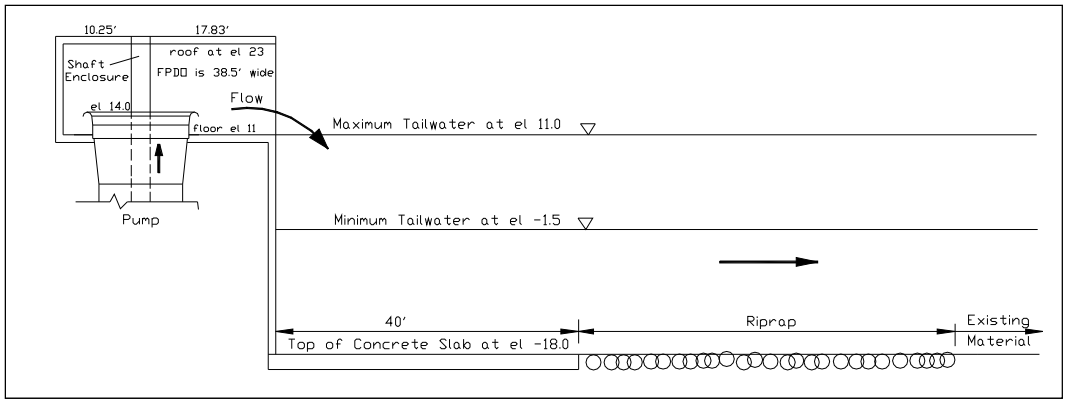

Figure 39. Schematic of FPDO and discharge area downstream of pump station.

4.2 Model description and scale effects

The model used for the riprap stability tests was the 1:15-scale model described previously that had the pump immediately below the FPDO. As stated previously, the inner flume width of 41.5 ft represents the correct width of the discharge channel for one pump. At all but the highest

tailwater, the FPDO had a plunging jet, which entrained significant quantities of air. Although the model used for the riprap tests was relatively large, models would generally entrain less quantities of air than the full size system. With less air in the model, the water-air mixture was denser in the model. Although the density increase was not large, the greater density should produce greater stress on the rock, therefore, making model results conservative. The amount of conservatism was unknown and may not be significant.

Tailwater in the inner flume was controlled by a series of equally spaced boards placed vertically to block a portion of the flow at the downstream end of the inner flume. To raise the tailwater, more boards were added with lesser spacing to increase loss through the boards. This design allowed flow to exit the inner flume over the full width and depth of the flume as opposed to an overflow tailwater control device where flow only exited at the water surface. This was important because the inner flume was not long enough to allow the use of an overflow tailwater control device.

4.3 Description of riprap gradations

Standard USACE gradations given in EM 1110-2-1601 (1994), "Hydraulic Design of Flood Control Channels", were used in the WCC project. Upper and lower gradation limits for 18-in. maximum stone size and 24-in. maximum stone size USACE gradations are shown in Figure 40 along with the gradations tested in the model. The gradations tested in the model were mixtures of several rock sizes from a sieving operation. The model riprap had a unit stone weight of 165 lbs/cu ft. The model gradations were mixed to follow the lower or minimum limit curve in the USACE standard gradations. The sizes from the sieving operation were converted to weight based on a sphere and a unit stone weight of 165 lbs/cu ft.

4.4 Test descriptions and results

The Type 1 Riprap Design used the 18-in. USACE gradation placed 25 ft downstream from the slab. The 18-in. maximum stone size gradation with unit stone weight of 165 lbs/cu ft had a minimum, median diameter D_{50}(min) = 0.88 ft. Tests were conducted at tailwater elevations of -1.5, 3.0, and 9.0. The 18-in. maximum size riprap placed to a thickness of 18 in. failed and exposed the underlying plywood base, as shown in Figure 41. The smooth, hard plywood base likely provides some conservatism to these results. Because failure occurred at the end of the slab, this test indicates

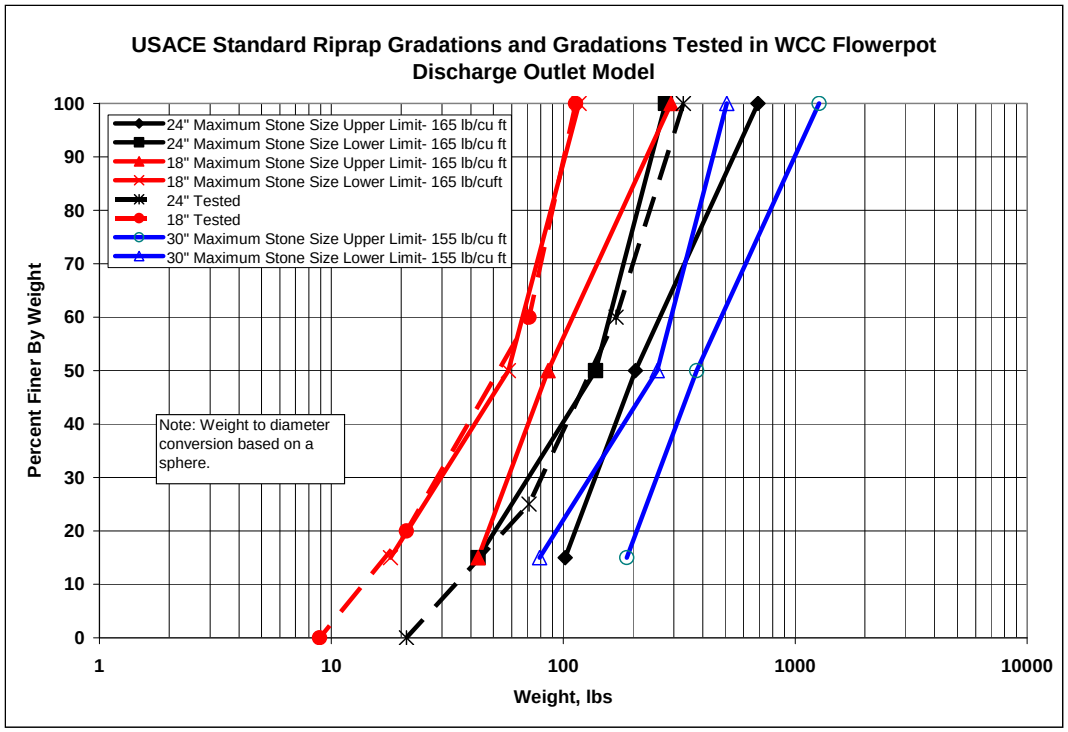

Figure 40. Gradation limits and gradations used in FPDO model.

Figure 41. Failure of Type 1 Riprap Design consisting of 18-in. maximum stone size gradation placed downstream of 40-ft concrete slab for a distance of 25-ft.

that the 18-in. riprap size was not adequate. Several alternatives were available to insure the stability of the downstream channel. First, baffle blocks and/or an end sill could be placed at the downstream end of the slab and the 18-in. riprap might be stable. Second, the concrete slab could be extended further downstream. Third, the riprap size could be increased. The District stated that increasing the riprap size would likely be the most cost effective solution.

The Type 2 Riprap Design used the 24-in. USACE gradation placed 25 ft downstream from the slab. The 24-in. maximum size riprap placed to a thickness of 24 in. was tested at a range of tailwater. Although minor movement of stones was seen with the 24-in. maximum stone size, the underlying plywood base was never exposed after more than 12.5 hr (model) of testing and was concluded to be stable. The remaining issue was the required distance downstream of the 24 in. riprap.

The Type 2 Riprap Design was tested with 25 ft of sand placed downstream of the riprap to a scaled depth of 7.5 in. Scour of the non-cohesive sand in the model could not be related to scour of the existing, far more complex, material in the WCC channel but was used as a qualitative indicator of scour potential. The model was run for 30 minutes at a tailwater el -1.5. The time-scale for converting scour time in the model to scour time in the prototype in a Froude model with sand used as a scour indicator was unknown. Sand scoured as shown in Figure 42. The plywood beneath the sand was exposed in similar locations as the riprap failure with the 18-in. riprap.

The Type 3 Riprap Design used the 24-in. USACE gradation placed 50 ft downstream from the slab. The Type 3 Riprap Design was tested with 25 ft of sand placed downstream of the 24-in. riprap to a scaled depth of 7.5 in. The model was run at tailwater el -1.5 until the scour pattern had similar total area of exposed plywood to the scour pattern from the Type 2 riprap. Similar scour pattern required two hours with the Type 3 Riprap Design and is shown in Figure 43. The scour with the Type 3 Riprap Design still showed significant lateral variations in scour.

The Type 4 Riprap Design used the 24-in. USACE gradation placed 75 ft downstream from the slab. The Type 4 Riprap Design was tested with 25 ft of sand placed downstream of the 24- in. riprap to a scaled depth of 7.5 in. The model was run at tailwater el -1.5 until the scour pattern had similar

Figure 42. Scour of sand downstream of Type 2 Riprap Design after 30 min of flow in model.

Figure 43. Scour of sand downstream of Type 3 Riprap Design after two hr in model.

total area of exposed plywood to the scour patterns from the Type 2 and Type 3 Riprap Designs. Similar scour pattern required eight hours in the model with the Type 4 Riprap Design and is shown in Figure 44. Although the amount of plywood base exposed was similar, the exposed areas were well downstream of the end of the riprap. The scour with the Type 4 Riprap Design had less lateral variation of scour.

Figure 44. Scour of sand downstream of Type 4 Riprap Design after eight hr in model.

4.5 Adjustment for unit stone weight

The riprap readily available to the New Orleans area had a unit stone weight of 155 lbs/cu ft. The tests were conducted using model rock having a unit weight of 165 lbs/cu ft. The gradation limits shown in Figure 40 from EM 1110-2-1601 (1994) for the 18-in. and 24-in. gradations were based on a unit stone weight of 165 lbs/cu ft. Converting results from one unit weight to another must be done using a stone size equation to account properly for the effects of unit weight on stone stability. The Isbash (1935) equation was the applicable equation. The equation for riprap size versus bottom velocity, V, in highly turbulent zones like downstream of the WCC pump station is:

$$V = 0.86\left[2g\left(\frac{\gamma_s - \gamma_w}{\gamma_w}\right)\right]^{1/2} (D_{50})^{1/2} \quad (1)$$

where g = gravitational constant, γ_s = unit weight of stone, and γ_w = unit weight of water. The 24-in. gradation determined during the model testing

had a minimum, median diameter D_{50}(min) = 1.17 ft. Substitution of D_{50}(min), γ_s = 165 lbs/cu ft, and γ_w = 62.4 lbs/cu ft into the equation was used to back-calculate a reference velocity of 9.57 ft/sec. Inserting this reference velocity and unit stone weight of 155 lbs/cu ft into the equation resulted in a D_{50}(min) of 1.30 ft. This D_{50}(min) and unit weight corresponded to a minimum, median riprap weight W_{50}(min) of 177 lbs. From EM 1110-2-1601 (1994), the gradation having a W_{50}(min) ≥ 177 lbs and γ_s = 155 lbs/cu ft was the 27-in. maximum stone size.

4.6 Velocity measurement and calculated stone size

A Pitot tube was installed in the model in an attempt to measure the bottom velocity and to use stone stability equations to calculate the riprap size. The Pitot tube was positioned 2.0 ft (prototype) above the concrete slab at the downstream end of the slab and the tailwater was set at el -1.5. The flow in the model (Figure 45) was so highly aerated that the Pitot tube would fill up with air immediately and a valid reading could not be obtained. A second method used a 2-in. (model) wide board placed down into the water at the downstream end of the slab to determine where the flow transitioned from the upstream directed roller in the upper part of the depth to the downstream directed submerged jet that was riding along the concrete slab. The transition point was at about 30 percent of the depth above the bottom. It was also apparent that the flow became stronger close to the slab and the flow was highly turbulent. Forces on the board varied significantly with time. As stated previously, the average unit discharge across the FPDO was 55.8 cfs/ft and across the 41.5 ft wide discharge channel was 43.7 cfs/ft. The riprap failure shown in Figure 41 indicates that the unit discharge was non-uniform across the 41.5 ft width. If the average of the two unit discharges above is assumed to occur in the lower 30 percent of the depth, the velocity in the bottom jet equals 10.1 ft/sec. Using Equation 1 and unit stone weight of 155 lbs/cu ft, the calculated D_{50}(min) was 1.45 ft, which was similar to the 1.30 ft determined from the model test results. This exercise was done as a check of the model test results.

4.7 Adjustment for 3-D effects

The model used herein was a model of one of the 11 FPDOs. Consideration must be given to the effects of how multiple outlets might affect the riprap requirements. Since the failure shown in Figure 41 occurred at the edges

Figure 45. Aeration and turbulence of flow in the 1:15-scale FPDO model.

of the flume, it was possible that two outlets operating next to each other could result in increased turbulence and more stress on the rock. Under another scenario, if the station was operated with less than all pumps on such as five or six pumps operating on the west side or five or six pumps operating on the east side, an eddy would form in the area where the pumps are not operating. This eddy would move flow along the down-stream face of the structure toward the operating pumps. This flow would have momentum and tend to contract the jet of the first operating pump that it ran into. Any lateral contraction of the jet would likely result in increased stress on the riprap. These effects of adjacent pump operation were felt to be small and the effects were addressed by increasing the velocity by five percent. The reference velocity becomes 10.05 ft/sec. The required D_{50} (min) for 155 lbs/cu ft was 1.43 ft. The corresponding W_{50} (min) was 238 lbs. From EM 1110-2-1601 (1994), the gradation having a

W_{50} (min) >= 238 lbs and 155 lbs/cu ft was the 30-in. maximum stone size gradation. The 30-in. maximum stone size gradation limits having unit weight of 155 lbs/cu ft are shown in Figure 40.

4.8 End protection

Although not tested, the downstream end of the riprap should be terminated with a thickened section to insure stability of the downstream end of the riprap. Figure 46 shows a thickened section that should allow at least 5 ft of scour at the downstream end of the riprap.

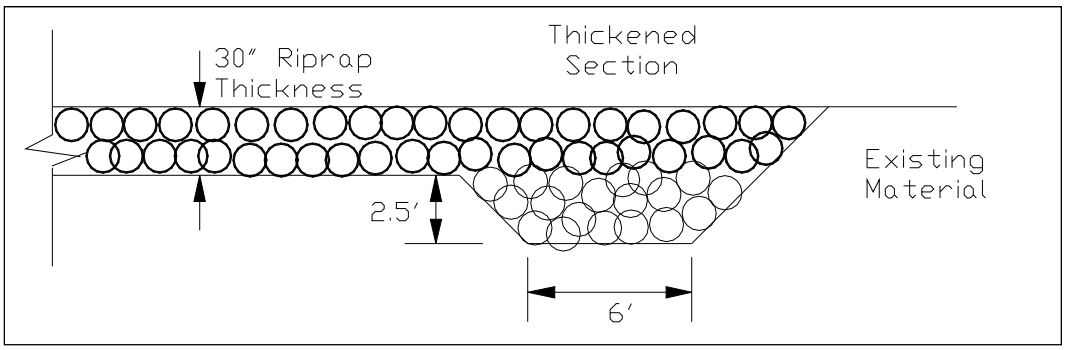

Figure 46. Thickened section of riprap recommended for both the upstream and downstream ends of the riprap protection.

While the 24-in. maximum stone size riprap in the model (increased to 30 in. due to unit weight and 3-D effects) was stable, the area just downstream of the slab was the primary point of possible instability that could cause problems to the structure if it were to fail. Riprap is not a uniform material and thus has the possibility of certain areas having primarily the small rocks in a gradation. The ERDC recommends that this possibility be handled by also using the thickened section at the upstream end of the riprap where it abuts the concrete slab. On the upstream end, the full 5 ft thickness of the thickened toe would abut the downstream face of the slab.

5 Keel Cooler Performance in the FPDO

5.1 General

Radiator type devices, called keel coolers, were used to keep the mechanical equipment cooled and were mounted where flowing water passes along and through the bars of the coolers. The intake bay of the pumps, inside the FPDO, and the downstream tailwater are three locations that were considered for placement of the keel coolers. The intake bay tests of the keel coolers are presented in the separate WCC pump intake report. The evaluation of the keel coolers inside the FPDO and in the tailwater locations are discussed herein.

5.2 Keel cooler tests in tailwater downstream of pump station

The initial design of the keel coolers was mounted on the downstream face as shown in Figure 47. Figure 47 also shows the trajectory of the jet leaving the FPDO for tailwaters lower than about el 9.8. Concern was expressed regarding the heat transfer environment at the pump station because of air entrainment in the water and if any dead zones would be present in which heat would not be removed away from the cooler. As stated previously, the models did not scale air bubble size and quantity correctly and the observations reported herein must take that into consideration.

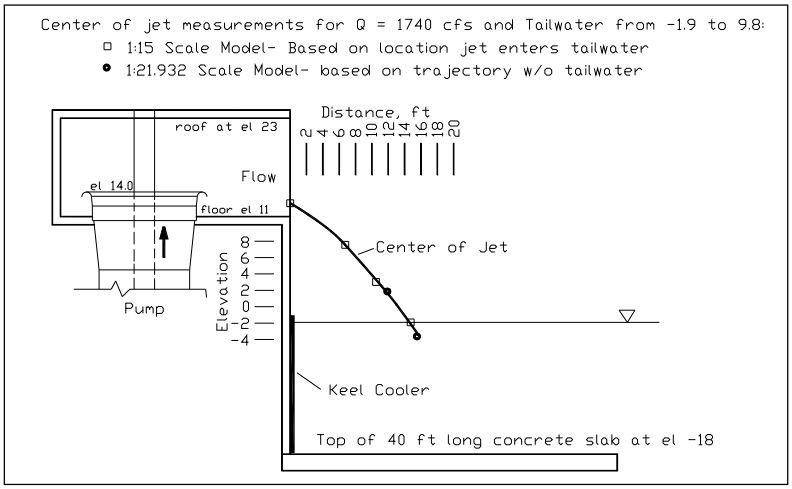

Figure 47. Initial design location of keel coolers and trajectory of jet leaving FPDO.

Figures 48 to 52 show the flow conditions in the 1:15-scale model for 1,815 cfs and tailwater elevations at el -1.5, el 2, el 5, el 8, and el 11, respectively. The primary difference between the various tailwater elevations was that the tailwater at el 11 resulted in the flow riding on the surface. In addition to high velocity at the surface, the downstream channel had significant wave activity at tailwater el 11. At the four lower tailwater elevations, the jet dove into the tailwater and the downstream wave activity was less.

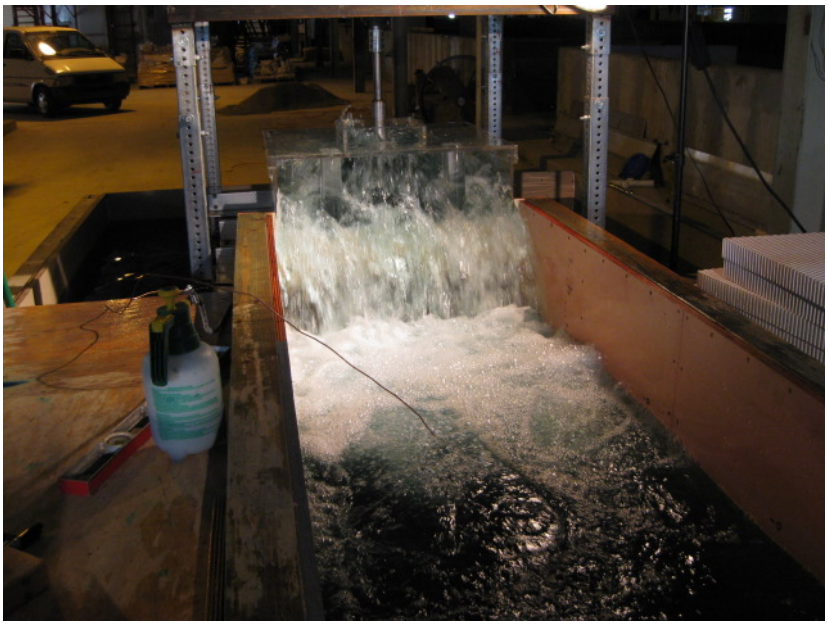

Figure 48. 1,815 cfs at tailwater el -1.5.

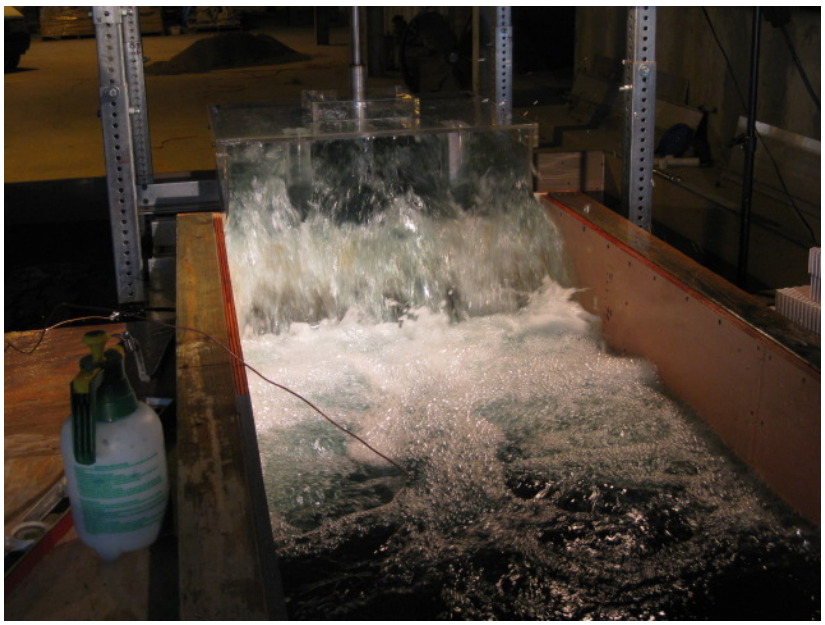

Figure 49. 1,815 cfs at tailwater el 2.

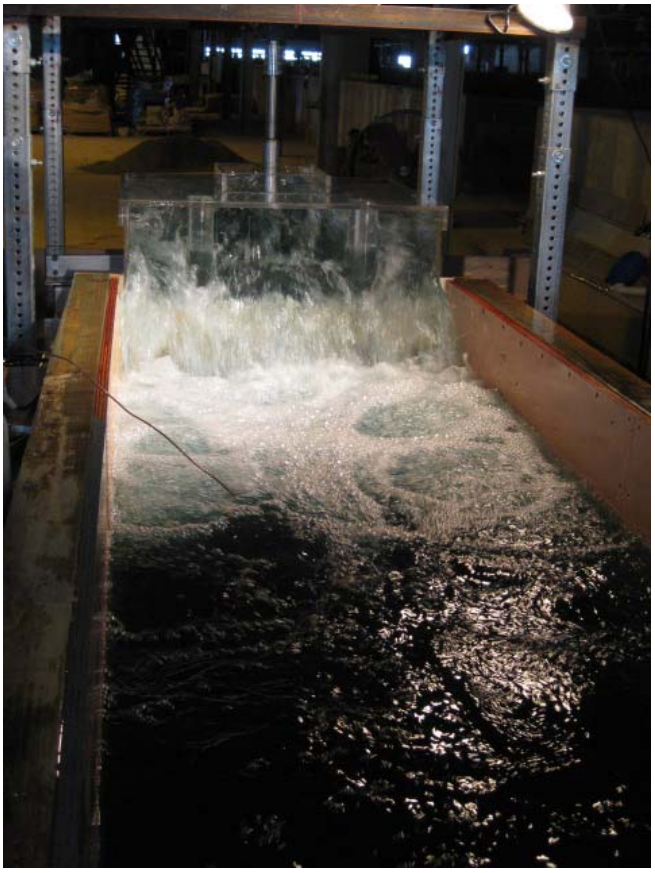

Figure 50. 1,815 cfs at tailwater el 5.

Figure 51. 1,815 cfs at tailwater el 8.

Figure 52. 1,815 cfs at tailwater el 11.

An underwater video camera was used to evaluate flow conditions near the downstream face of the pump station. At the downstream face of the pump station, the following observations were made concerning air entrainment next to and downstream of the downstream face of the pump station:

- At tailwater el 11, the jet riding on the surface resulted in almost no air bubbles near the vertical wall. Looking downstream from the vertical wall, the air bubbles in the falling jet only penetrated to about 8.0 ft above the slab.
- At a tailwater el 8, a portion of the diving jet rolled back upstream and carried bubbles near the wall. Occasionally a turbulent burst of the jet was found to bring bubbles all the way to the wall. Looking downstream from the vertical wall, the air bubbles in the falling jet only penetrated to about 5.0 ft above the slab.
- At a tailwater el 5, a portion of the diving jet rolled back upstream and carried bubbles near the wall. Occasionally, a turbulent burst of the jet was found to bring bubbles all the way to the wall. Looking downstream from the vertical wall, the air bubbles in the falling jet occasionally reached the slab.

- At a tailwater el 2, a portion of the diving jet rolled back upstream and carried bubbles near the wall. Occasionally a turbulent burst of the jet was found to bring bubbles all the way to the wall. Looking downstream from the vertical wall, the air bubbles in the falling jet frequently reached the slab.
- At a tailwater el -1.5, the flow pattern was similar to el 2, 5, and 8 but the frequency of occurrence and amount of air reaching the wall was greater, but not significantly greater. Looking downstream from the vertical wall, the air bubbles in the falling jet always reached the slab.

Velocities were measured by using a 1/8-in. diameter Pilot tube at the face of the keel coolers mounted on the vertical wall in the tailwater of the FPDO. The purpose of these velocity measurements was to insure adequate velocity magnitude to obtain heat dissipation in the keel coolers used for engines and gear drives in the pump station. Type 3224 keel coolers were used in the tests. The Type 3224 was 200-in. long by 22.3-in. wide by 2.5-in. deep. Type 3224 had 24 bars that are 0.5-in. thickness by 2.5-in. deep by 0.435-in. clear spacing. The loss coefficient (K) for flow through the full scale cooler was based on Osborn (1968). Osborn uses f = (flow area in rack)/(total cross section area) = 0.435/ (0.5+0.435) =0.465. Osborn investigated depth (d)/thickness (t) ratio from 1.0 to 6.0 and found loss coefficient for d/t from 3.0 to 6.0 to be constant. WCC keel coolers have bars with d/t = 5.0. Figure 7 in Osborn for f = 0.465 results in a loss coefficient K of about 3.0. According to the plot in Osborn (1968), Kirschmir (1926) gives K = 2.9. Based on the various sources, K = 3.0 was used to represent the cooler for perpendicular flow through the rack having square corners. The keel coolers have rounded corners having radius of 0.126 × bar thickness. The Hydraulic Design Criteria (HDC) chart number 010-7 (WES 1952) shows that slight rounding of the corners (amount not specified) reduced loss coefficient by about 14 percent for d/t = 10. The plot of the bar cross section of the slight rounding in the HDC chart shows more rounding than was present in the Louisiana Machinery bars. Papworth (1972) shows that full rounding (r = 0.5xt) of d/t = 5.0 bars reduced the loss coefficient by 24 percent. Using the radius to scale the amount of reduction from Papworth (1972) results in 24 percent times 0.126/0.5 = 6.0 percent reduction. Based on using the average of these two sources, the loss coefficient of 3.0 for square corners was reduced 10 percent to 2.7 for the slightly rounded corners. A loss coefficient K = 2.7 was the ERDC's best estimate of the K for perpendicular flow through the full scale coolers (angle = zero deg).

The model keel coolers needed to exhibit the same loss characteristics as the full scale coolers. This was difficult because almost all data on screens and bar racks were to flow through the rack at angles of less than 60 deg. Keel coolers have traditionally been used on ships where flow was along the length of the cooler. It was not possible to simply geometrically scale the bars and spacing of the coolers and expect the correct answer. If the coolers are scaled geometrically in the 1:15 scale model, the bars would be 1/30-in. thick and the spacing would be 1/34 in. Based on tests of screens, thicknesses, and spaces this small would have significantly more loss in the model than in the full scale for perpendicular flow at an angle of zero deg. Higher losses would also be expected for flow along the bars. In addition, geometrically scaled bars would be unacceptably flimsy. The model scale effects are generally dependent on the Reynolds number in the model. The information in the literature on effects of Reynolds number on loss coefficients is limited to screens and no information was found for Reynolds number effects on bar racks. If flow was normal to the racks, a screen could be substituted for the bar rack. For WCC, the desired flow orientation was parallel to the bars as opposed to perpendicular to the bars and a screen would not exhibit the correct loss characteristics. Based on Papworth (1972), screens in a model exhibit the same loss coefficient as the full scale if the percent open area was the same and if the model screen wire diameter and model velocity result in a large enough model Reynolds number. The 1:15-scale model had a Reynolds number based on bar thickness above this range for large enough bar thickness. The approach used herein was to use model bar racks having both correct open area and members large enough based on the circular wire screen information. In addition, the ratio of bar rack K to wire screen K was used to adjust the results. Based on the previous paragraph, the full scale cooler results in $K = 2.7$ for the 0.5 in. bars spaced at 0.435 in. at an approach velocity of 1.69 ft/sec (1.0 knot). Application of Idelchik (1986) wire screen equations for large Reynolds number to the full scale bar rack using equal open area/total area = 0.465 results in $K = 2.0$. Thus K from the wire screen equations have to be increased by 2.7/2.0 = 1.35 to equal the bar rack loss coefficient. The wire screen equations from Idelchik (1986) are relatively constant above $R = 600$ as are the Papworth (1972) equations. R was based on wire screen diameter and velocity through the rack as used above from Papworth (1972). Table 8 shows required spacing and Reynolds number for various sizes of bars.

Table 8 shows that a 3/32-in.-thick bar was the minimum thickness to exceed the $R = 600$ limit at the 1.0 knot full scale velocity. Nine of these bars at a spacing of 0.08 in. results in a keel cooler width close to the required width = (22 5/16 in. divided by 15 = 1.488 in.). The bars were

Table 8. Model rack for various bar sizes based on Papworth.

Bar thickness, in.	Space, in.	fraction blocked = S	Number of bars	Total model width, in.	R*	K x (1-S)²/S (K_{screen})	$K_{bar\ rack}$ = 1.35 x K_{screen}
1/16	0.054	0.5365	13	1.461	527	0.8 (2.00)	2.70
3/32	0.080	0.5396	9	1.484	796	0.8 (2.04)	2.75
1/8	0.108	0.5365	7	1.523	1054	0.8 (2.00)	2.70

*Papworth Reynolds number $R = V(through\ screen) \times Bar\ Thickness/v$

made 1/4 in. deep, resulting in an aspect ratio of 2.7. Idelchik (1986) shows little effect on K of aspect ratio of 2.7 used in the model versus an aspect ratio of 5.0 used in full scale. All of these calculations were for flow at zero deg (perpendicular) to the rack. The conclusions from these calculations are applied to racks having flow along the bars because no better information was found.

Figure 53 shows the Type 3224 keel cooler design tested in the 1:15-scale model. The model cooler was built using a water jet that cut slots in 1/4-in. thick steel. Rather than the 0.08-in. uniform spacing over the full depth of the bar, the water jet produced an opening of 0.09 in. on one side and 0.075 in. on the other side. This was felt to be adequate for the model coolers.

Figure 53. Keel cooler type 3224 used in 1:15-scale model.

The eleven Type 3224 keel coolers were mounted vertically on the wall below the FPDO. The coolers' bottom was at el -18 and top was at about

el -1.3. The coolers were mounted 10 in. from the vertical wall and 3.0 in. apart. Vertical velocities were measured 10 in. from the face of the coolers. Velocities were measured at the centerline of the FPDO along the middle cooler of the eleven coolers. Velocities were measured with a miniature propeller meter made by Nixon flowmeters. The propeller meter had a diameter of 0.46 in. (model dimension). Figure 54 shows the velocity meter in the 1:15-scale model with the eleven keel coolers.

Figure 54. 1:15-scale model with 11 type 3224 coolers and Nixon velocity meter looking upstream.

The Nixon meter is subject to debris collecting around the shaft, which can affect the readings. The meter was cleaned of debris and a check of calibration was conducted. The calibration was conducted in a separate flume with discharge measured with a Venturi meter, fine screens to produce a uniform velocity distribution, measured flume depth and width, and short distance from screen to measurement to result in minimal boundary layer growth. The calibration check and the factory curve are shown in Figure 55 and the factory curve was accepted as being valid.

The Nixon meter only provides velocity magnitude and flow direction must be determined by some other method. The Nixon meter can average measured frequency of revolution of the rotor in Hz over 1.0 sec or over 10 sec duration. Frequency of revolution of the rotor was measured for six 10 sec durations and they were averaged.

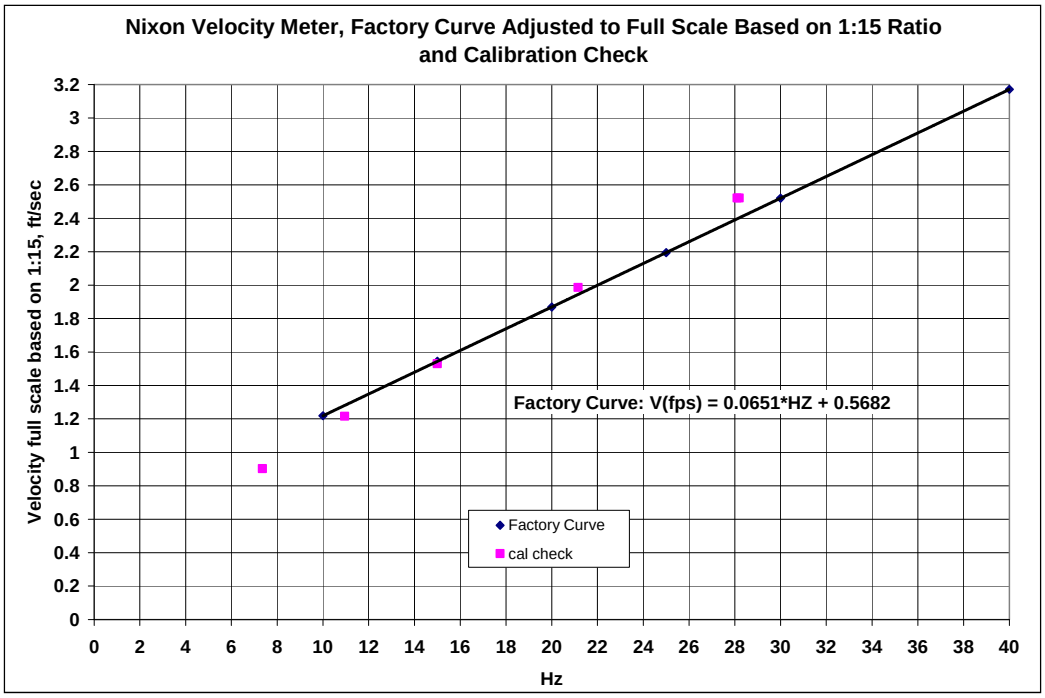

Figure 55. Check of calibration of Nixon velocity meter.

Tailwater at the FPDO varies from a minimum of -1.9 to a maximum of 11, which was the elevation of the floor of the FPDO. At the highest tailwaters, flow rides along the surface. At lower tailwaters, the jet leaving the FPDO dives into the tailwater. Tests were conducted to determine the tailwater at which the breakpoint occurs between the diving and surface flow conditions. It should be noted that finding a breakpoint separating two different flow regimes is a rigorous test of any model. The 1:15-scale FPDO model was large and was the best tool to make this determination. Tests were conducted using a discharge of 1,740 cfs. The test started with a tailwater of el 8 and the diving jet mode was present. The tailwater was increased to about el 9.2 and after 10 minutes in model time, the diving mode persisted. The tailwater was increased to about el 9.8 and after about three minutes (model time) of the diving mode, the model switched to the surface jet condition. With the tailwater at el 9.8, the jet stayed in the surface flow condition for about 10 minutes and never switched back to the diving mode. During this time, velocities were measured. Several other factors could affect the tailwater at which the breakpoint occurs including adjacent pumps operating or not operating and the presence of waves in the discharge channel.

One factor that can affect a free overfall like the FPDO was the aeration of the nappe. If air cannot get below the falling jet, the jet trajectory and

stability will be affected. The FPDO could get air from the 3-ft space between adjacent bays of the outlet. In addition, the area downstream of the two piers in the FPDO was another source of aeration. If adjacent pump bays are not operating, the nappe was easily aerated from each side. If all pumps are operating, the downstream end walls on each side of the pump station preclude significant aeration from the ends. The 1:15-scale model can only get air from the 3-ft side gap between FPDOs and downstream of the two piers inside the FPDO. Measurements were made of the pressure below the nappe using a piezometer inverted into a "U". The manometer showed a reduced pressure under the nappe of about 0.02 in. in the model, which would correspond to a reduced pressure of about 0.3 in. full scale. The difference was so small in the model that any lesser reading would have been recorded as zero. The magnitude of reduced pressure under the nappe was not believed to be significant because a test was run with a plate on one side of the FPDO to deflect the jet to provide a large area for air to reach the underside of the nappe. The trajectory and stability of the nappe on the other side of the model were unchanged indicating the FPDO responds like a fully aerated nappe.

Vertical velocity magnitude along the face of the keel coolers is plotted in Figures 56, 57, and 58 for low tailwater with diving flow, intermediate tailwater with diving flow, and high tailwater with surface flow, respectively. The velocities were presented in knots because this type of keel cooler is typically used on a ship hull and were stated to need a 1 knot current. Based on an underwater camera of confetti, dye, and a string mounted on a stiff wire showed that the flow direction was up with two exceptions where the direction was variable. At the lowest tailwater of el -1.9 and at the velocity reading near the water surface, dye, confetti, and string in this area showed variable flow direction. At the highest tailwater of el 11, flow in the corner of the slab at el -18 and the vertical wall was variable in direction. Vertically upward flow could be assumed at all other locations.

All six velocities, over the length of the cooler, were averaged for each tailwater and are shown in Table 9. Velocity magnitude ranged from 0.68 to 1.28 knots and was less than 1.0 knot for all but two of the tailwaters tested. The highest tailwaters where flow rides along the surface had the lowest average velocities.

The next tests with the keel coolers in the downstream tailwater were conducted to examine alternate positions of the coolers in the tailwater. All tests were conducted at a discharge of 1,740 cfs and tailwater at el -1.9.

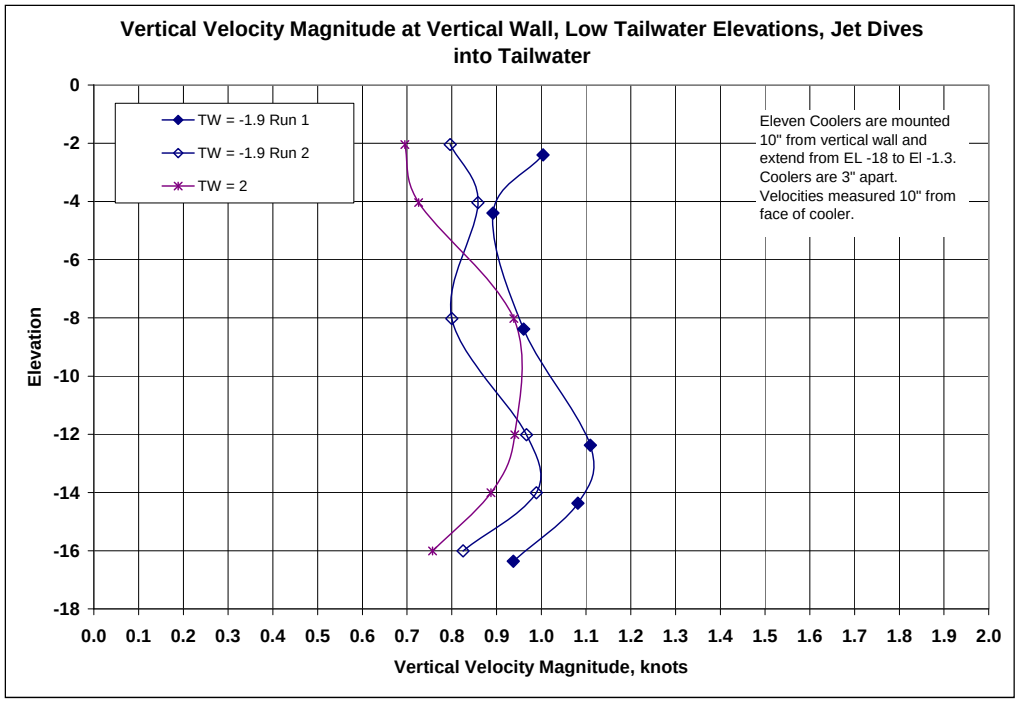

Figure 56. Vertical velocity magnitude along coolers for lowest tailwaters at EL -1.9 and el 2.0 having diving flow.

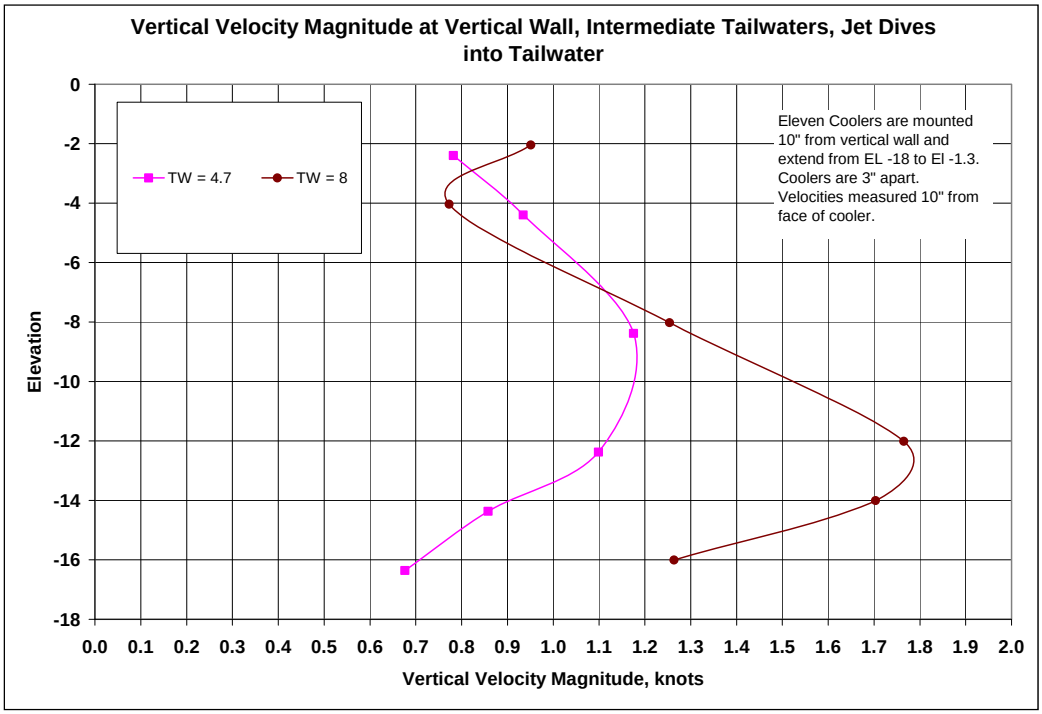

Figure 57. Vertical velocity magnitude along coolers for intermediate tailwaters at el 4.7 and el 8.0 having diving flow.

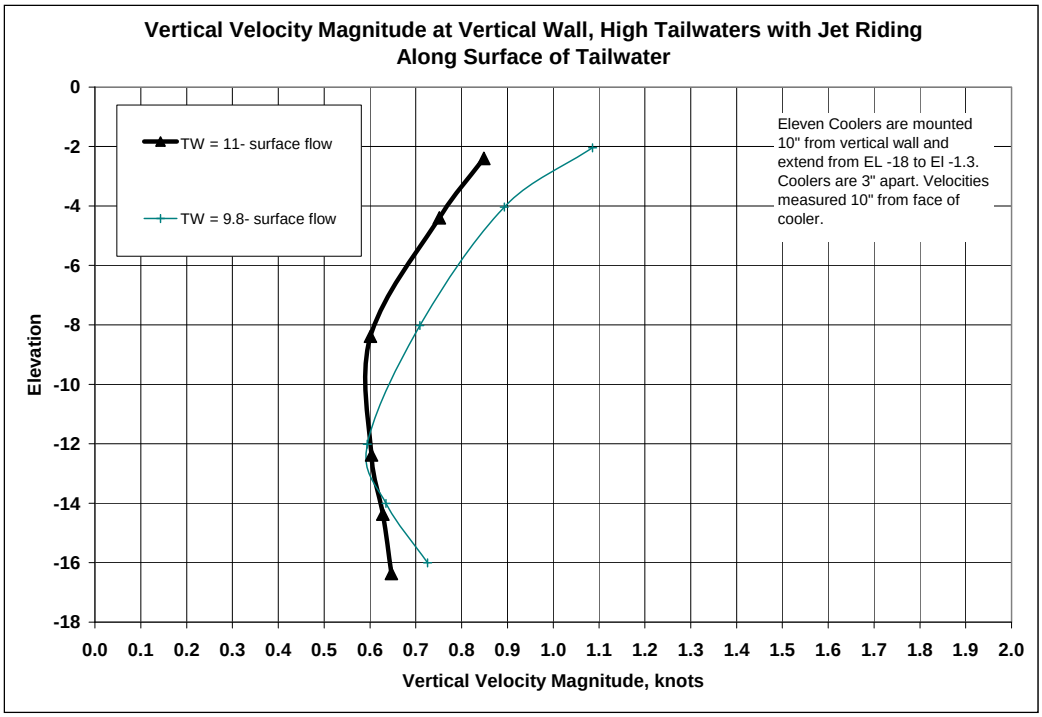

Figure 58. Vertical velocity magnitude along coolers for high tailwaters at el 9.8 and el 11.0 having surface flow.

Table 9. Average velocity over length of cooler. Note that two runs were made for the lowest tailwater elevation.

Tailwater elevation at	Average velocity over length of cooler, knots
-1.9 Run 1	1.0
-1.9 Run 2	0.87
2	0.82
4.7	0.92
8	1.28
9.8	0.77
11	0.68

These tests were intended to examine the feasibility of different design concepts and were not a comprehensive evaluation over a full range of operating conditions.

In the first phase of testing alternate keel cooler locations, the coolers were laid flat on the floor as shown in Figure 59. The upstream end of the coolers was 12 in. downstream of the vertical wall. The coolers were placed against the glass sidewall of the flume to allow viewing of the cooler relative to the plunging jet. The downstream quarter of the keel coolers was subjected to

Figure 59. Keel coolers laid flat on floor. Five coolers were placed adjacent to the glass sidewall to allow viewing in the model.

the zone of large fluctuations on the upstream side of the plunging jet. This area had large air concentration and therefore velocity measurement would have been difficult. Unless a significant research effort was conducted, it was unknown how the forces on the keel cooler would be quantified for design purposes in this highly turbulent zone.

The next phase of testing was the option with sloped keel coolers in the tailwater. By sloping the coolers, the downstream ends of the coolers were farther away from the high turbulence on the upstream side of the plunging jet. The downstream end of the coolers was about 11.5 ft from the vertical wall in the sloped design compared to about 17.6 ft in the design with the coolers lying flat on the slab at el -18. Top of coolers was at el-3.

The air bubbles in the model are relatively larger and rise quicker than air bubbles in the full scale. Even with the coolers further upstream, some of the air reached the sloped coolers, but turbulence was far less. Figures 60 and 61 show the initial sloped design with eleven Type 3224 coolers spaced at 1.0 ft apart at a 39-deg angle relative to vertical. The lower ends of the coolers were 2.0 ft above the concrete slab. A 45-deg slope wedge was placed below the coolers to direct flow along the coolers. An underwater camera was used to observe dye injections. Flow came around the sides of the cooler array and passed upward through the coolers rather than the desired motion of moving along the cooler. This was not considered acceptable because debris could become trapped beneath the cooler, which could reduce heat transfer and be difficult to clean.

Figure 60. View looking upstream at eleven Type 3224 keel coolers placed 1.0 ft apart.

Figure 61. Side view of eleven Type 3224 keel coolers placed 1.0 ft apart.

In the next sloped keel cooler design, the coolers were moved adjacent to each other with about a 2.0 in. (full scale) spacing between coolers. This design also included the 45-deg bottom wedge. As with the initial sloped cooler design, flow entered the sides and came up through the rack. This design was considered unacceptable because debris could become trapped on the underside of the coolers.

In an attempt to promote flow along the coolers, the coolers were kept at the 2.0-in. spacing with bottom wedge and the sides were closed with a sheet of Plexiglas to prevent flow from entering the sides as shown in Figure 62. Dye injections showed that the lower half of the rack had flow going up through the rack in a downstream direction and the upper half of the rack had flow going down into the rack in an upstream direction. This design had the advantage of flow coming up through the rack on the bottom that would have passed through the rack on the top half and have much less debris to become trapped on the underside of the coolers. However, this design did not achieve the desired flow along the coolers and the possibility of debris becoming trapped under the coolers was still a concern.

Figure 62. View looking upstream at eleven Type 3224 coolers spaced at 2.0 in. with bottom wedge and sides closed with a Plexiglas sheet.

In the last sloped cooler design, a plate was installed on the bottom side and parallel to the coolers to replicate the hull of a ship in the traditional use of keel coolers. The gap between the bottom plate and the coolers was 12 in. and coolers were spaced 4 in. apart. The plate was extended to the floor and leaned up against the vertical wall. The bottom of the cooler was 18 in. above the concrete slab. This allowed flow to go between the plate and the cooler as well as above the cooler. Figures 63 and 64 show the bottom plate design. Dye injections showed the design promoted flow along the coolers. Flow was along the coolers both between the coolers and above the coolers. Flow was along the cooler in an upward direction from the bottom of the cooler to about 2/3 to 3/4 of the length of the cooler where it turned and came out of the cooler. Flow was along the cooler in a downward direction from the top of the cooler to about 1/3 to 1/4 of the length of the cooler where it turned and came out of the cooler. Figure 65 shows a schematic of the flow patterns along and through the cooler. While this design showed improved flow patterns, any debris entering at the bottom opening or the top opening between the plate and the cooler could become trapped on the bottom side of the cooler.

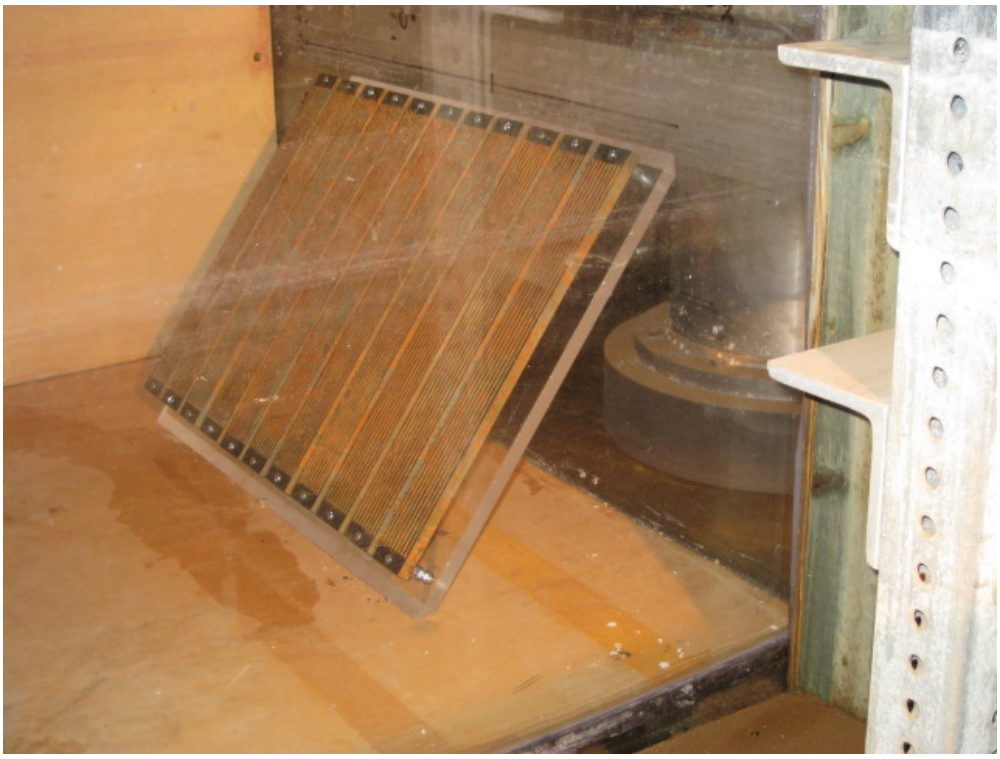

Figure 63. Side view of sloped keel coolers with bottom plate.

Figure 64. View looking upstream of sloped keel coolers with bottom plate.

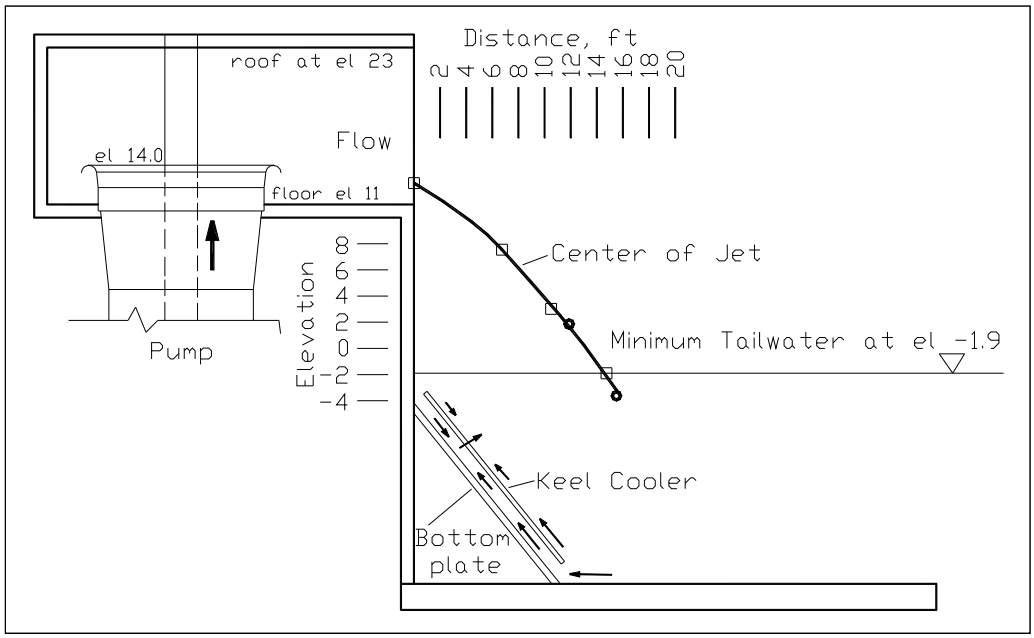

Figure 65. Schematic of flow patterns with sloped keel cooler having bottom plate.

6 Keel Cooler Tests Inside the FPDO

6.1 General

Three issues were evaluated with keel coolers placed inside the FPDO. First, the coolers could not increase the pump head enough to reduce the discharge from the pump significantly. Second, the velocity past the coolers had to be high enough to transfer heat away from the coolers. Third, the coolers had to be able to withstand the dynamic forces from the flow in the FPDO. Each of these three issues was addressed by testing in the 1:21.932-scale FPDO model used previously to determine head on the discharge side of the pump.

6.2 Pump head increase with coolers in FPDO

Tests were conducted in the 1:21.932-scale model of the FPDO to determine if the proposed keel coolers had an effect on pump discharge head and flow stability. The eleven coolers were placed on the backwall and floor of the FPDO, as shown in Figures 66 and 67, respectively.

The model keel coolers were designed and built to minimize scale effects that could result if model openings and bars were too small, resulting in losses and loss coefficients in the model that were too large as discussed in a previous section. Some of the details were repeated in this section because different model coolers had to be used in the 1:21.932-scale model but the design principles were the same. The full-scale keel coolers had 24 bars that are 0.5 in. wide, 2.5 in. deep, and 0.435 in. clear spacing. Based on analysis of bar rack data, the loss coefficient for flow through the full scale cooler was $K = 2.7$. Geometric scaling of the bars from full-scale to model would have resulted in bars that were 0.5 in./21.932 = 0.023 in. thick. This thickness would have been too weak for stability in the model. In addition, the spacing would have been 0.435 in./21.932 = 0.020 in. The Reynolds number effect data on screens (Papworth 1972) show that the 0.023 in. bar thickness and 0.020 in. spacing in the model would result in a larger loss coefficient than in the full scale. Based on the screen loss data, the model coolers were built with seven bars 0.084-in. thick having a spacing of 0.073 in. The percent open area was the same in model and full scale. The fewer and relatively larger bars and spacing along with the equal percent open area resulted in similar loss coefficient in model and prototype. This scale effect analysis was based on flow through the cooler because no literature was found for flow along the cooler. Figure 68 shows the model coolers and grate in the 1:21.932-scale model.

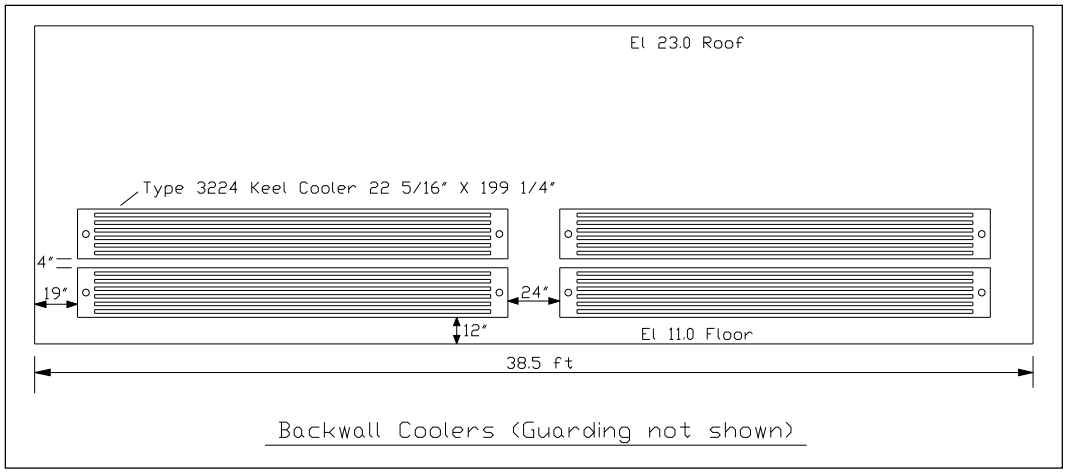

Figure 66a. View of backwall keel coolers looking upstream.

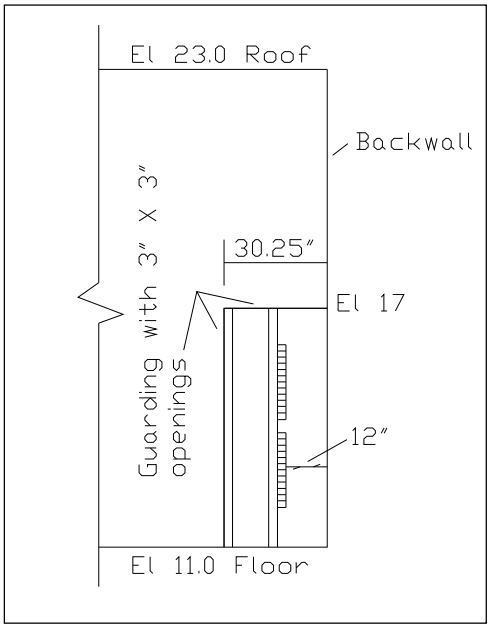

Figure 66b. Side view of backwall keel coolers.

The coolers were protected with a grate having 3.0 in. by 3.0 in. openings. The full scale grate was constructed of 1.5-in.-wide by 1/4-in.-thick stainless steel bars running parallel to the bars in the coolers and 3/8-in.-diameter stainless steel rods running perpendicular to the bars of the coolers. The full scale grate was 8.0 in. above the top of the floor coolers and 15.5 in. from the downstream face of the backwall coolers. The amount of open area in the full scale grate was about 79 percent. The full-scale grate had the 1.5-in.-wide by 1/4-in.-thick bars running about parallel with the flow direction based on dye injections. The primary blockage was the 3/8-in.-diameter rods that are perpendicular to the flow. This fact was critical to the design of

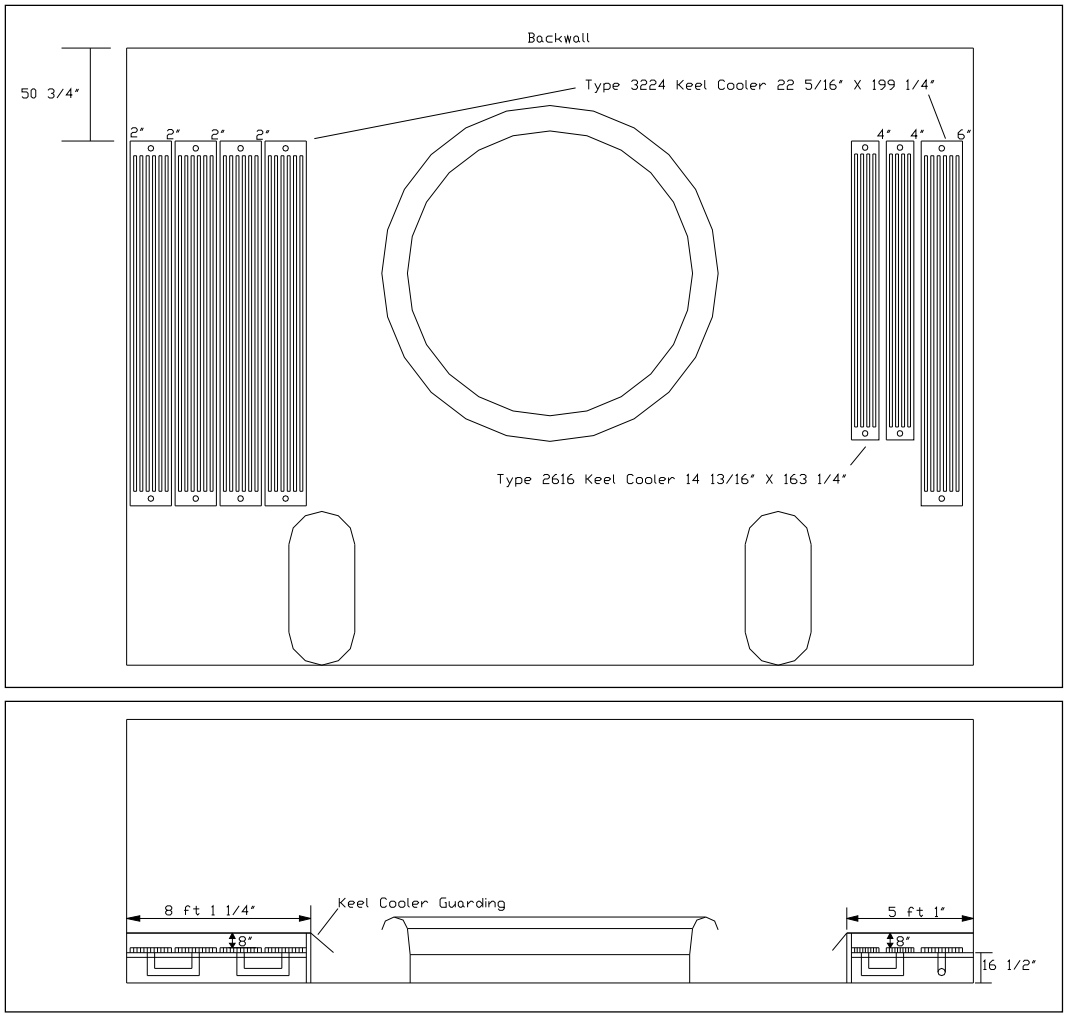

Figure 67. Keel cooler schematic of floor coolers.

the model grate and allowed the use of a simple wire mesh to simulate the full scale grate. Had the 1.5 in. bars been perpendicular to the flow, the grate would have exerted significantly more resistance to flow and the model grate would have been far more difficult to simulate losses. The grate in the model was composed of a wire mesh having four openings per in. (model), 81 percent open area, and wire diameter of 0.025 in. (model).

Because of concern about scale effects and making certain that the grate effect on pump head was not underestimated, a second model grate used a wire mesh having eight openings per inch, 74.6 percent open area, and wire diameter of 0.017 in. (model). Both grates were tested as described subsequently.

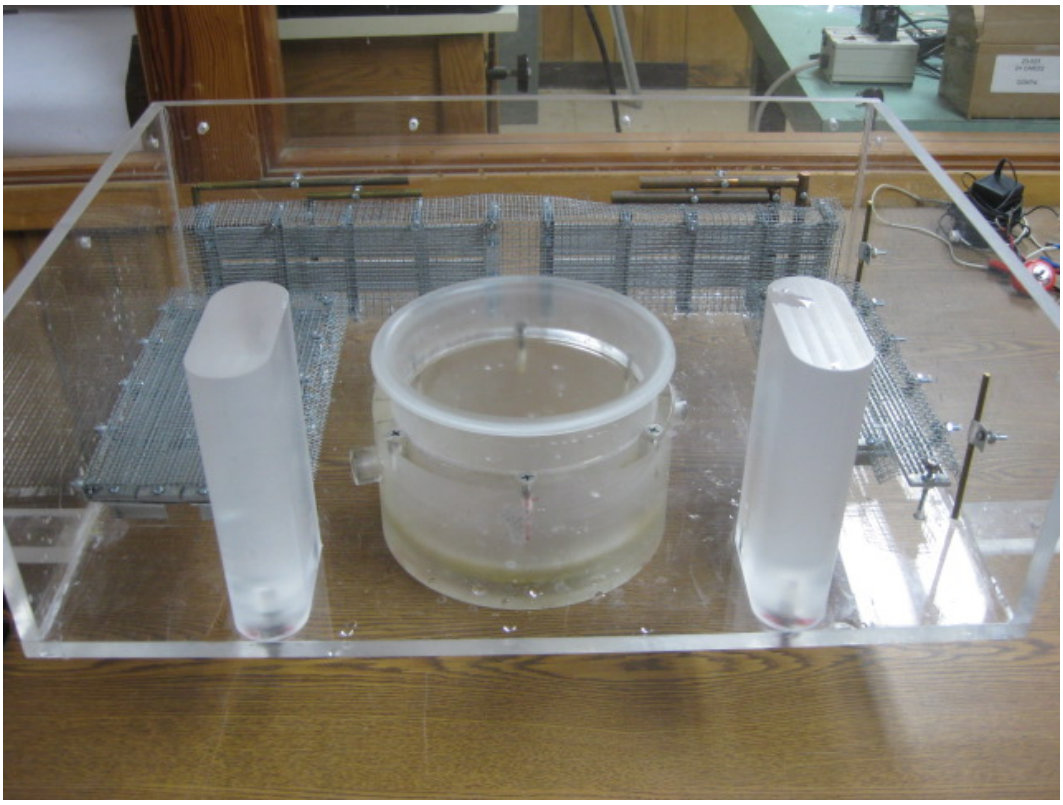

Figure 68. Detailed coolers in 1:21.932-scale model.

Figure 69 shows discharge head data from the FPDO without the keel coolers that was presented previously in this report. Also shown is a best fit curve to represent all of the tests without the keel coolers. Figure 69 shows data from tests with the detailed coolers protected by the 4-mesh grate. As stated previously, there was concern about scale effects from the grates and the need to insure that the effects of the grate and coolers on pump head was not underestimated. Figure 69 also shows data from tests with the 8-mesh protective grate placed on top of the 4-mesh protective grate. The added grate had little impact on the measured total energy on the discharge side of the pump. The lack of effect was likely due to the large percent of open area of the two grates. The proposed coolers increased pump discharge head by 0.6 ft at a discharge of 1,740 cfs.

Dye injections in the flowerpot section showed no change in flow stability with and without the coolers. Figure 70 shows pressure measurements in the pump column section beneath the flowerpot section. As indicated by the standard deviation, pressure fluctuations in the pump column section with the keel coolers were no different from pressure fluctuations measured without the keel coolers.

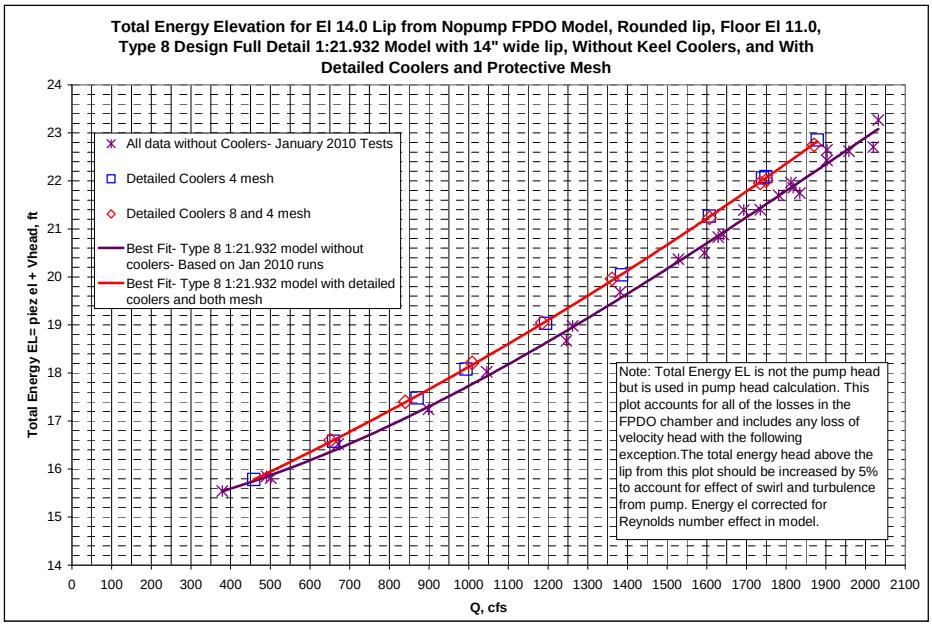

Figure 69. Pump discharge total energy without coolers, and with detailed keel coolers having two designs of protective grate.

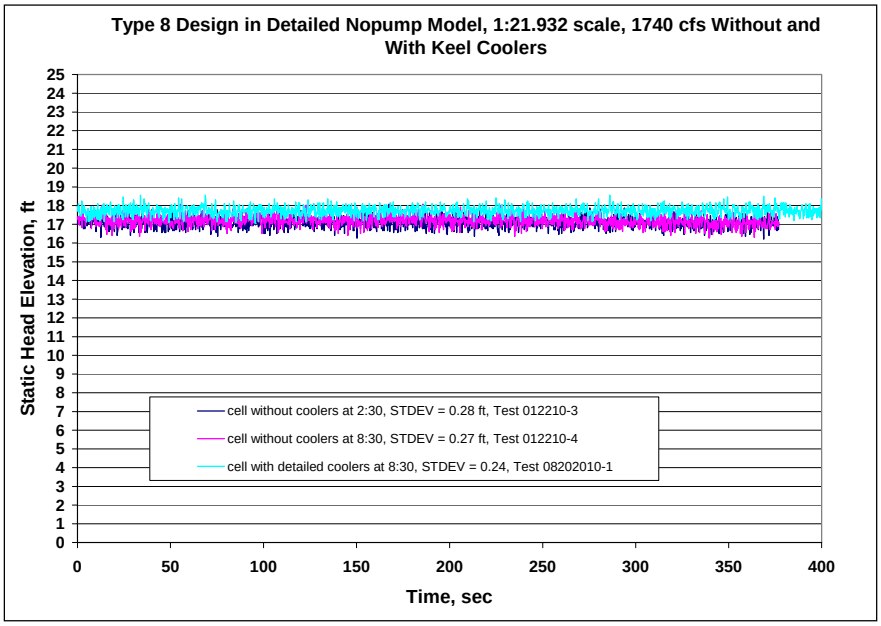

Figure 70. Pressure cell measurement in pump column beneath flowerpot section at el 7.7 with and without keel coolers.

6.3 Velocities near coolers in the FPDO

Velocities in the FPDO were measured with the detailed coolers and the protective grate using a 1/8-in. (model dimension) diameter Pitot tube. At the 1: 21.932-scale, the Pitot tube was not accurate for velocities less than about 1.0 knot. Any reading less than 1.0 knot was stated as “less than one

knot." Holes were drilled in the roof and sidewalls to position the Pitot tube at various locations. Except as noted, velocity measurements were made between the protective grate and the cooler. Dye was injected to determine flow patterns at various locations. The dye injections were important to align the Pitot tube with the flow to obtain a valid reading.

Figure 71 shows the velocity magnitude and direction where arrows indicate dye movement near the four floor coolers mounted on the right side of the FPDO. All velocities were measured between the protective grate and the cooler except for a single velocity that was measured beneath the cooler near the downstream end. All velocities exceeded 2.0 knots and flow directions were generally parallel with the bars of the cooler.

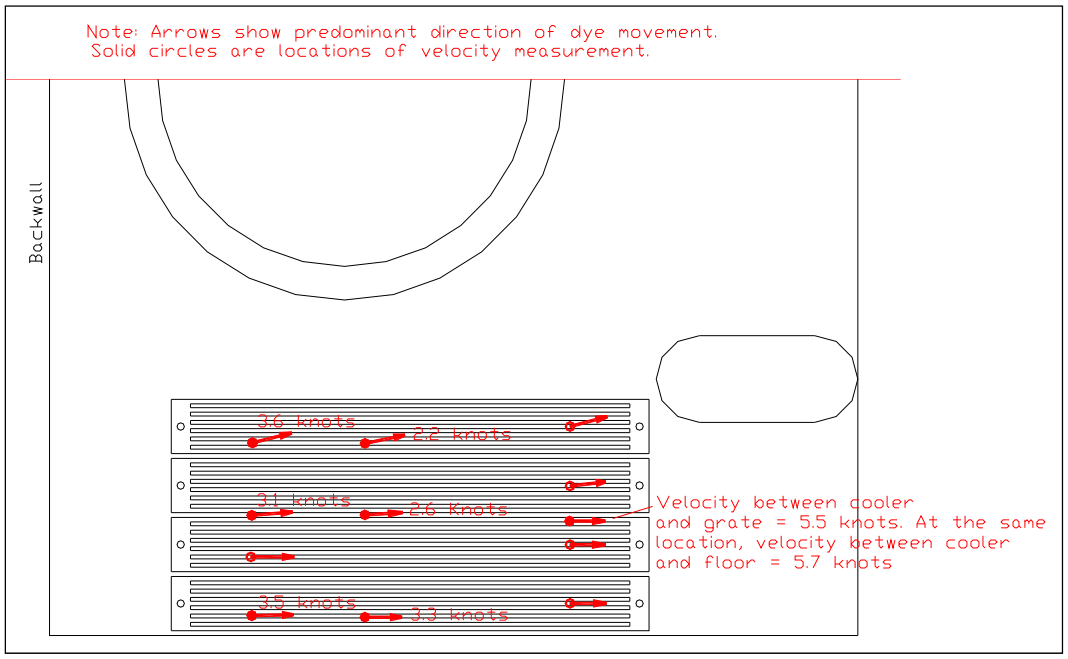

Figure 71. Velocities near the four floor coolers on right side (looking downstream) of FPDO.

For the floor cooler on the right side closest to the flowerpot, very little dye moved down or up through the cooler. Stated otherwise, the flow was parallel to the coolers. The other three of the right side floor coolers closer to the sidewall had an increasing amount of flow down through the cooler that reached a maximum at the cooler nearest the sidewall. Stated otherwise, flow was angling down through the cooler. The dye injections showed that the dye moved rapidly in a periodic manner down through the grate, which was consistent with the model observations that showed a rapid rise in water level above the grate and along the sidewall.

Figure 72 shows the velocities between the grate and coolers of the three floor coolers on the left side of the FPDO. Velocity magnitudes and directions were similar to the floor coolers on the right side of the FPDO.

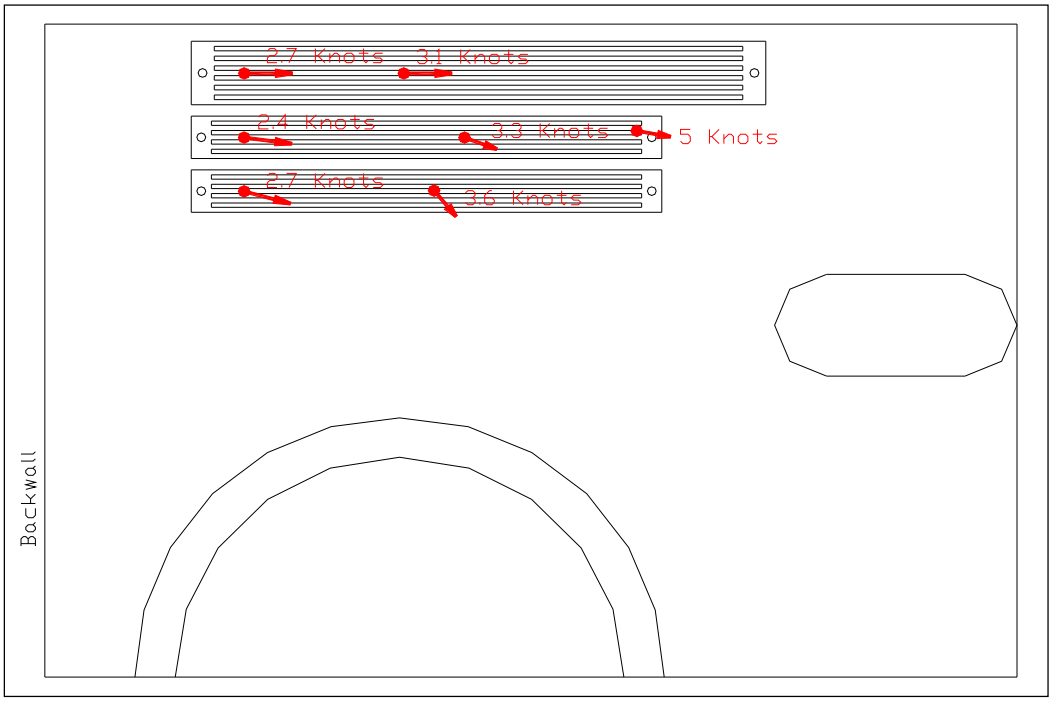

Figure 72. Velocities near three floor coolers on left side (looking downstream) of FPDO.

Velocities along the backwall coolers were far more complex than the velocities near the coolers on the floor and were difficult to explain. On the coolers on the right side of the backwall, detailed dye observations were made for the zone between the backwall and coolers (Figure 73). The dye direction is shown by an arrow with an open circle. Figure 73 also shows locations of velocities taken with the Pitot tube by a solid circle. As shown in Figure 73, flow between the backwall and the cooler was generally in a downward direction rather than along the bars of the coolers. Although predominantly downward, the flow had a significant downstream component through the coolers at some locations as indicated by the arrows having "DS" next to the open circle. Velocities measured just above the coolers and between the backwall and the coolers ranged up to 8.0 knots as shown in Figure 73. The direction of these velocities can be inferred from the dye arrows.

Detailed dye observations were also made for the zone between the coolers and the protective grate (Figure 74). They showed a predominant flow in a downstream direction normal to the cooler face. The predominant

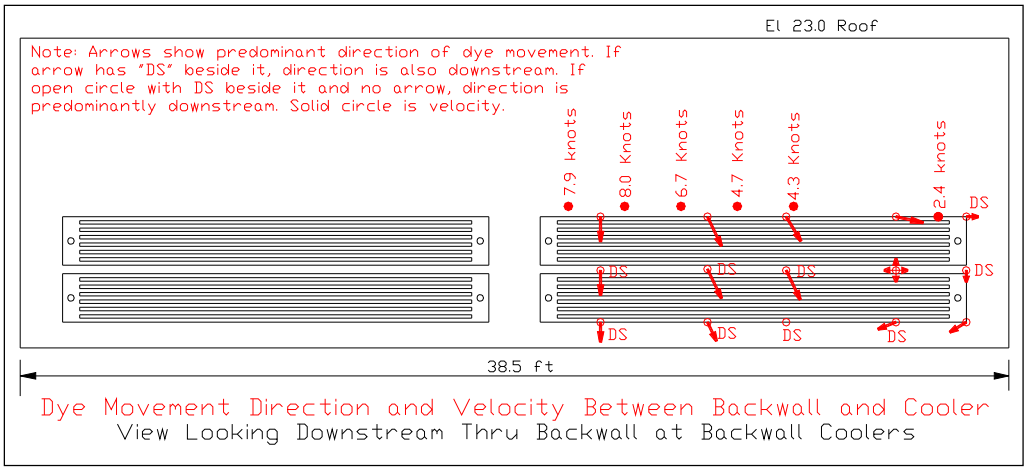

Figure 73. Dye movement direction and velocity between backwall and coolers on right side. Dye arrows at top edge of upper cooler show direction of measured velocity. Looking downstream.

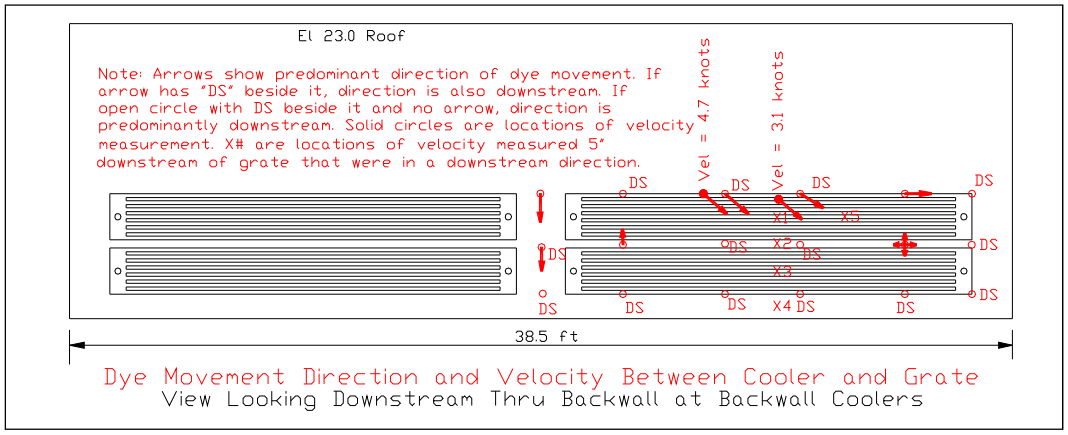

Figure 74. Dye movement direction and velocity between coolers and protective grate on right side.

downstream-directed flow was shown by the letters "DS" next to an open circle. Only near the top of the coolers where velocities were measured was the flow moving along the face of the coolers as well as some directed downstream.

Velocity measurements were made at the "X#" locations shown in Figure 74 to determine if downstream velocities were present and significant in magnitude. The Pitot tube was positioned 5.0 in. (full-scale) downstream of the protective grate. At X1 and X5, velocity was less than 1.0 knot. At X2 through X4, velocity magnitude was 2.9 knots, 3.6 knots, and 4.0 knots, respectively. Little flow came through the top cooler. A significant amount of flow came out the bottom cooler and beneath the bottom cooler.

The only zone where velocities appear to be the lowest was the 1/3 of the cooler length closest to the sidewall. At the middle of this zone, between the upper and lower coolers, the dye arrows showed flow in all directions. This area appeared to be a circulation zone having a clockwise direction on the right side of the backwall. One velocity measurement between the backwall and the cooler (Figure 73) shows the top of this circulation to have a velocity of 2.4 knots. Dye was repeatedly introduced into the center of the circulation zone to see if the dye stayed for any significant length of time. The implication of this qualitative test was that if the dye stayed, heat transfer would be hindered and the cooler would not function as intended. In every case the concentration of dye returned to ambient concentration after about 1.0 sec in the model.

Velocity measurements and dye observations were conducted at the two backwall coolers on the left side of the FPDO. The primary difference between the two sides on the backwall was the diameter and location of the pipes connected to the coolers, as shown in Figure 75. The pipes on the right side were 6-in. diameter whereas the pipes on the left side were 8-in. diameter.

Figure 75. View of backwall showing pipes between backwall and coolers. Pipes blocked some of the flow between the backwall and cooler.

This was important mainly in the area between the vertical pipes and the corner of the FPDO because the distance from the backwall to the cooler was 12 in. and the pipes blocked some of the flow. Another potential

difference was that there were four floor coolers on the right side versus three floor coolers on the left side. The difference in width and configuration of the floor coolers could affect flow at the backwall, but observation of flow in the model did not lead to that conclusion.

Dye was injected at the top of the left backwall coolers between the backwall and the coolers. As in the coolers on the right side, flow direction was generally downward, as shown in Figure 76. Velocities were measured at the same X# locations (Figure 76) downstream of the grate as in the right side backwall cooler tests. The velocity at X1 was less than one knot. The velocities at X2 to X4 were 3.4, 3.8, and 4.2 knots, respectively. These values were close to the values measured on the right side backwall coolers. Because of the similarity of dye direction and velocity magnitude at both backwalls, not all velocities were measured on the left side.

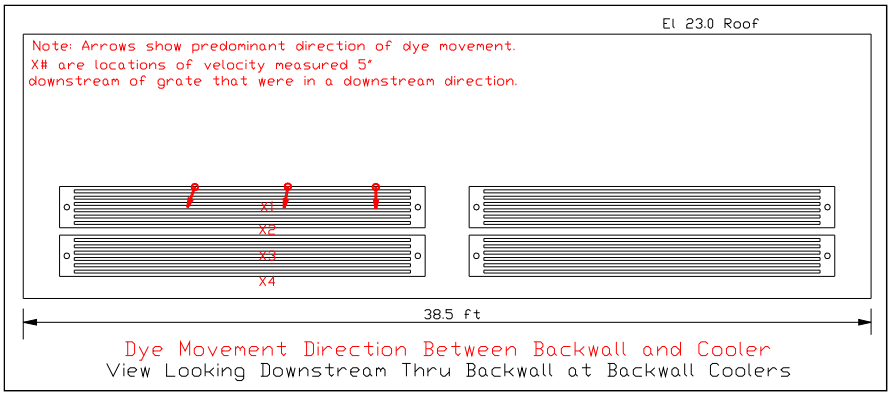

Figure 76. Dye movement direction between backwall and coolers on left side.

The area between the corner and the vertical pipes was examined closely on both sides of the backwall. Although difficult to quantify, it did appear that the larger 8.0 in. pipes on the left side were reducing dye movement intensity near the corner more than the 6.0 in. pipes on the right side. However, dye placed in the corner near the face of the cooler did not stay in this area on the left side similar to the dye movement tests on the right side reported previously.

Principal characteristics of the velocities measured near the coolers are summarized as follows:

- Four floor coolers on right side: No velocity parallel to bars < 2.0 knots. 2/3 of cooler area had velocity parallel to bars greater than 3.0 knots.

- Three floor coolers on left side: No velocity parallel to bars < 2.0 knots. 1/2 of cooler area had velocity parallel to bars greater than 3.0 knots.
- Upper backwall coolers: 2/3 of cooler area had flow along back side of cooler that was perpendicular to bars and exceeded 4.0 knots, 1/6 of cooler had velocity greater than 2.0 knots parallel to bars. The velocity over 1/6 of the cooler area was uncertain but dye quickly moved away from cooler.
- Lower backwall coolers: 2/3 of cooler area had flow through the cooler exceeding 2.0 knots. The velocity over 1/3 of the cooler area was uncertain but dye quickly moved away from cooler.

6.4 Dynamic loadings on keel coolers

Tests were conducted to determine the hydrodynamic loading on the keel coolers in the FPDO. Figures 77-79 show a discharge of 1,740 cfs in the 1:21.93-scale model of the FPDO with the keel coolers. Flow was turbulent with significant fluctuations, particularly over the floor mounted coolers. Observation of large turbulence in the FPDO resulted in concern about dynamic loading on the coolers. Physical model tests were conducted in the 1:21.932-scale model of the FPDO to determine the dynamic loadings on the four floor coolers on the right side (looking downstream) of the FPDO. Results are presented herein in model dimensions and model frequencies until the end of this section where values are scaled up to the full scale system. One exception to this was the use of references to discharge that are always presented in full scale.

Figure 77. View of FPDO model looking upstream into chamber with 1,740 cfs.

Figure 78. View of back of FPDO model with 1,740 cfs.

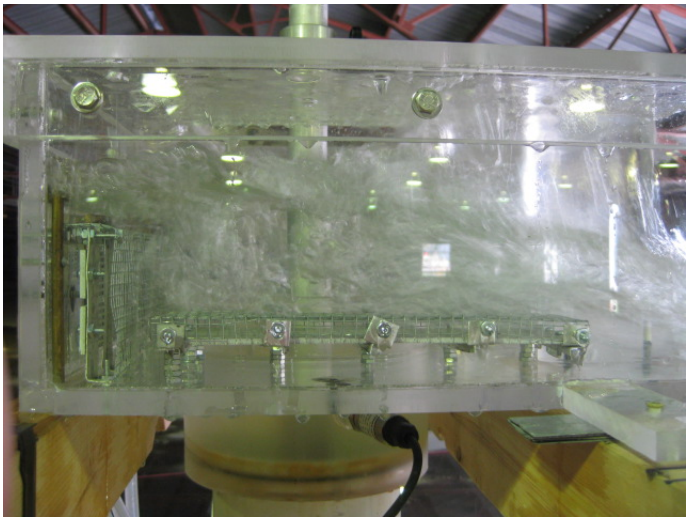

Figure 79. View of side of FPDO model with 1,740 cfs.

Determining dynamic loading in the highly complex flow environment of the FPDO is a significant undertaking. Two types of loading tests could be conducted with the coolers. The first type of loading test would be with a load cell attached to one end of an individual cooler that was hinged on the other end. The tests would be run and the load cell and hinge location swapped. This type of test would provide needed information, particularly about the total load on an individual cooler. The second type of loading test would be using a differential pressure cell to measure the pressure difference above and below the cooler. The pressure difference would be multiplied by a representative area to determine load. The second type of loading test with the pressure cell gives pressures at a point representative of a local area and thus local force on the cooler. Both of these load test types have their own set of problems that would have to be overcome. The

WCC FPDO was under construction and the RINO Districts needed loading estimates as soon as possible.

ERDC hypothesized that structural failure of the keel cooler from the dynamic loading of the turbulent flow would likely occur as fatigue at a connection of the bars to the manifold on the ends of the coolers or the bar connections to the intermediate supports. Either location would need a local force, as opposed to the total force, over the entire cooler. The full scale keel cooler was 200-in.-long and was supported at three intermediate locations, resulting in about a 50-in.-long clear span of each tube between supports. As a result of this hypothesis, the availability of an appropriate differential pressure cell, and the need to expedite this study, the differential pressure cell approach was selected for this study. The load cell measurements would have been a valuable addition to provide a check on the magnitudes from the pressure cell approach if time had allowed.

As background for the pressure cell tests, the 1:21.932-scale model of the FPDO was designed and constructed to determine the head on the discharge side of the pump in the WCC pump station. The FPDO model used the water supply system of a different model to construct the FPDO model rapidly. The straight pipe upstream of the FPDO required that the model be raised well above the floor and supported by a framework (Figure 80). Preliminary tests showed that the framework supporting the FPDO was vibrating. These vibrations could compromise the pressure measurements. The wooden framework supporting the FPDO was stiffened by adding numerous braces and stiffening members. The jet leaving the FPDO fell about 6.0 ft into a basin whose walls provide the structural support for the framework supporting the FPDO. A separate support stand was built to hold only the differential pressure cell to reduce vibration of the cell. However, this did not eliminate pressure cell vibration because the cell was connected to the FPDO framework by the two tubes connecting the differential pressure cell and the FPDO.

A PX2300 differential pressure cell by Omega was used to measure the differential pressures on the coolers. The pressure cell was bidirectional and ± 0.5 lb/in.^{2}. The pressure cell was connected to 1/8-in.-diameter piezometer taps on the sidewall and floor of the FPDO with a type of plastic tubing that could bend but was resistant to deformation of the diameter or length. The 0.17-in. inside diameter plastic tubing was used for two reasons. First, it was clear enough to see if air bubbles were present, which could affect the measurement of pressures.

Figure 80. Framework supporting 1:21.932-scale model of FPDO. Picture taken after braces and stiffeners were added.

Second, the flexible tubes allowed the pressure cell to be moved, rotated, and bumped so that any air bubbles in the tubes, fittings, and pressure cell could be moved toward the air-bleed ports located on each side of the diaphragm of the pressure cell. Inserts were placed inside any fittings and the body of the pressure cell to minimize changes of the inside pipe diameter that could affect the pressure readings. The tubes were kept as short as possible but had to be 11-in. long to connect to the two piezometers (Figure 81). Purging air bubbles from the system was a challenge because the pressure at the piezometers to move water and air bubbles through the tubes was extremely low. The cell needed to be below the elevation of the water level in the FPDO to force flow to the pressure cell and the air-bleed ports. At the same time, the cell could not be too far below the FPDO because the air bubbles would not move down through the tubes. Unfortunately, one can never be certain that all air bubbles have been removed from the system because not all parts of the system are visible. The approach used herein was to purge the air, run the test, and repeat the process until results were repeatable.

Concern existed about the response time of the system of piezometer taps, tubing, connections, and pressure cell. A study by Reader-Harris and McNaught (2005) summarized some of the issues concerning tubes connecting differential pressure cells to flowmeters that have applicability to this study. They refer to the tubes as "impulse lines." They summarize results from other studies and state "…..pulsation data from impulse lines cannot necessarily be relied upon unless impulse-line lengths are very much shorter than a quarter wave length for the highest frequency existing in the

Figure 81. Pressure cell and plastic connecting tubes attached to FPDO.

piping, and then only if there are no constrictions or volumes in the impulse line that would lower its resonant frequency." Another source in the Reader-Harris and McNaught study stated the line should not be longer than 10 percent of the quarter wave length. To check against this criterion, the wave speed in the model tubes was calculated using acoustic speed equations from Wylie and Streeter (1983). The tubes are made of polyethylene by Imperial Eastman and have an inner diameter of 0.17-in. and a wall thickness of 0.04-in. Polyethylene has a range of Young's modulus. The only information about the polyethylene used in the tube was that it had a Shore D hardness of 50. Young's modulus for a Shore D hardness of 50 was about 9,080 lb/in.^{2}. Using bulk modulus of elasticity of water of 320,000 lb/in.^{2} along with tube characteristics including a Poisson ratio of 0.25, resulted in a wave speed in the tubing of 411 ft/sec.

Seven Hz was measured previously as the maximum frequency in the system. The wave length for this highest frequency was (1/7 sec) x (411 ft/sec) = 59 ft. One-fourth of this wave length was 14.7 ft. The tubing used herein was 11 in. in length (= six percent of quarter wave length) and meets the Reader-Harris and McNaught (2005) criterion for tube shortness and thus provided reliable pulsation data.

Regarding sampling rate, the response time of the PX2300 was 50 ms, which limited the data collection rate to 20 Hz. Sampling rate selection must consider aliasing, which refers to an effect that causes different signals to become indistinguishable when the sampling frequency was too low. Aliasing was avoided if the sampling rate satisfies the Nyquist requirement,

which states that the sampling rate must be greater than twice the maximum frequency of the problem being studied. The Nyquist frequency insured that the sampling was adequate to reconstruct the original signal from the sampled data. The Nyquist frequency does not insure that the sampled data captures all the peaks and valleys of the original signal. The pressure differential had a maximum frequency of about 7.0 Hz in the model. Using 7.0 Hz as the maximum frequency of interest, the sampling rate that satisfies the Nyquist requirement was 14 Hz. The PX2300 differential cell was sampled at 20 Hz and the single cell PX309 was sampled at 37 Hz, both of which were greater than the Nyquist frequency. Even though the Nyquist frequency was exceeded, some of the peaks and valleys of the time series were clipped, particularly with the 20 Hz sampling. The amount of data clipping was investigated using the 20 Hz sample data with the Whittaker-Shannon interpolation formula (Whittaker 1935) to reconstruct the time series from the sampled data. The reconstructed time series for ten seconds of test 08302010-1 using the differential pressure cell is shown in Figure 82. While some clipping of the data was present such as at time 38.5 sec (Figure 82), the one percent exceedance values for the reconstructed signal and the sampled data were the same and the sample rates were considered acceptable.

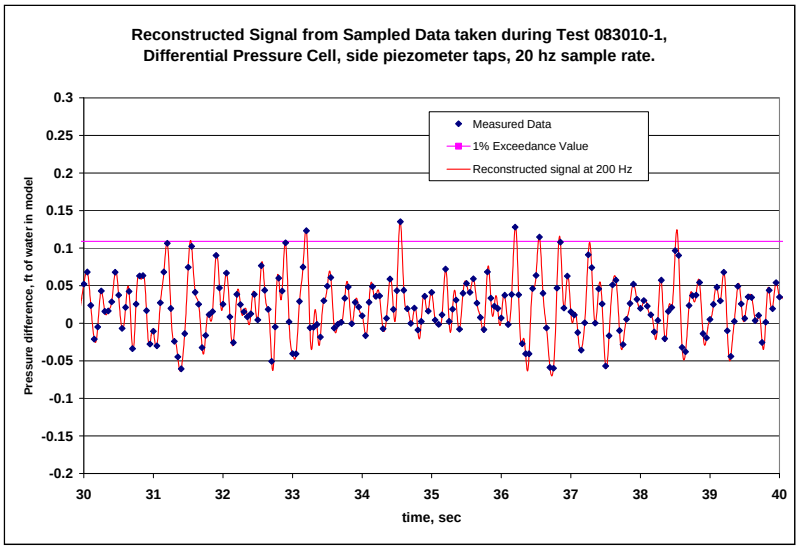

Figure 82. Reconstructed signal from sampled data.

The piezometer taps connecting the pressure cell to the FPDO were positioned above and below the floor coolers at three locations along the cooler as shown in Figure 83. The piezometer on the top side of the cooler through the sidewall was 0.55 in. above the top of the cooler (Figure 84). This position was 0.09 in. above the protective grate. The bottom

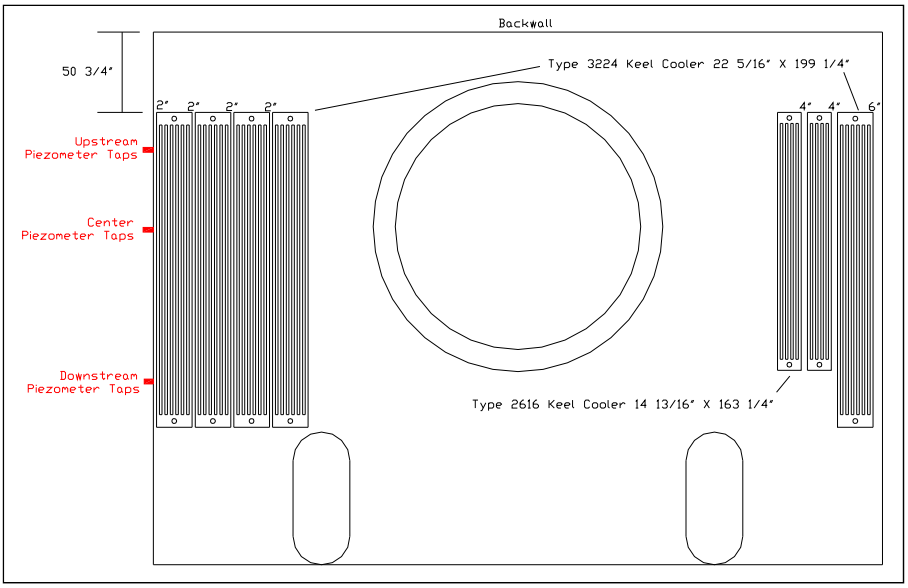

Figure 83. Piezometer locations along floor coolers.

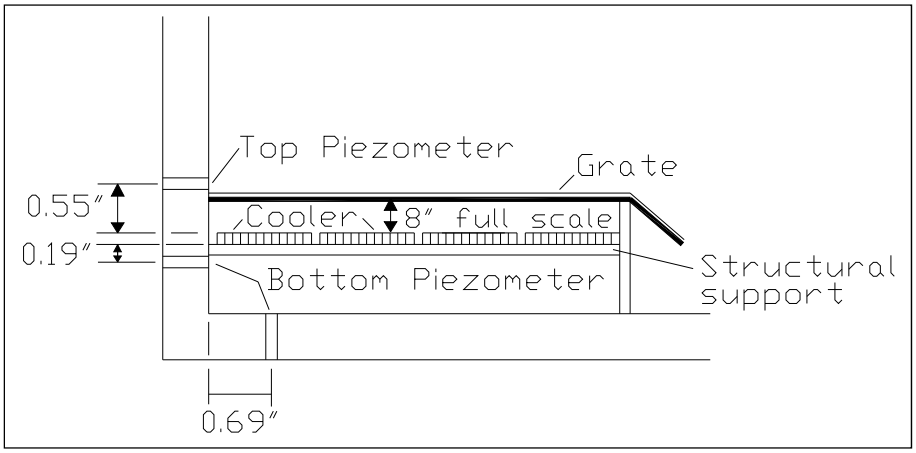

Figure 84. Schematic of piezometer tap locations. Looking upstream at four floor mounted keel coolers.

piezometer was placed on the sidewall directly below the top piezometer and 0.19 in. below the bottom of the cooler. This initial location of the bottom piezometer was in an area where flow came down between the cooler and the sidewall and was also affected by turbulence from the structural support members on the bottom of the keel coolers. Because of those two factors that might affect pressures in an unknown way, a few tests were also conducted with a bottom piezometer located on the floor of the FPDO for the center piezometer location only. This floor piezometer was located 0.69 in. away from the sidewall and even with the pump centerline.

Data were recorded using a laptop computer and each test met the following two criteria for duration: (1) greater than 100 sec and (2) the number of samples was equal to or greater than 2^n, where n was an integer that resulted in 2^n being greater than 100 times the sample rate. For example, 100 sec of 20 Hz sampling would be 2,000 samples. The test would be run for at least 2^{11} = 2,048 samples and then 2,048 samples were analyzed. The 100-sec minimum duration was based on comparing a change in mean value with a size of sample until the mean changed less than one percent.

Initial tests were conducted to determine the frequencies at which the model system vibrates that could interfere with the differential pressure measurements. The model was started at a low flow that submerged the piezometer taps but had few bubbles near the piezometer taps. This low flow was used to purge the tubes and pressure cell of any air bubbles for all tests reported herein. After purging air off, the pump supplying the flow was stopped. All water was drained out of the FPDO, but the tubes and pressure cell remained full of water and free of air. The discharge valve was closed such that the vertical riser pipe up to the lip of the outlet remained full of water. The data acquisition system was started and a hammer was used to tap the framework at various locations. The system vibrated and the vibrations quickly decayed. The frequency of vibration ranged from 14 to 18 Hz.

A test was conducted using the piezometer tubes that were connected to the center piezometer taps, but were disconnected from the pressure cell and using them as simple piezometers to determine which side of the cooler had the highest pressure and the magnitude of the average differential. The test was conducted with 1,740 cfs using both side piezometers. The top side of the cooler had the highest pressure, which averaged 0.01 to 0.02 ft higher than the bottom side. Periodically, the high side would jump about 0.05 ft above the low side.

The initial production test with the differential pressure cell was conducted with the tubes connected to the center piezometers on the sidewall and 1,740 cfs passing through the FPDO. The time history of differential pressure for test 09272010-13 is shown in Figure 85 for the center piezometer location having both taps on the side wall. The one percent exceedance differential for this test was 0.087 ft. Results are summarized in Table 10 for all three piezometer locations. The power spectral density for this run (Figure 86) shows significant power spectral density between 2.0 and 7.0 Hz.

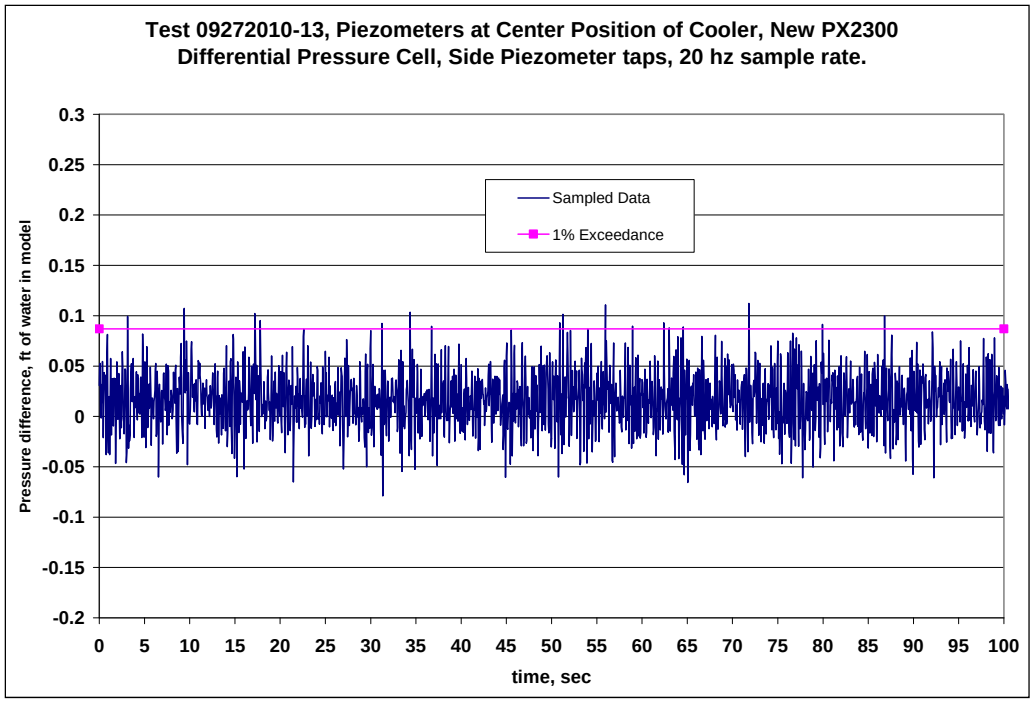

Figure 85. Time history of differential pressure across cooler for 1,740 cfs using both piezometer taps on side wall at center piezometer location, test 09272010-13.

Table 10. Results from differential pressure cells.

Test#	Piezometer Location	1 percent differential, ft of water in model	Tube restraint method
09272010-13	Center	0.087	3
09272010-14	Center	0.079	3
09272010-15	Center	0.090	3
09272010-16	Center	0.097	3
09232010-2	Downstream	0.129	1
09232010-3	Downstream	0.131	1
09232010-4	Downstream	0.116	1
09232010-5	Downstream	0.129	1
09232010-6	Downstream	0.118	1
09272010-2	Downstream	0.119	1
09272010-3	Downstream	0.116	2
09272010-4	Downstream	0.116	2
09272010-5	Downstream	0.123	2
09272010-6	Downstream	0.122	2
09272010-7	Downstream	0.119	2

Test#	Piezometer Location	1 percent differential, ft of water in model	Tube restraint method
09272010-8	Downstream	0.118	3
09272010-9	Downstream	0.112	3
09272010-10	Downstream	0.113	3
09242010-2	Upstream	0.078	1
09242010-3	Upstream	0.068	1
09242010-4	Upstream	0.074	1
09242010-5	Upstream	0.079	1

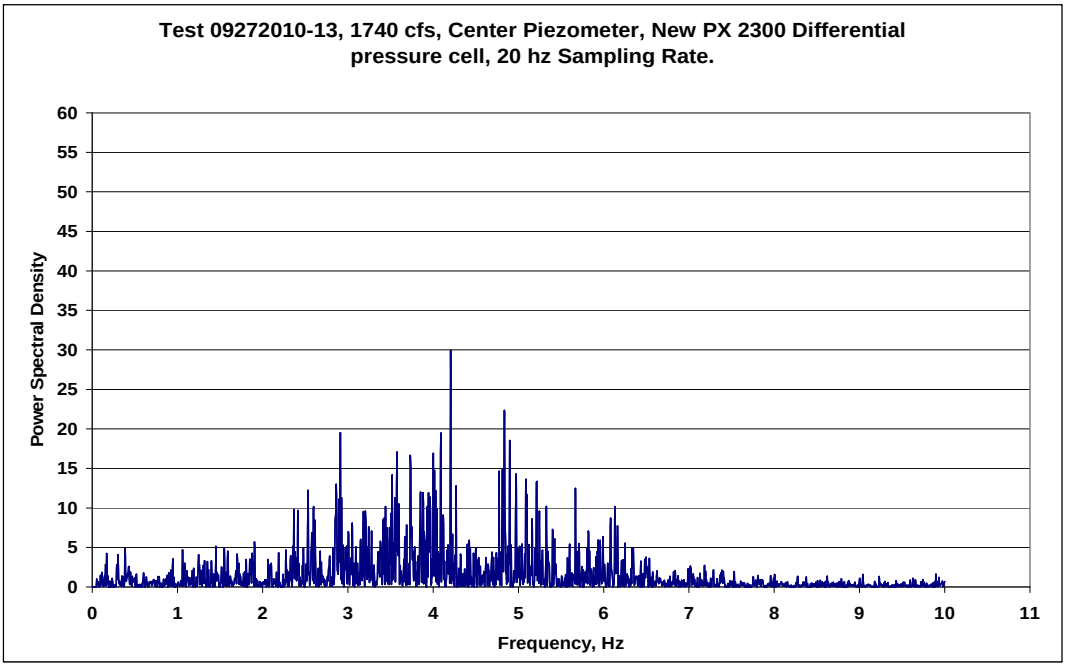

Figure 86. Power spectral density of differential pressure across cooler for 1,740 cfs using both piezometer taps on side wall at center piezometer location.

Tube restraint method: 1 = no restraint along the 11-in. length, 2 = connected to framework supporting FPDO at midpoint of tube, 3 = midpoint of tube connected to cross member but not connected to framework.

Figure 87 shows pressure differential for test 09272010-2 at the downstream piezometer position and Figure 88 shows the power spectral density. Table 10 shows test results from the downstream piezometer position with various methods to restrain the flexible tubing between the differential pressure cell and the piezometer at the sidewall of the FPDO. The ERDC was concerned that the tubes could be vibrating at frequencies of interest to this study.

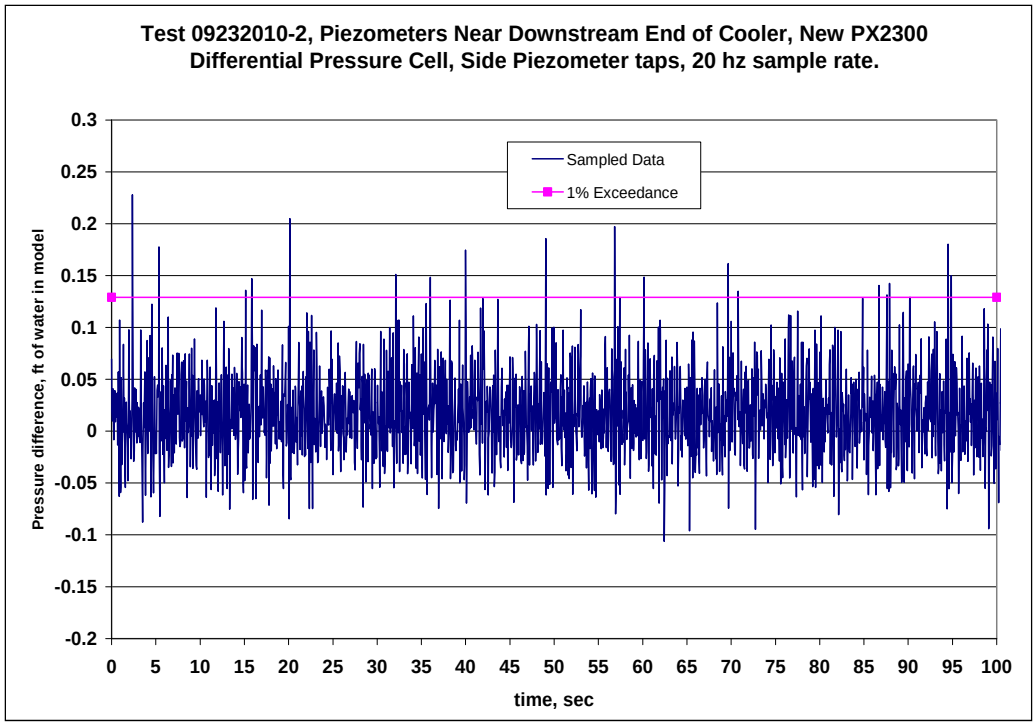

Figure 87. Time history of differential pressure across cooler for test 09232010-2 for 1,740 cfs using both piezometer taps on side wall at downstream piezometer location.

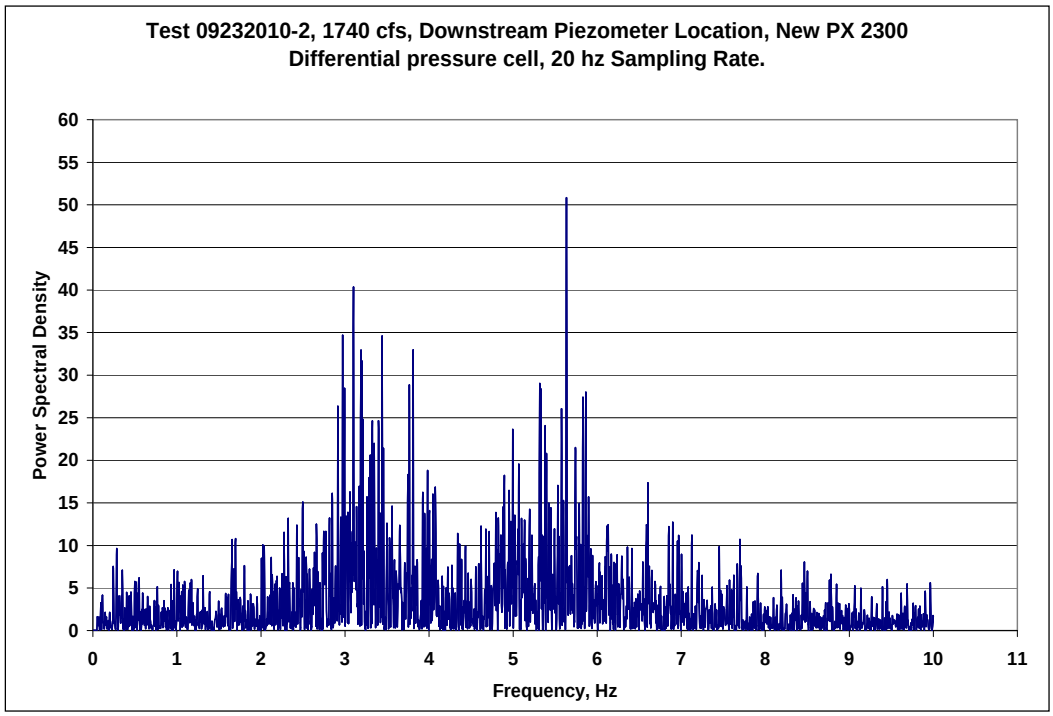

Figure 88. Power spectral density of differential pressure across cooler for test 09232010-2 for 1,740 cfs using both piezometer taps on side wall at downstream piezometer location.

None of the restraint methods had a significant effect on either the one percent exceedance values or the power spectral density distribution plots. Figure 89 shows pressure differential for test 09242010-2 at the upstream piezometer position and Figure 90 shows the power spectral density. The plots at the three locations along the coolers show some variation in pressure difference and frequency along the coolers. From the data summarized in Table 10, the downstream piezometer location had the highest 1 percent exceedance differential, which was about 0.13 ft in the model.

A method was needed to check results from the differential cell. Two single pressure cells (not differential) were available to mount in the piezometer taps. Rather than using tubes, the pressure cell was directly screwed into the sidewall and bottom of the FPDO, but the diaphragm was recessed about 0.5 in. from the 1/8 in. piezometer. The 2.0 lb/in.^{2} Omega PX 309 pressure cell had a one millisecond response time, which suggests an allowable sampling rate up to 1000 Hz. Omega was contacted to see if the response time was in air or water but they had no data to address this issue. One caution with using these cells was that the average pressures in the model are about 0.1 lb/in.^{2}, which was only five percent of the full scale signal with the 2.0 lb/in.^{2} cells. Since these cells are primarily being used to check the differential results, the low percentage of full scale was accepted. The signal was sampled at a rate of 37 Hz, which was the limit for two cells simultaneously in the data acquisition system used on this project. The 37 Hz rate was almost twice the rate used with the differential cell. The difference between the cells was calculated at each sampling time and was plotted in Figure 91 for the center piezometer location for test 09152010-1. The difference was adjusted for the difference in elevation between the piezometer above and below the cooler. Table 11 summarizes the one percent exceedance values based on the difference between the two individual cells for all three piezometer locations.

The one percent exceedance differentials measured with the differential pressure cell in Table 10 were similar to the differentials measured with the two single pressure cells in Table 11. This agreement provided a good check on the data and the Table 10 differential pressure cell data were accepted. The peak differential was located at the downstream piezometer position and equaled about 0.13 ft in the model.

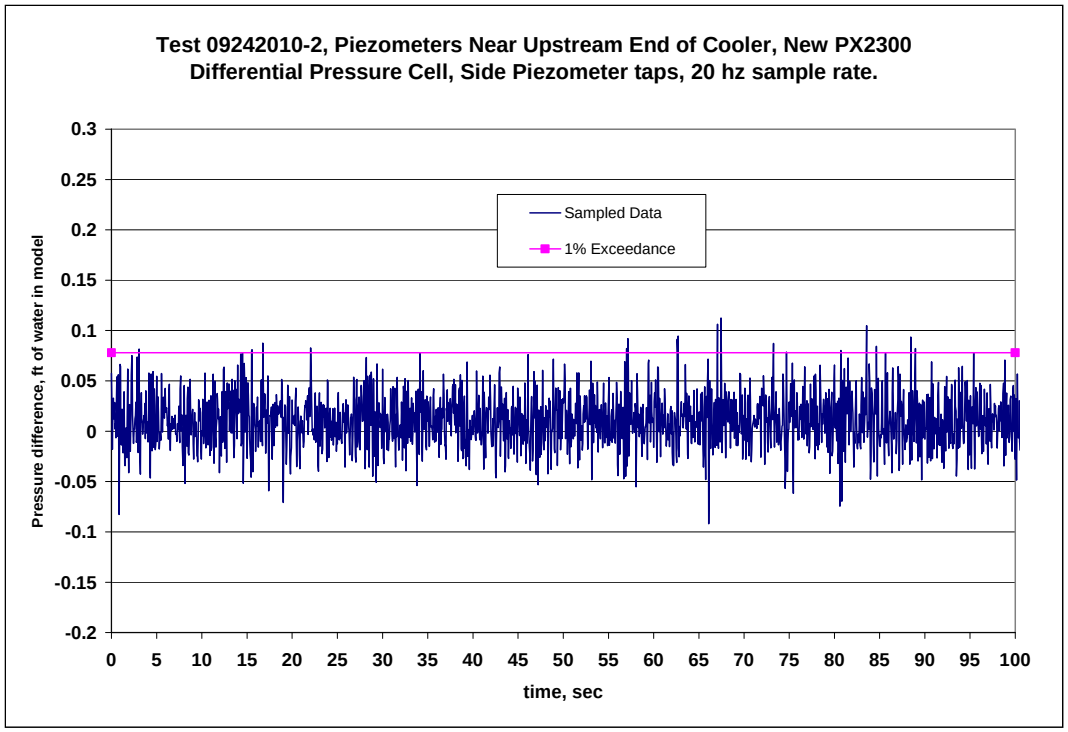

Figure 89. Test 09242010-2 for piezometers near upstream end of coolers.

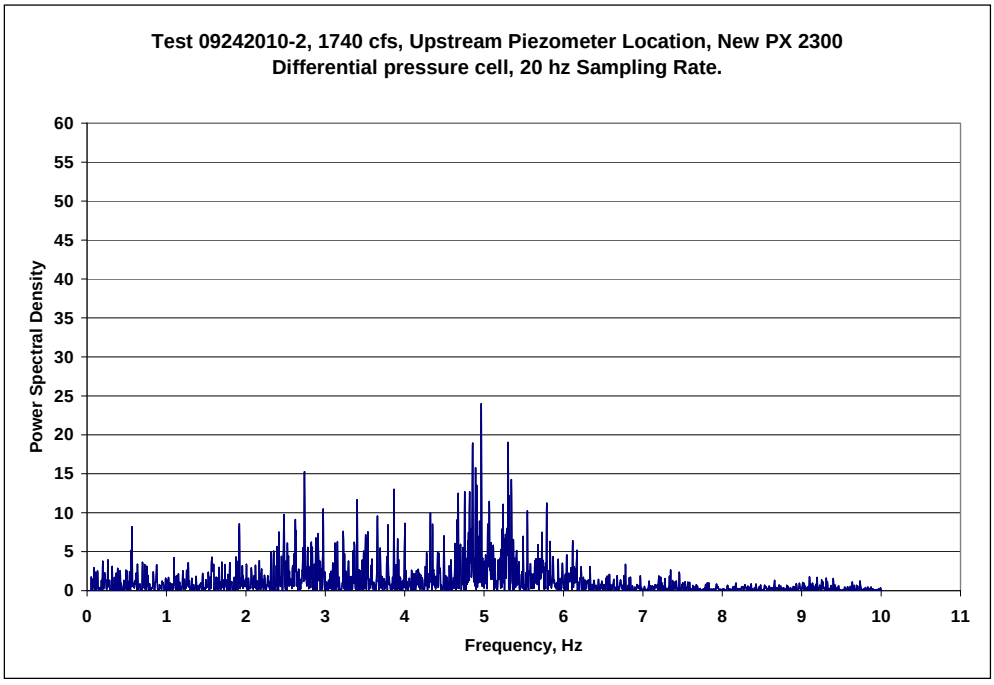

Figure 90. Power spectral density for test 09242010-2 for piezometers near upstream end of coolers.

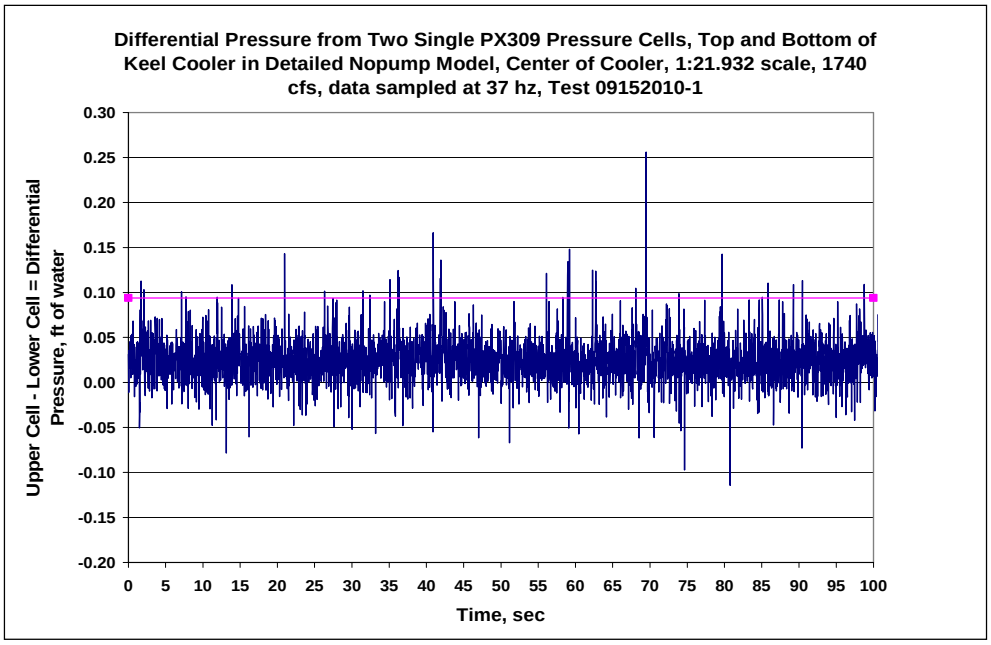

Figure 91. Differential pressure at center piezometer location from two single pressure cells for test 09152010-1.

Table 11. Differential pressure based on two single pressure cell measurements. All values in ft of water in the model.

Test	Piezometer Location	1-percent Exceedance, ft of water in model
09152010-1	Center	0.094
09152010-2	Center	0.079
09152010-3	Center	0.077
09152010-6	Downstream	0.126
09152010-7	Downstream	0.139
09152010-8	Downstream	0.131
09152010-10	Upstream	0.071
09152010-11	Upstream	0.070
09152010-12	Upstream	0.070

As a check on the frequency response, the power spectral density for the upper pressure cell for test 09152010-1 is shown in Figure 92 and the lower cell in Figure 93. Similar to the differential cell, most power was below 7.0 Hz but the upper cell showed power at some frequencies not found in the lower cell such as more power below 3.0 Hz.

A limited set of measurements was made to compare the single pressure cell below the cooler mounted on the sidewall versus the cell mounted on the floor. These tests were only conducted for the center piezometer

location. Results were similar for both locations below the cooler and all tests were conducted using the sidewall position to represent the zone below the cooler.

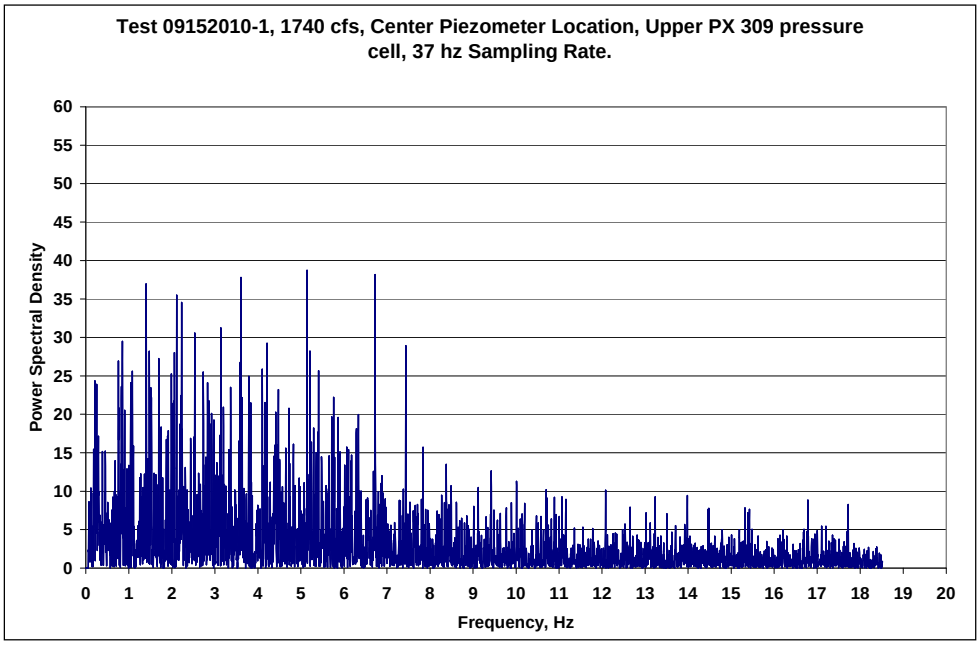

Figure 92. Power spectral density for pressure at piezometer on top of keel cooler for center piezometer location, test 09152010-1.

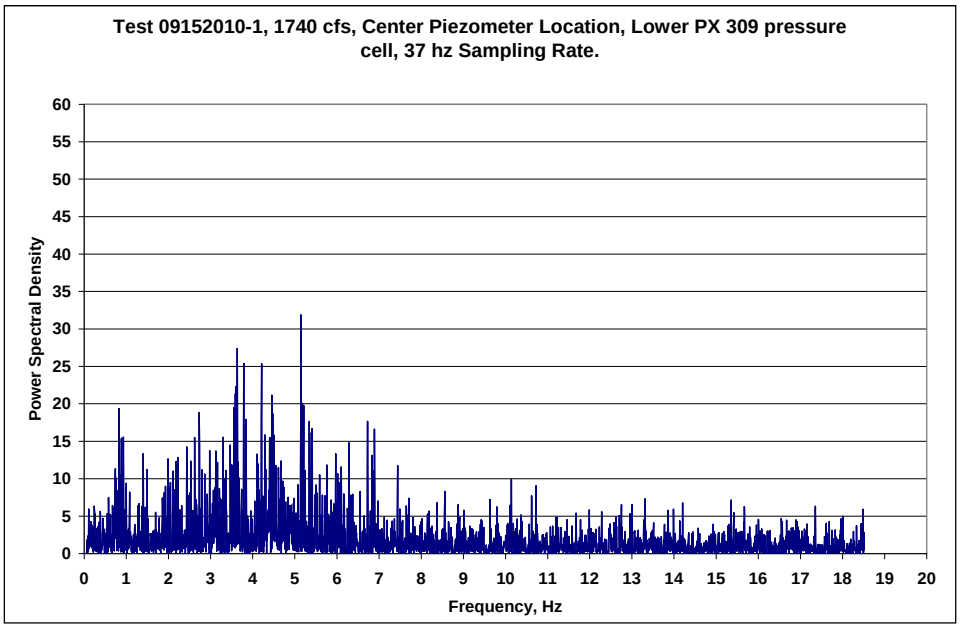

Figure 93. Power spectral density for pressure at piezometer below keel cooler for center piezometer location, test 09152010-1.

The next step was to integrate the pressure differential data to obtain the loading for structural calculations. A significant amount of information about using pressure fluctuations to determine loading is available from stilling basin slabs and buildings subject to fluctuating winds. Two of the important issues from those studies that must be addressed herein are explained in the next two sections.

6.4.1 Number and location of pressure measurements

Pressure differentials were measured at three locations along the sidewall. While more locations along the length of the cooler would have been better, ERDC believes the three measured locations were adequate to capture close to the maximum pressure differential and thus loading on the cooler. No data were collected concerning lateral variation of the pressure difference away from the sidewall. While lateral variation across the cooler existed, the rise of water level along the sidewall of the FPDO suggested the cooler near the wall would experience the largest pressure differential. In addition, dye injections discussed in the previous section on velocities showed that the highest flow through the floor coolers in a downward direction occurred at the wall cooler.

6.4.2 Correlation of point pressures

Depending on the nature of the flow turbulence, extent of flow separation, shape of structure, and numerous other factors, studies have shown that point pressures can be highly correlated with pressures at adjacent locations or not correlated at all. In other words, turbulence induced pressure fluctuations may not rise and fall over the entire cooler simultaneously. Wacker and Plate (1992) showed that using peak pressures to determine peak wind load on buildings and assuming that all peak pressures were completely correlated, peak load was overestimated. Stated otherwise, if all peak pressures were assumed to act simultaneously, peak load was over-estimated. This study did not have time to develop the correlations between point pressures at enough locations along and across the cooler and conservatively assumed that the highest measured one percent exceedance point pressure difference at any of the three locations along the length of the cooler applied to the entire area of the cooler.

From the data, the largest one percent exceedance pressure difference at the three piezometer locations (center, downstream, or upstream) was 0.13 ft of water in the model at the downstream piezometer (Table 10). A

statistical analysis of the one percent exceedance values from the 14 tests taken at the downstream location resulted in a mean value of 0.12 ft and a standard deviation of 0.006 ft. If uniformly distributed, the mean and the standard deviation show that a one percent exceedance value of 0.13 will be exceeded five percent of the time. Therefore, the use of the maximum of the fourteen one percent exceedance values of 0.131 ft should be conservative.

Up until this point, values have been presented in model quantities. At full scale, the one percent exceedance pressure difference was 0.131 x 21.932 = 2.87 ft or 1.245 lb/in.^{2}. The bars in the four full-scale floor coolers were 0.5 in. wide. The resulting uniformly distributed force on each bar was 12 in./ft x 0.5 in. width x 1.245 lb/in.^{2} = 7.47 lb/ft.

In a model where the Froude number must be the same in model and full-scale, frequencies scale in model to full-scale according to the inverse of the square root of the length scale or 4.68:1 in a 1:21.932-scale model. This means that the 2-7 Hz frequencies in the model correspond to 0.4 to 1.5 Hz in the full scale FPDO. The largest pressure differentials occurred at full scale frequencies between 0.4 and 1.0 Hz.

7 Summary and Recommendations

The physical model investigation of the WCC flowerpot discharge outlet (FPDO) reported herein evaluated stability of flow in the FPDO, head loss through the FPDO to use in pump head estimation, downstream riprap stability, and performance of keel coolers both inside the FPDO and downstream of the FPDO in the tailwater. Testing was based on the final eleven pump design of the pump station having a discharge of about 1,740 cfs/pump at an intake water level at el 2.0.

The recommended Type 8 Design FPDO has a 14-in.-wide rounded lip with its top located at el 14, the chamber floor at el 11, and the roof at el 23. The diameter of the outlet at the top of the semicircular lip at el 14 was 169.5 in.

Two 3-ft-wide piers at the downstream end of the chamber were found to not have adverse effects on pump head or flow exiting the chamber.

Both the pump column and flowerpot sections above the pump have a 6.1-deg divergence angle, which was found to be stable with respect to flow separation.

Pressures measured in the pump column and dye injections in the flowerpot section showed stable flow conditions in the vertical column above the pump. Water levels in the chamber were well below the roof and should allow air bulking of the flow without filling of the chamber.

Tests in the FPDO model without the pump immediately beneath the FPDO were used to develop pump discharge head data to be used in developing a system curve.

Riprap stability tests in the 1:15-scale model were used to size the riprap and determine the required channel-protection distance downstream. It was found that a stable riprap required a 30-in. maximum stone size for the 155 lb/ft^3 riprap available in the New Orleans area. The required downstream length of the stable riprap was 75 ft. A 6-ft-long thickened section on both the upstream and downstream ends of the riprap was also recommended.

Flow remained stable and pressure fluctuations were not changed when seven keel coolers were installed of the floor and four coolers on the backwall of the FPDO. The addition of the 11 keel coolers on the floor and backwall of the FPDO increased the discharge head by 0.6 ft at a discharge of 1,740 cfs.

A differential pressure cell was used to determine dynamic loadings on the keel coolers mounted on the floor. Loads were highest at the downstream end of the floor cooler and the one percent exceedance pressure difference resulted in a uniform load of 7.4 lb/ft of bar length.

Velocities measured near the seven floor keel coolers always exceeded 2.0 knots. More than 2/3 of the four backwall keel cooler area had velocity exceeding 2.0 knots. Less than 1/3 of the backwall keel cooler area had velocity that was difficult to quantify, but dye in the model quickly moved away from these areas. The dye movement indicates heat transfer will not be hindered in these areas.

An alternate location for the keel coolers was in the tailwater immediately below and downstream of the FPDO. This location was considered unacceptable because vertical velocities along the coolers were generally less than 1 knot. The safest location from impingement forces from the falling jet was with the coolers mounted on the vertical wall just below the lip of the FPDO.

References

Idelchik, I. E. 1986. Handbook of Hydraulic Resistance. 2nd ed. New York: Hemisphere Publishing Company.

Isbash, S. 1935. Construction of Dams by Dumping Stones in Flowing Water. Leningrad.

Kirschmir, O. 1926. Investigation regarding the determination of head loss. Mitteilungen des Hydraulischen Institute der Technischen Hochschule Munchen, Heft 1.

Lawrence, F. E., and P. L. Braunworth. 1906. Fountain Flow of Water in Vertical Pipes. ASCE Transactions, Paper No 1035.

Miller, D. S. 1978. Internal Flow Systems. BHRA Fluid Engineering Series, Volume 5.

Osborn, J. F. 1968. Rectangular-Bar Trashrack and Baffle Headlosses. *ASCE J of the Power Division*, 94(2).

Papworth, M. 1972. The effects of screens on flow characteristics. BHRA TN 1198.

Reader-Harris, M. J., and J. M. McNaught. 2005. Impulse Lines for Differential-Pressure Flowmeters, Best Practice Guide. TUV NEL, Glasgow, England.

US Army Corps of Engineers (USACE). 1994. Hydraulic Design of Flood Control Channels. EM 1110-2-1601, Washington DC.

Wacker, J., and E. J. Plate. 1992. Correlation of Structure of Wind Pressure Buffeting on Cuboidal Buildings and Corresponding Effective Area Wind Loads. *J of Wind Engineering and Industrial Aerodynamics*, 41-44.

Whittaker, J. M. 1935. Interpolatory Function Theory. London: Cambridge University Press.

Wylie, E. B., and V. L. Streeter. 1983. Fluid Transients. FEB Press, Ann Arbor.

REPORT DOCUMENTATION PAGE

Form Approved
OMB No. 0704-0188

1. REPORT DATE *(DD-MM-YYYY)*	2. REPORT TYPE	3. DATES COVERED *(From - To)*
May 2013	Final - TR	

4. TITLE AND SUBTITLE

Physical Model Study of Flowerpot Discharge Outlet, Western Closure Complex, New Orleans, Louisiana

5a. CONTRACT NUMBER

5b. GRANT NUMBER

5c. PROGRAM ELEMENT NUMBER

6. AUTHOR(S)

Stephen T. Maynord

5d. PROJECT NUMBER

5e. TASK NUMBER

5f. WORK UNIT NUMBER

7. PERFORMING ORGANIZATION NAME(S) AND ADDRESS(ES)

Coastal and Hydraulics Laboratory
3909 Halls Ferry Road
Vicksburg, MS 30180

8. PERFORMING ORGANIZATION REPORT NUMBER

ERDC/CHL TR-13-3

9. SPONSORING / MONITORING AGENCY NAME(S) AND ADDRESS(ES)

U.S. Army Corps of Engineers
441 G Street NW
Washington, DC 20314-1000

10. SPONSOR/MONITOR'S ACRONYM(S)

11. SPONSOR/MONITOR'S REPORT NUMBER(S)

12. DISTRIBUTION / AVAILABILITY STATEMENT

Approved for public release; distribution is unlimited.

13. SUPPLEMENTARY NOTES

14. ABSTRACT

The physical model investigation of the West Closure Complex (WCC) Pump Station evaluated flow leaving the 1740 cfs pumps through the flowerpot discharge outlet (FPDO). The model study evaluated stability of flow in the FPDO, head loss through the FPDO to use in pump head estimation, downstream riprap stability, and performance of keel coolers both inside the FPDO and downstream of the FPDO in the tailwater. The recommended Type 8 Design FPDO has a 14-in. wide rounded lip with its top located at elevation (el) 14, the chamber floor at el 11, and the roof at el 23. The diameter of the outlet at the top of the semicircular lip at el 14 was 169.5 in. Two 3-ft wide piers at the downstream end of the chamber were found to not have adverse effects on pump head or flow exiting the chamber. Pressures measured in the pump column and dye injections in the flowerpot section showed stable flow conditions in the vertical column above the pump. Water levels in the chamber were well below the roof and should allow air bulking of the flow without filling of the chamber.

15. SUBJECT TERMS

Keel coolers	Pump diffuser	Pump impeller
Physical model	Pump discharge	Pumps
	Pump head	Riprap design

16. SECURITY CLASSIFICATION OF:			17. LIMITATION OF ABSTRACT	18. NUMBER OF PAGES	19a. NAME OF RESPONSIBLE PERSON: Richard B. Styles
a. REPORT	b. ABSTRACT	c. THIS PAGE			19b. TELEPHONE NUMBER *(include area code)*
Unclassified	Unclassified	Unclassified	Unclassified	107	(601) 634-4065